THE UNIVERSITY OF MICHIGAN

COLLEGE OF ENGINEERING
Department of Mechanical Engineering
Heat Transfer Laboratory

Technical Report No. 6

AN EXPERIMENTAL STUDY OF THE INFLUENCE OF
LOCALIZED, NORMAL SURFACE OSCILLATIONS
ON THE LAMINAR FLOW OVER A FLAT PLATE

James M. Deimen
John A. Clark

ORA Project 05065

This report was also a dissertation submitted by
the first author in partial fulfillment of the require-
ments for the degree of Doctor of Philosophy in The
University of Michigan, 1965.

ACKNOWLEDGEMENTS

TABLE OF CONTENTS

CHAPTER

LIST OF TABLES

LIST OF ILLUSTRATIONS

NOMENCLATURE

Small letters

a	thermal diffusivity
b	the uncertainty of a variable
c	conversion factor $lb./ft^2$ to "Hg
d	the measured variable in uncertainty analysis
e	distance from membrane centerline
f	frequency
g_o	gravitational constant
h	center of gravity of a circular ring sector
k	diameter of inside crescent of eccentric
ℓ_c	length of eccentric
ℓ_{cw}	length of counterweight
m_1	connecting rod crank end mass
m_2	connecting rod wrist pin end mass
m	shape factor of probability curve
m'	dimensionless shape factor of probability curve (mL^2)
r	radius of counterweight ring
s	membrane tension
t	time
u	velocity component in x-direction
v	velocity component in y-direction
w	membrane deflection
x	distance along plate from leading edge
y	distance normal to plate
z	center of gravity of eccentric

Capital letters

B   bore of eccentric

D   outside radius of eccentric

F   denotes function

$F_3(X')$ geometric oscillation profile factor

I   outside radius of counterweight

L   distance of membrane centerline from leading edge

P   pressure

R   gas constant

T   temperature

U'   dimensionless velocity (u/u_∞)

V   velocity

X'   dimensionless length (x/L)

Re   Reynolds Number with respect to distance
           from plate leading edge

N   hot wire resistance ratio

Greek letters

δ laminar boundary layer thickness

ϵ amplitude of oscillating membrane

ϵ' dimensionless membrane amplitude (ϵ/L)

η Blasius variable $\sqrt{\dfrac{u}{\nu x}}$

μ viscosity

ν kinematic viscosity

λ_f amplitude frequency parameter

ξ Pohlhausen similarity parameter

ρ density

ϕ_s' steady disturbance function $(\exp[-m(x-L)^2]$)

ω circular frequency

ω' dimensionless circular frequency ($\omega L / u_\infty$)

Subscripts

∞ free stream

w plate surface

a   air

m   membrane

s   static conditions

o   stagnation conditions

B   brass

Dissertation Abstract

AN EXPERIMENTAL STUDY OF THE INFLUENCE OF
LOCALIZED NORMAL, SURFACE OSCILLATIONS
ON THE LAMINAR FLOW OVER A FLAT PLATE

By James M. Deimen

The purpose of this investigation is to study the
effect of a finite localized surface oscillation on the
mean value velocity profiles in the laminar boundary
layer of a flat plate and compare the results with an
analytic solution.

The experimental program consisted of the design,
construction and testing of a flat plate with a flexible
membrane located in the surface and driven by an oscil-
lating device. The flat plate was located in a low
turbulence, low speed wind tunnel. The principal
measuring instrument was a hot wire anemometer mounted on
a bridge over the plate with its position normal to the
plate controlled from outside the tunnel.

Experimental data was taken at free stream velocities
of 20 and 40 feet per second. The surface oscillation amp-
litude was 0.050 inches and the frequency range 15 to 100
cycles per second.

The results of the investigation show that a definite
change in the mean value velocity profile in laminar flow occurs
and is a function of free stream velocity, frequency and
location on the plate surface. In addition, early transition
is promoted. The analytic solution is found to be qualitat-
ively valid in the laminar flow region downstream of the
membrane.

CHAPTER I

Introduction and Literature Survey

Although a large number of boundary layer studies both theoretical and experimental have been conducted and reported, only a relatively small number have been concerned with the effects of an artificial time varying disturbance located in the boundary layer region. This is a report of an experimental study of one such type of disturbance, namely the effect of an oscillatory disturbance in the boundary layer induced by the oscillatory movement of a small region normal to the surface of a flat plate. The flat plate is located in a steady parallel flow field with no pressure gradient. This experimental study is based upon a theoretical study conducted by Na (56) in which the disturbance is an oscillating bulge in the flat plate transverse to the mean velocity of the flow and sinusoidally varying in amplitude with respect to time.

The literature survey was conducted with two primary objectives. First, to review previous theoretical and experimental research concerning disturbed boundary layer flows along a flat plate. Primary interest was centered upon the laminar profile and transition regions. Second, to study and analyze the techniques utilized by previous investigators in their studies of turbulent flow and boundary layer flow. Emphasis was placed on hot wire anemometry technique since this method of measurement is

1

used for this investigation. The following paragraphs contain brief resumes of the more important references.

Liepmann and Dhawan (43,16) studied the skin friction due to the laminar boundary layer. They utilized a flat plate with a small moveable section in its surface. Movement of this section gave a direct indication of skin friction. The flat plate was mounted in a wind tunnel of low turbulence level (0.03%). With a hot wire anemometer they studied the effect of small gaps in the plate surface and the Tollmien-Schlichting waves. They also studied the pressure gradient due to the leading edge of the flat plate.

Schubauer and Skramstad (67) conducted an experiment in which they found the Tollmien-Schlichting waves as predicted by the Tollmien-Schlichting stability theory. In order to obtain the low turbulence levels necessary, extensive experimental work was performed to find the best combination of screens and cloth for the tunnel settling chamber and to isolate the test section from the rest of the tunnel. The results of their turbulence measurements and the effect of fan noise on turbulence are given in the report. They developed the method of producing oscillations in the boundary layer by electrodynamically vibrating a thin metallic ribbon in the boundary layer.

Dryden, Schubauer, Mock and Skramstad (17) experimentally determined tables of turbulence level versus mesh length for various screens and developed corrections for

wire length when the wire length and the scale of
turbulence are of the same order.

Schubauer and Klebanoff (65) conducted a detailed
investigation of the transition region with naturally and
artificially induced turbulence spots. They used the
vibrating ribbon flat plate and wind tunnel of reference (67)
and developed a method of dual mounting for two hot
wires so that a turbulent spot could be observed with
respect to time and distance simultaneously. They compared
their experimental results in regard to turbulent spot
movement and calming effect with Emmons (20).

Emmons (20) developed a probability transition theory
from observations of turbulent spots on a tilting water
table. He then applied this theory to transition on a
flat plate with fair results.

Charters (5) conducted experiments to investigate
the effect of transverse contamination of laminar boundary
layer flow by turbulence. He studied the edge effect of
the wind tunnel walls with the flat plate fastened to the
walls and also the turbulent wake of a rod or airfoil set
perpendicular to the plate in the boundary layer. He
found that the transverse effect spread linearly with
distance downstream.

Liepmann and Fila (44) conducted studies on the
effect of roughness elements and heating on the boundary
layer of a flat plate mounted vertically in the flow. Their
method of reducing wind tunnel turbulence level is given in

the report including the components and measurements.
Blasius profile measurements were taken with both hot wire
and total head tube. In addition, temperatures were taken
with the hot wire.

Dryden (18) gives a very detailed account of problems
met in hot wire boundary layer measurements and includes
leading edge effects and heat loss due to the proximity
of the hot wire to the wall. He includes a detailed
study of the effect of a pressure gradient along the surface
of the plate and a thorough investigation of the laminar,
transition and turbulent flow regions.

McPhail (46) conducted measurements to determine the
effect of the wind tunnel contraction section on the turbu-
lence components and turbulence level. In addition, he
studied the effect of fan noise on the turbulence level.

Klebanoff and Tidstrom (39) utilizing the vibrating
ribbon technique to induce vibrations in the boundary
layer, made measurements of fluctuation in the laminar
boundary layer just upstream of transition. They used
two hot wires mounted in two positions with simultaneous
observation on an oscilloscope to observe the movements
of turbulent spots.

Hill and Stenning (34) measured boundary layer profiles
on a flat plate in a mainstream flow possessing pressure
oscillations which were varied over a wide frequency
range. They compared the profiles with oscillations to
those without and found no change in the mean values from
the theoretical or experimental Blasius profiles.

Moore and Ostrach (54) developed a theoretical analysis of the boundary layer profiles due to the oscillation of a plate about its steady mean velocity. They found a second order quasisteady effect on the mean boundary layer velocity profiles in compressible flow.

Kestin, Maeder and Wang (37) developed a theoretical analysis of the boundary layer equations including first and second order effects. Their solutions are in the form of infinite series of trigonometric functions. Computer calculations indicate that oscillations due to a free stream turbulence level of 5% would produce a second order effect of only 0.25% on the mean velocity profile.

Klebanoff, Tidstrom and Sargent (38) present detailed measurements of boundary layer instabilities including secondary vortex streaming both for naturally and artificially induced oscillations in the boundary layer. A vibrating ribbon was used to induce oscillations and two hot wires were used to simultaneously pick up two components of the velocity for display on an oscilloscope.

Criminale and Kovasznay (12) developed a theoretical analysis of the growth of a three dimensional wave packet begun by an impulsive instability and located in a Blasius boundary layer flow.

Greenspan and Benney (23) have recently developed a theoretical analysis which indicates a sudden growth of secondary oscillations in flat plate boundary layer flow. Their linearized analysis possesses good agreement with

the experimental observations of sudden violent velocity

changes in the transition region as indicated by Klebanoff,

Tidstrom and Sargent (38).

CHAPTER II

Statement of the Problem

The problem is purely experimental in nature, conducted primarily to ascertain the validity of a mathematical model by Na(56). A physical system was designed and constructed to approximate the mathematical model. The mathematical model including the basic assumptions and results of the perturbation analysis developed by Na are as follows.

Let a semi-infinite "flat" plate be placed in a flow of constant velocity such that the mean pressure gradient on the surface of the plate is zero (Figure 2.1). The following assumptions are made:

a) Let L, the distance of the localized disturbance from the leading edge, be significantly greater than the boundary layer thickness δ, i.e., $L \gg \delta$, such that leading edge effects can be neglected.

b) Let the fluid be incompressible so that the induced pressure waves travel with infinite velocity.

c) Let the surface of the plate be given by the probability curve for the two dimensional space-wise coordinates (Figure 2.2) and the time-wise periodic disturbance by complex notation for a steady periodic disturbance. Therefore, the surface may be given by the following expression:

$$y = \epsilon \exp \left[-m (x - L)^2 + i\omega t \right] \qquad (2.1)$$

7
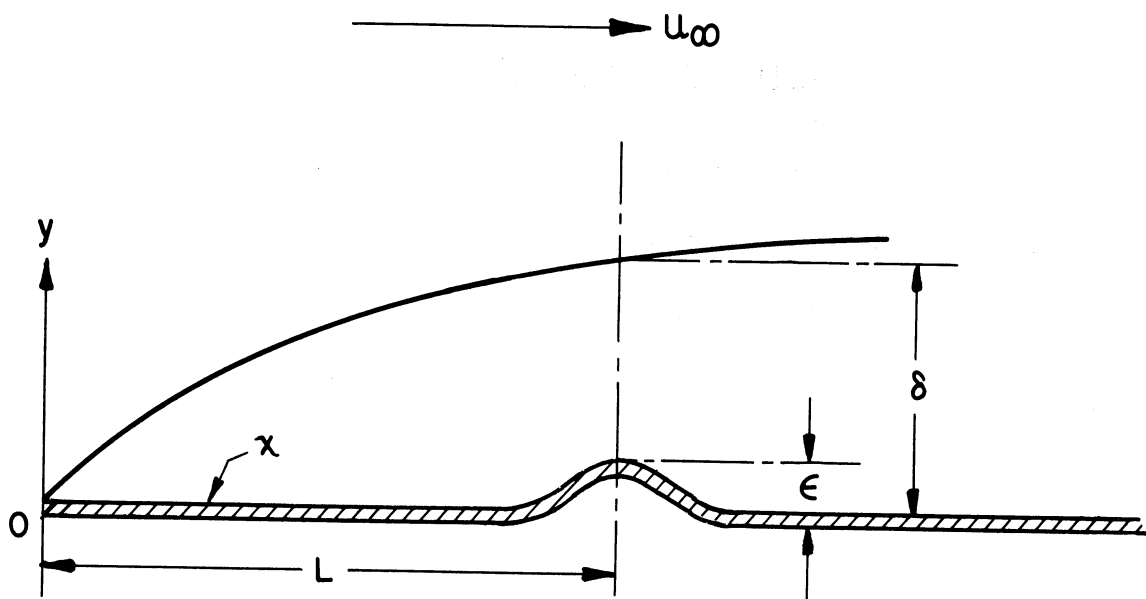
Figure 2.1 Model of the flat plate
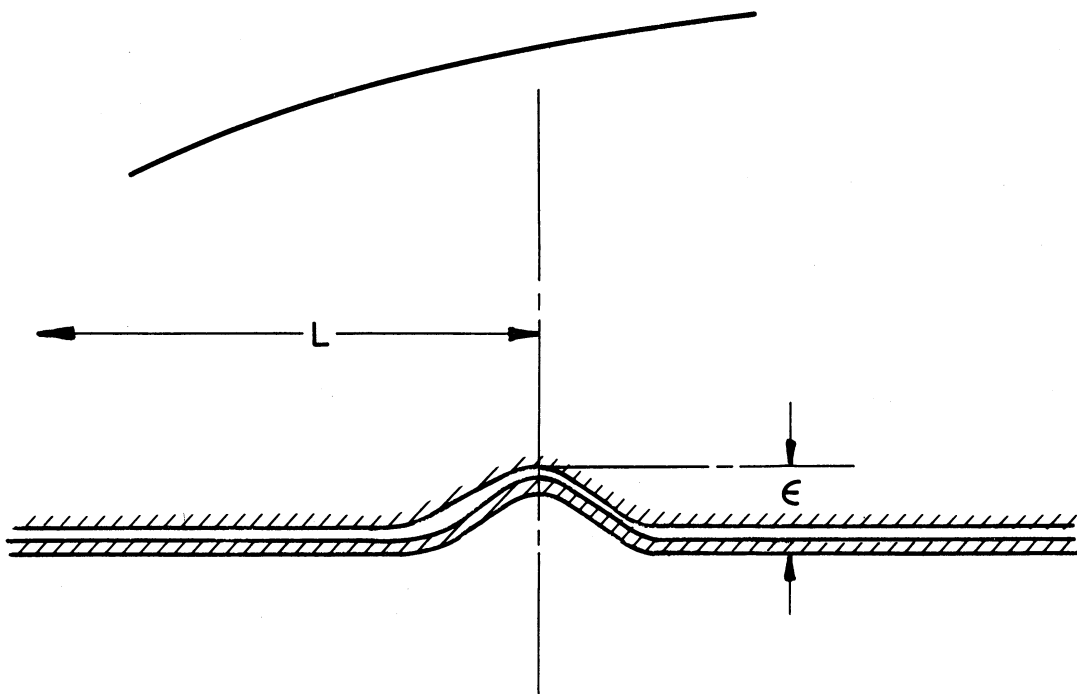
Figure 2.2 Analytical model of the disturbance

d) The effect of localized oscillations on the potential flow is neglected. The potential flow is assumed to be a flow of constant velocity

e) The velocity component of the plate in the x direction is zero.

The continuity, momentum and energy equations for Cartesian coordinates can be thus expressed,

Continuity,

$$\frac{\partial u}{\partial x} + \frac{\partial v}{\partial y} = 0 \tag{2.2}$$

Momentum,

$$\rho\left(\frac{\partial u}{\partial t} + u\frac{\partial u}{\partial x} + v\frac{\partial u}{\partial y}\right) = -\frac{\partial P}{\partial x} + \mu\left(\frac{\partial^2 u}{\partial x^2} + \frac{\partial^2 u}{\partial y^2}\right)$$

$$\rho\left(\frac{\partial v}{\partial t} + u\frac{\partial v}{\partial x} + v\frac{\partial v}{\partial y}\right) = -\frac{\partial P}{\partial y} + \mu\left(\frac{\partial^2 v}{\partial x^2} + \frac{\partial^2 v}{\partial y^2}\right) \tag{2.3}$$

Energy,

$$\frac{\partial T}{\partial t} + u\frac{\partial T}{\partial x} + v\frac{\partial T}{\partial y} = a\left(\frac{\partial^2 T}{\partial x^2} + \frac{\partial^2 T}{\partial y^2}\right) \tag{2.4}$$

The boundary conditions are,

$$y = \epsilon \exp\left[-m(x-L)^2 + i\omega t\right]$$
$$T = T_w$$
$$u = 0$$
$$v = i\omega\epsilon \exp\left[-m(x-L)^2 + i\omega t\right]$$
$$y \rightarrow \infty$$
$$T = T_\infty \tag{2.5}$$
$$u = u_\infty$$

The final result obtained by Na expressing the
equation for the velocity profile in the boundary layer under
perturbed conditions is,

$$u' = u_o' + \frac{\epsilon'^2}{Re} u_{20}' = 2\zeta - 2\zeta^3 + \zeta^4 + \frac{\epsilon'^2 \omega'^4}{Re} F_3(X')\{-53.749(\zeta - 3\zeta^3 + 2\zeta^4)\}$$

(2.6)

where,

$$\zeta = \frac{y}{\delta}$$

and

$$F_3(X') = X' \phi_s'^2 [m'(X'-1)X' - 0.25] \{[1.50 - 4m'X'(X'-1)][m'(X'-1)X' - 0.25] + 2m'X'(2X'-1)\}$$

(2.7)

The primes denote non-dimensional quantities and η
is the Blasius non-dimensional variable, defined as $y\sqrt{\frac{U_\infty}{\nu x}}$.

The first three terms on the right s ide are an
approximate representation of the boundary layer laminar
profile over a flat plate with no oscillation, i.e., the
zeroeth order solution (36,59). This non-oscillatory case
may also be represented by the Blasius profile (2). The
purpose of this investigation is the effect of the last
term. Scrutiny of this term reveals that it may be
divided into $\epsilon'^2 \omega'^4$ /Re multiplied by a geometric
quantity. Therefore, the effect of this term can be in-
vestigated by the alteration of the amplitude and frequency

of the bulge in the plate. Since the frequency enters
to the fourth power, the effect of frequency alteration will
be sudden and rapid.

The experimental program is concerned with two
comparisons. a) A comparison of the mean velocity profile
with oscillation with the mean measured velocity profile
without oscillation. b) A comparison of the mean velocity
profile with oscillation with the prediction of the per-
turbation theory. Since the small perturbation solution
is very restrictive in regard to the size of $\epsilon'^2 \omega'^4/Re$
the theoretical solution is not expected to hold when the
last term reaches a few percent of the sum of the first
three terms.

The experimental investigation utilizes relatively
large values of amplitude and moderate values of frequency,
i.e., on the order of the boundary layer thickness at the
bulge and frequencies up to 100 cps. In effect, a
finite disturbance is introduced into the boundary
layer. Therefore, the theoretical solution is only a
qualitative indication of the physical problem when applied
to finite disturbances.

CHAPTER III

Experimental Equipment

The experimental program is conducted in a low speed,
low turbulence wind tunnel of the Aerospace Engineering
Department. Inside the tunnel test section is a flat
plate assembly with a flexible membrane located in the
surface. The principal measuring instrument is a boundary
layer hot-wire probe located on a bridge over the plate
(Figure 3.1). The flat plate and supporting assembly
is mounted vertically with the flexible membrane drive
mechanism mounted on one side of the tunnel test section
wall and the hot-wire position control passing through the
opposite wall. The roof of the test section is removable
glass panes to allow adjustment and visual inspection. Views
of the electronic instruments and controls are shown in
Figures 3.2 and 3.3.

3.1   Flat Plate Configuration

The plate is 13 inches by 31 inches, 6061-ST6
aluminum plate ¼ inches thick (Figure 3.4). The plate is
split at the membrane location 9 inches from the leading
edge with the downstream section fastened to the T-section
rails and the leading edge section moveable to facilitate
adjustment of the membrane tension. The membrane is glued
to the clamping bars on the underside of the plate (Figure 3.5).
The dimensions of the downstream section are based upon the
length of the membrane across the plate. Charters (5)
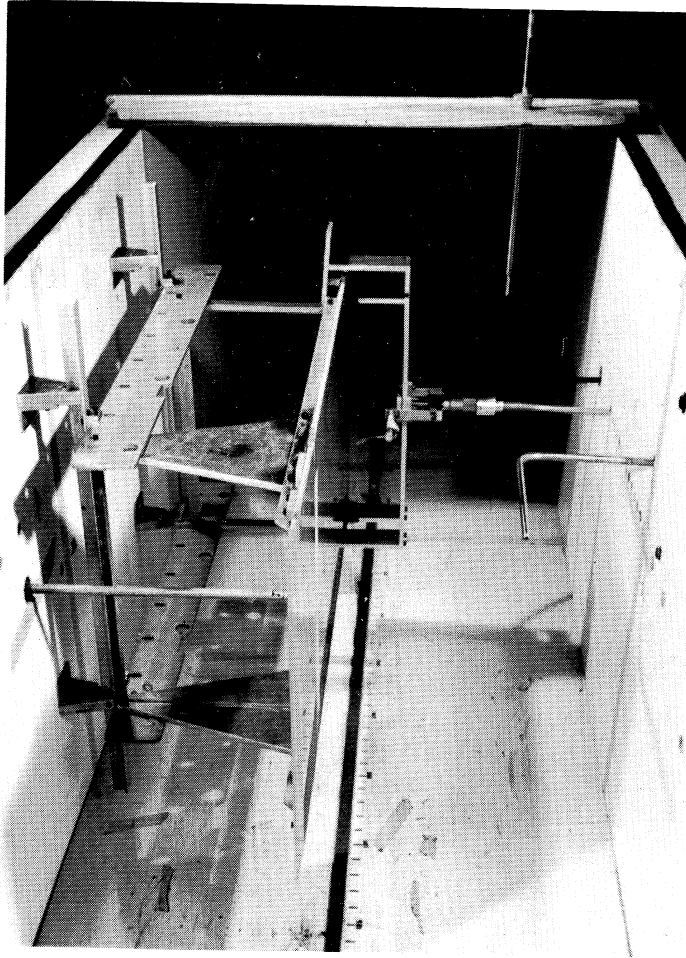
Figure 3.1   Flat Plate test apparatus mounted in
tunnel test section
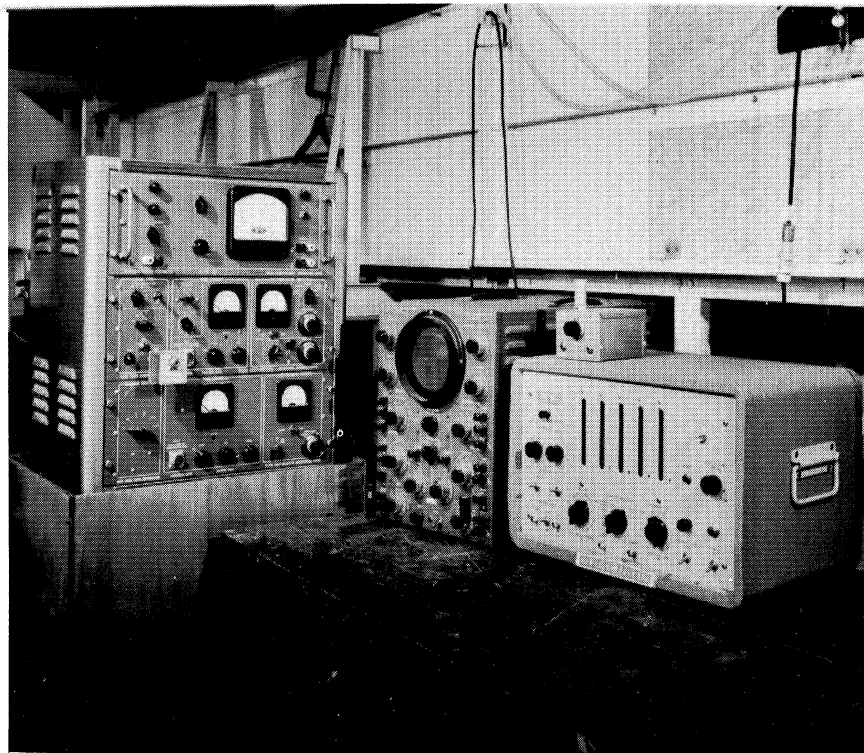
Figure 3.2 Electronic instruments
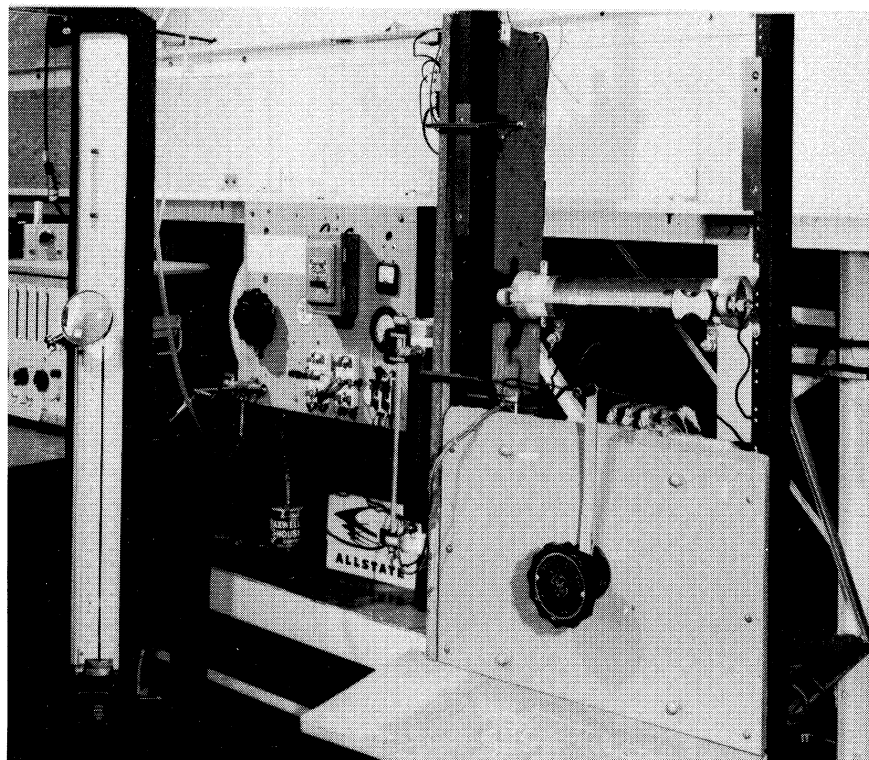
Figure 3.3 Micromanometer, oscillator and wind
tunnel controls

13 - IN.

FLOW

A'

LEADING EDGE

9.0-IN.

FLOW

IO-IN.

A'

OSCILLATING MEMBRANE

31- IN.

I 3/8 -IN.

A

T RAIL

A
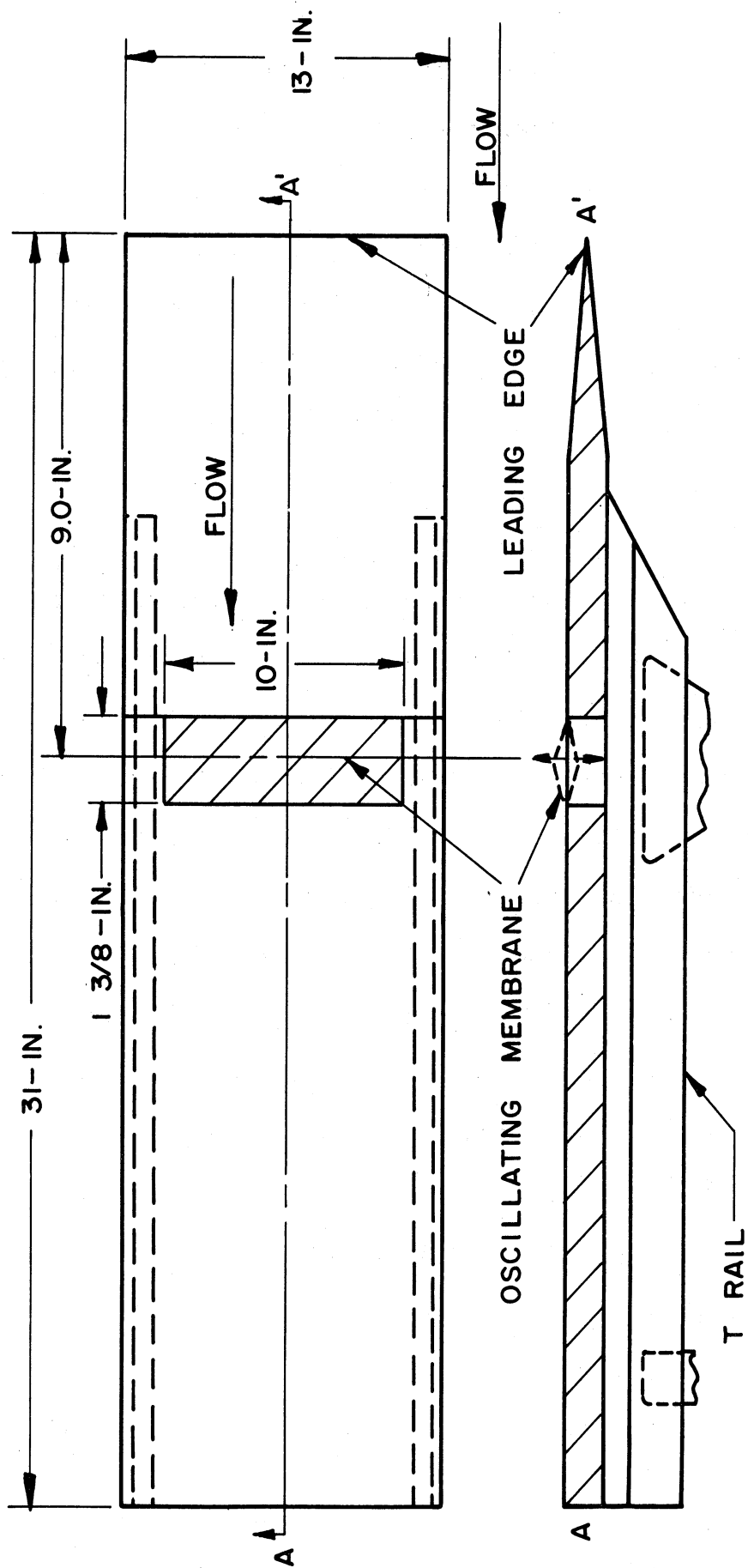
Figure 3.4 Flat plate configuration

found that an edge effect would expand over the surface of
a plate with a constant angle of less than 10° in the
downstream direction. Therefore, for a 10°-angle and 8-inches
membrane length the edge effects would meet at a downstream
distance of approximately 22 inches. The membrane is 10-inches
long to insure two dimensional flow over the full central
8-inches. The supporting structure allows the plate to be
adjusted for angle of attack and pivots approximately at
the membrane location. The structure holds the plate
rigidly 12-inches from the wall approximately in the
center of the tunnel test section. The leading edge is
symmetric and razor sharp, with each surface approximately
parabolic (Figure 3.6). The plate surface was hand sanded
with #250 wet sandpaper to obtain a satin finish before the
plate was split at the membrane location. The T-rails
insure that there is no change of elevation on the plate
at the membrane. The membrane clamping bars are shimmed
to adjust the membrane level with the plate. The gap in
the surface between the membrane and the plate is less than
1/16-inches which is less than the 1/8-inches tested by
Liepmann and Dhawan (16.43). The membrane material is a
thin very elastic rubber commonly known as rubber dam.
The surface roughness is comparable to the surface
roughness of the plate. The width under tension is 1 3/8-in.
Glued to the centerline of the membrane is the aluminum
driven link of the oscillating linkage.
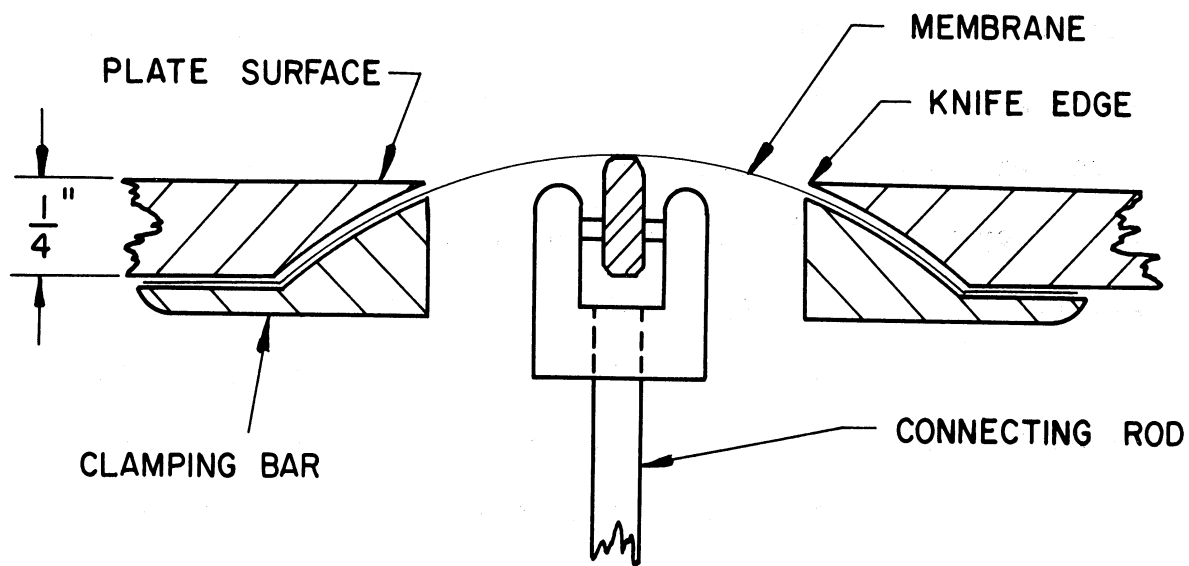
Figure 3.5 Detail of membrane configuration
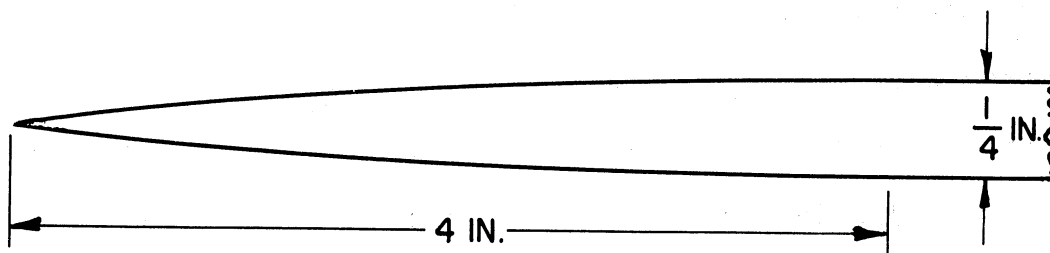
Figure 3.6 Leading edge configuration

3.2 Oscillator

The device to oscillate the membrane in the plate surface required the most effort in the development of the test apparatus. The initial goals of the investigation were set high and required an oscillating device with a frequency range of 10-1000cps and with an amplitude greater than 0.010 inches. In addition the driving device would have to be located within an area less than one inch below the plate or outside the tunnel test section. The frequency requirement indicated that an electromagnetic device would be most promising. The first test device utilized a 0.001 inches aluminum foil membrane above a specially constructed D.C. electromagnet. The membrane lay parallel to the magnetic field lines. An electric A.C. current oscillating at the desired frequency was passed through the membrane in a direction perpendicular to the magnetic field lines. Thus, an electromotive body force was developed in the membrane with its direction perpendicular to the plane of the membrane. The intensity of the oscillating disturbance generated was so small that a stethoscope had to be utilized to hear the sound. Therefore, a second electromagnetic oscillator of similar design was constructed but with an iron foil membrane of 0.003 inches thickness. The effectiveness of the superior magnetic permeability is partially nullified by the increase in stiffness and inertia in comparison with the aluminum foil. The electromagnet was operated to produce a magnetic flux ten times that necessary to produce magnetic

saturation in the foil. The signal was audible but of such low intensity that the oscillation amplitude was insufficient for the purpose of this investigation. Since the iron foil was magnetically saturated and thickening of the foil would increase the stiffness and inertia, the only alternative would be to increase the A.C. current level. Sufficient current for an appreciable oscillating amplitude would cause severe heating of the membrane. Heating of the membrane could not be permitted since heating a section of the plate would induce a change in the air flow over the plate that could not be tolerated. Therefore, the electromagnetic oscillator was abandoned.

Brief consideration was given to various forms of fluid powered oscillators but the best approach seemed to center on a mechanical oscillator with a frequency range of 10-200 cps. Therefore, a mechanical oscillator was constructed as follows.

The membrane is driven from outside the tunnel by a connecting rod of aluminum tubing 14-inches long. At the crank end the rod length is adjustable. The crank is an eccentric with a 9/16-inches connecting rod needle bearing. Eccentrics with 0.050 inches and 0.010 inches were constructed but only the 0.050 inches was used in this investigation. The connecting rod is connected to the driven link under the membrane with a small journal bearing. Dual counterweights on either side of the needle bearing complete the reciprocating mechanism.

The total reciprocating unbalance is less than 1/20 pound-
mass and the rotating unbalance is less than 1/20 pound
mass. The counterweights approximately eliminate the
rotating unbalance and shift the angular position of the
maximum reciprocating unbalance. See Appendix for the
design of the eccentric and counterweights.

The eccentric is driven through a gearbox (Figure 3.7)
The gearbox has interchangeable spur gears with possible
ratios of 10 to 1, 4 to 1 and 2 to 1. The gearbox
is driven by a shunt wound, 24 volt D.C, 10,000 RPM,
Robbins and Myers, $\frac{1}{4}$ Hp. aircraft motor. The motor is
capable of sustained operation over a range of 5000 to
12000 RPM. With the gearbox the useful frequency range is
10 to 100 cps. In addition, the eccentric can be mounted
directly on the motor shaft for frequencies from 100 to
200 cps. A thin iron disk with six teeth is mounted on the
motor shaft. Continuous monitoring of the motor speed is
obtained with an Electro Model 3010-A magnetic pickup and a
Hewlett-Packard Model 522-B electronic counter. Two 12-volt
storage batteries are connected in series through a
rheostat to control the motor speed by control of the
motor voltage. Figure 3.8 shows the control circuitry.

3.3 Membrane dynamic configuration

The instantaneous shape of the membrane at either
maximum or minimum position is assumed to be triangular
(Figure 3.9). Also shown is the analytical curve used
by Na(56) to describe the surface,
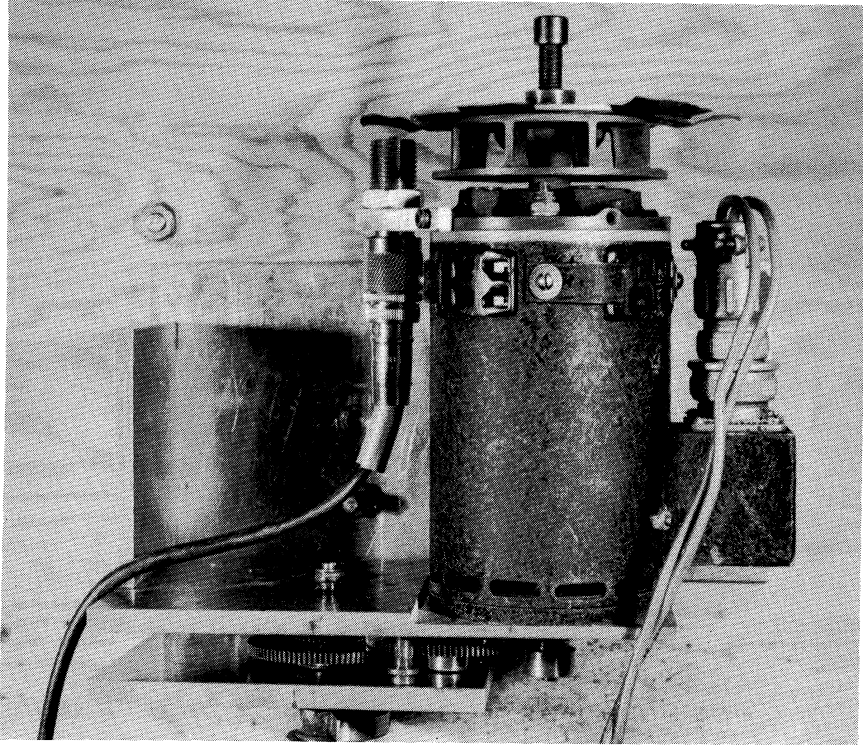
Figure 3.7   Mechanical oscillator drive
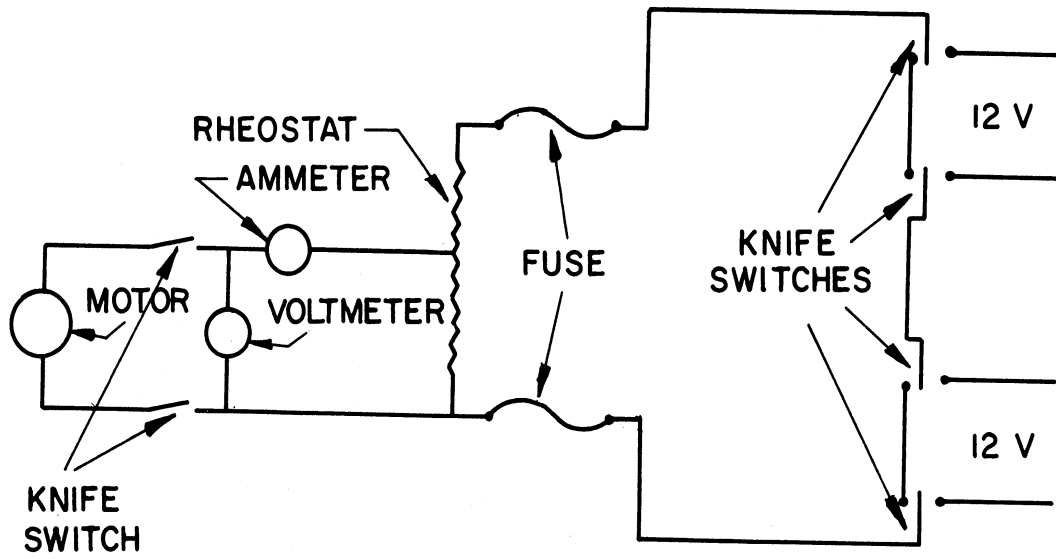
Figure 3.8   Motor control circuit for oscillator
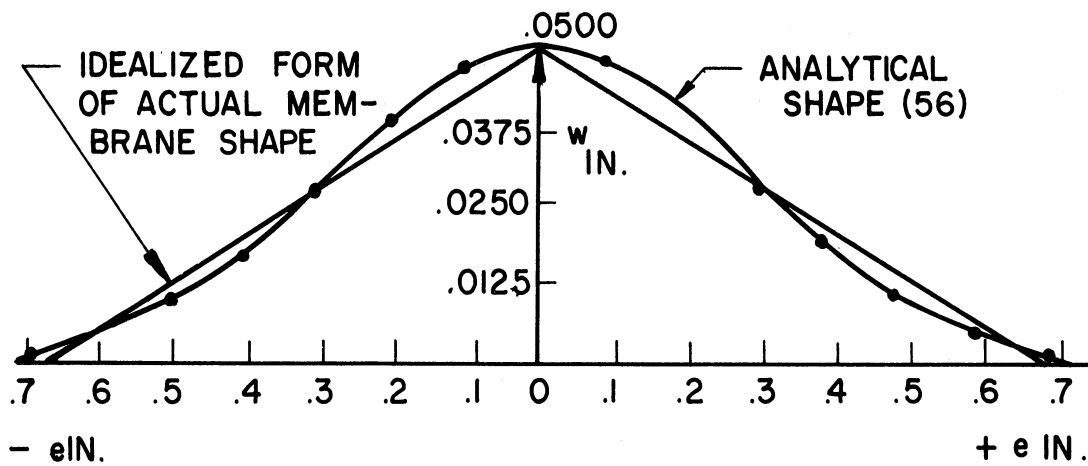
Figure 3.9   Membrane configuration

$$y = \varepsilon \exp \left[-m(x - L)^2 \right] \qquad (3.1)$$

In Figure 3.9 the analytical curve is made to equal the
idealized triangular shape at 0.3 inches from the center-
line of the membrane. The corresponding value of m' is
535 and the resulting analytical shape closely approximates
the actual shape. In fact any value of m' from 400 to 1000
will cause the analytical shape to closely approximate
the actual triangular shape.

The possibility of harmonics in the shape of the
membrane was checked analytically and experimentally.
The experimental check consisted of observing the membrane
in operation over the frequency range with a Strobotac
stroboscopic light. No harmonics appeared in the membrane.
In addition the membrane was simultaneously checked for
rocking about the wrist pin and no rocking was observed.

The analytical check utilized the following membrane
equation,

$$\nabla^2 w = \frac{1}{\alpha^2} \frac{\partial^2 w}{\partial t^2} \qquad (33)$$

$$\qquad (3.2)$$

which, for this case, reduces to

$$\frac{\partial^2 w}{\partial \ell^2} = \frac{1}{\alpha^2} \frac{\partial^2 w}{\partial t^2} \qquad (3.3)$$

where, $\quad \alpha^2 = \dfrac{S}{\rho_m} \qquad (3.4)$

The center of the membrane is displaced as $\epsilon \sin \omega t$. The following steady state solution is applicable,

$$w = F(l)\sin \omega t \tag{3.5}$$

The steady equation then takes the form,

$$F''(l)\sin \omega t = \frac{1}{\alpha^2}\left(-F(l)\omega^2 \sin \omega t\right) \tag{3.6}$$

The boundary conditions are as follows

$$l = 0 \qquad\qquad l = l_m$$
$$w = \epsilon \qquad\qquad w = 0 \tag{3.7}$$

The solution for F is,

$$F = \epsilon\left(\cos\frac{\omega}{\alpha}l - \frac{\cos\frac{\omega}{\alpha}l_m}{\sin\frac{\omega}{\alpha}l_m}\sin\frac{\omega}{\alpha}l\right) \tag{3.8}$$

and,
$$\frac{w}{\epsilon} = \left(\cos\frac{\omega}{\alpha}l - \frac{\cos\frac{\omega}{\alpha}l_m}{\sin\frac{\omega}{\alpha}l_m}\sin\frac{\omega}{\alpha}l\right)\sin \omega t \tag{3.9}$$

The membrane density $\rho_m = 0.0359$ Lbm/in^3. Table 3.1 indicates the elongation from a one inch relaxation length, the corresponding tension, the fundamental natural frequency and the first harmonic. Operation of the oscillating membrane was limited to elongations between $\frac{1}{4}$ and 3/8 inches with frequencies below 200 cps.

ELONGATION	TENSION	FUNDAMENTAL NATURAL FREQUENCY	FIRST HARMONIC FREQUENCY
.250 INCHES	27.5 $^{lbf}/_{IN^2}$	217 cps	434 cps
.375 INCHES	42.5 $^{lbf}/_{IN^2}$	246 cps	492 cps

Table 3.1 Natural frequency and first harmonic of membrane
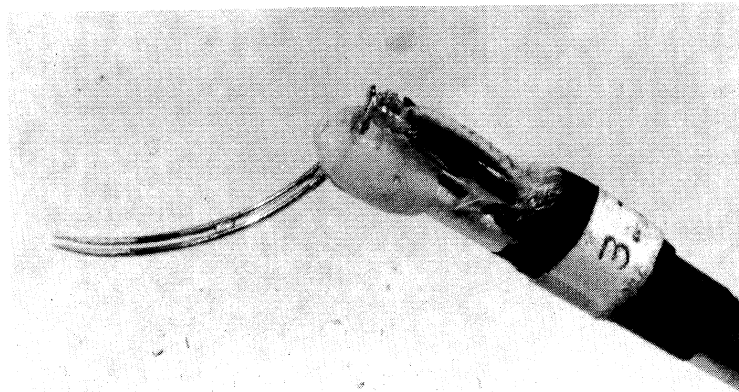
Figure 3.10 Hot wire probe

3.4 Hot-wire anemometer

The hot-wire probe is mounted on an aluminum bridge spanning the plate and clamped to the rails underneath the plate (Figures 3.1 and 3.4). The bridge may be clamped at any location along the plate. Mounted on the bridge is an assembly that may be clamped at any span-wise position on the bridge. This assembly contains a Starrett micrometer head for positioning the probe at any location normal to the plate. The micrometer head can be turned from outside the tunnel with a shaft passing through the tunnel test section wall. Various probes may be accommodated by the micrometer assembly.

The hot wire probe utilized for this investigation is shown in Figure 3.10. Two curved stainless steel surgeons needles are mounted in a streamlined plastic block which in turn is mounted on the end of a $\frac{1}{4}$-inch aluminum rod which fits into the micrometer assembly. Soft soldered across the tips of the stainless steel needles is the hot-wire itself. The hot-wire is a 0.0002 inches diameter tungsten wire 0.050 inches long. Since the length to diameter ratio of the hot wire is 200 to 1 the thermal end effects of the wire when heated may be ignored. The electrical leads are soldered into the eyes of the needles.

The hot-wire instrumentation consists of a Flow Corporation Model HWB3 constant current anemometer which includes the wire current circuit, galvanometer circuit, bridge circuit and voltage amplifier. This control unit utilizes a four-wire circuit where two leads to the hot-wire

carry the current for the hot-wire and the other two

leads are for measurement of the hot-wire voltage with the

galvanometer. The output voltage of the hot wire can be

fed into the amplifier which includes a compensating circuit

for the thermal lag in the hot-wire. The output of the

amplifier is fed through a 7 kc low pass filter to a

Dumont Model 322 oscilloscope. The oscilloscope

continuously monitors the instantaneous voltage drop

across the hot wire as compensated and amplified. In this

investigation the purpose of the oscilloscope is to

enable a qualitative instantaneous understanding of the flow

characteristics at each data point of each velocity profile.

Measurements of RMS voltage and current are made with the

galvanometer of the control unit.

The temperature of the air in the wind tunnel is

measured simply by means of a thermometer inserted through

the roof of the tunnel test section.

3.5 Wind Tunnel

All preliminary developmental testing was performed in

a wind tunnel with a test section of 2 feet by 2 feet cross

section and 4 feet in length. Unfortunately this tunnel

does not possess a calming section ahead of the convergent

section. Gross instabilities are present in the air flow

thus preventing its use for quantitative measurement in

this investigation.

The wind tunnel used to obtain the results of this

investigation is shown in Figure 3.11. The calming section
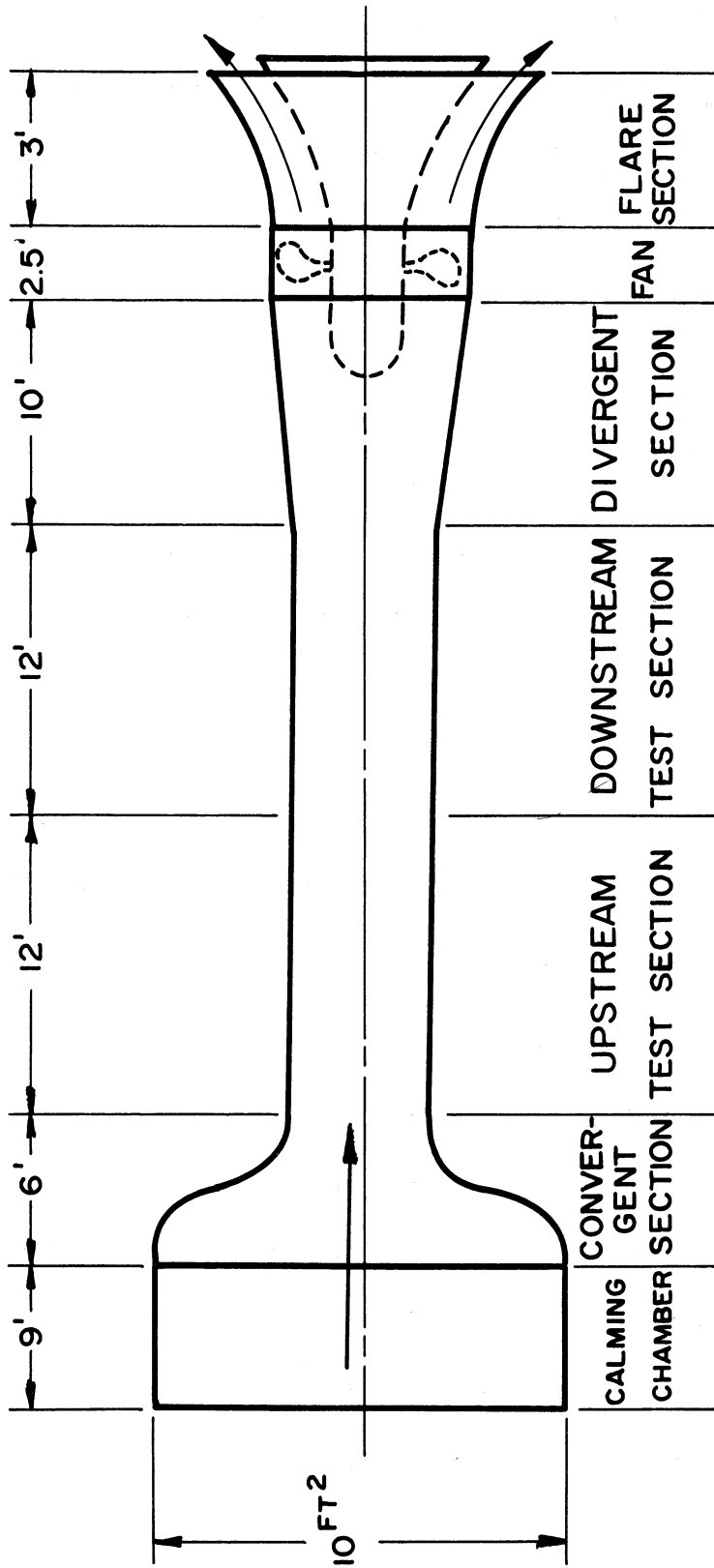
Figure 3.11 Wind tunnel

of the tunnel contains three turbulence screens followed
by a 25 to 1 convergent section. Two test sections in series
are located downstream of the convergent section. The test
section cross section area is 2-feet by 2-feet and 12-feet
in length. The downstream test section is utilized for
this investigation. Downstream of the test section is the
divergent section leading to the axial flow fan. The fan is
driven by a field controlled series wound D.C. motor.
The tunnel is capable of producing velocities ranging from
10 to 50 feet per second through fully open test sections.
The velocity of the free stream in the tunnel test section
can be kept within 0.001 inches of water in terms of the
dynamic head. The free stream turbulence level of the tunnel
is approximately 0.05% at 20 feet per second and 0.1%
at 40 feet per s econd.

For continuous monitoring of the test section free
stream velocity and the calibration of the hot wire probe
an F.W. Dwyer pitot static tube is utilized. The pitot
static tube is connected to a Merriam micromanometer
Model 34FB2 TM. A three way valve in the tubing leading
from the stagnation point tube is included with one branch
open to the ambient barometric pressure. Thus, either the
dynamic head inside the tunnel test section or the dif-
ference between the tunnel test section static pressure and
the ambient barometric pressure can be measured.

CHAPTER IV

Measurement Procedure

The operation of the hot-wire and associated equipment
for the purpose of quantitative velocity measurements
requires painstakingly careful measurement technique.
The following procedure was developed specifically for
the experimental program of this investigation but con-
tains methods common to most hot-wire procedures. The
measurement procedure may be divided into three major
categories: a) hot-wire calibration procedure,
b) profile measurement procedure, c) determination of
the locations of interest in the boundary layer of the
flat plate.

The hot-wire is calibrated with a pitot static
tube and micromanometer. The hot-wire probe is mounted in
a fixture fastened to the pitot tube with the hot-wire in
a plane normal to the end of the tube and about 4-inches
from the tube. The pitot tube is mounted about 7-inches
from the tunnel test section wall where the tunnel free
stream air flow is uniform. The following expression
derived from Bernoulli's equation and the perfect gas law
is used to determine the tunnel air speed.

$$(P_o - P_s) \, 2 g_o R T_s = P_s V^2 \tag{4.1}$$

$(P_o - P_s)$ is the dynamic head and is measured by the
micromanometer in inches of water. The gas constant R
is 53.35 pounds force feet per pound mass degree Rankin

and g_0 is 32.174 pounds force per pound mass. T_S is

the static temperature of the air in the tunnel test section

as indicated by an ice bath calibrated mercury thermometer.

Since the tunnel wind speed is always below a Mach number

of 0.05 the static temperature and stagnation temperature

are essentially alike. The static pressure inside the wind

tunnel is measured with the micromanometer by comparing the

static pressure of the pitot tube with the ambient outside

the wind tunnel and subtracting from the corrected

barometric pressure as measured by a mercury barometer.

The hot-wire is operated at a resistance ratio of 1.6.

The cold resistance is set with the galvanometer and bridge

circuit. Then the hot wire heating current is switched on

and balanced with the bridge circuit. Finally the wire

current is measured with the galvanometer. A typical

calibration curve of current versus velocity is shown

in Figure 4.1. Hot-wire calibration is affected by aging

of the hot-wire and by dirt depositing on the wire, thus

causing a change in the convection heat transfer. Large

changes in wind tunnel operating termperature will also

cause changes in calibration. Therefore the calibration

of the hot-wire is checked before and after each series

of tests on each testing day.

The flat plate is mounted vertically in the

tunnel test section with a minus $\frac{1}{2}$ degree angle of

attack with respect to the geometric center plane of the

tunnel. The measurement of profiles with the plate at

angles of attack from 0° to $-\frac{1}{2}^\circ$ indicate that profiles most
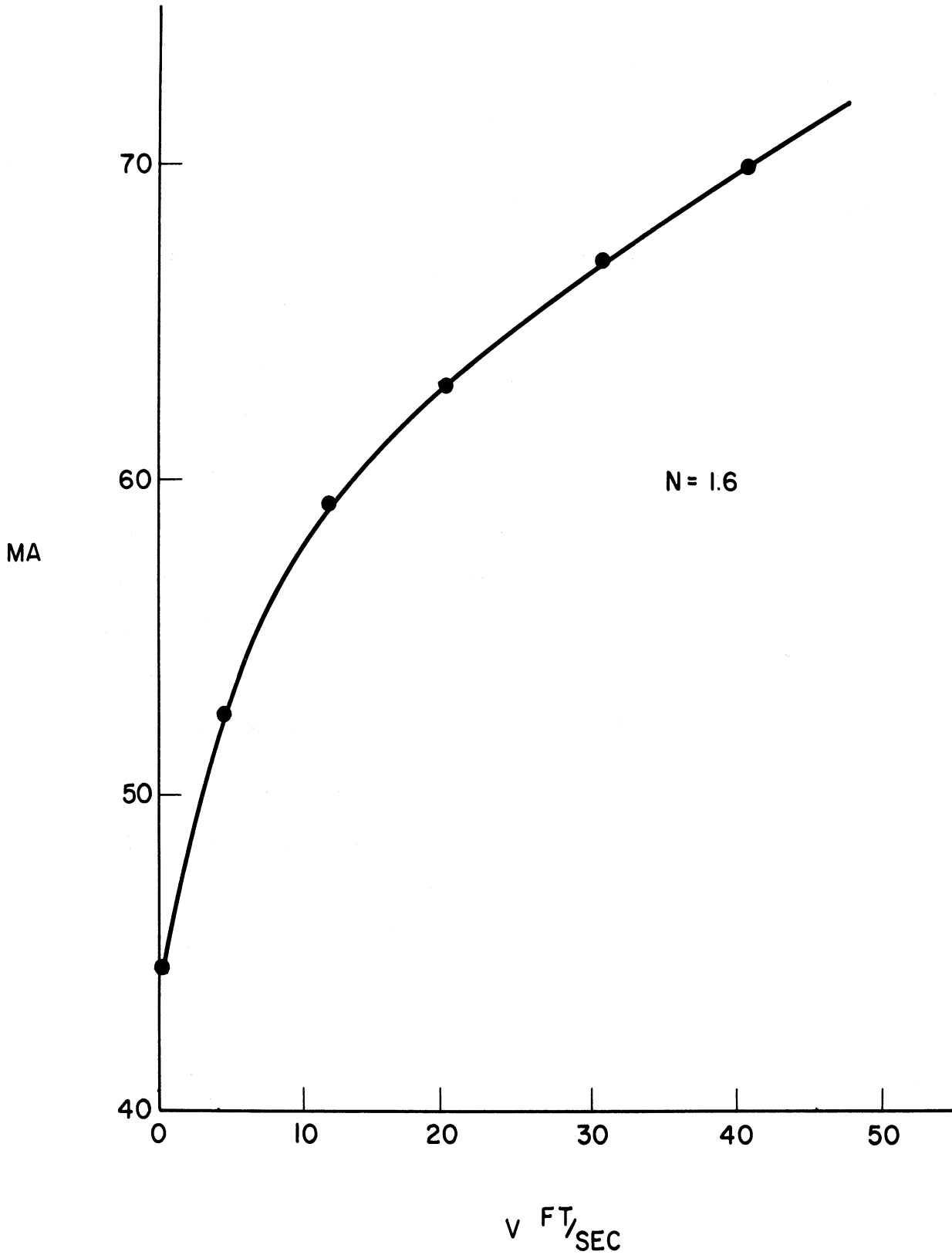
Figure 4.1   Calibration curve of hot wire current
versus velocity

closely approximating the theroetical Blasius profile
at all plate locations occur with the $-\frac{1}{2}^{\circ}$ angle of
attack. The reason for the small angle of attack may be
the slight asymmetry in the flow due to the necessary
supporting structure of the plate.

The measurement of profiles is as follows. The probe
bridge is clamped to the plate with the hot-wire located
at the desired distance downstream of the leading edge.
The probe is adjusted toward the plate until the tip of
the probe and its reflection in the plate just meet. Then
the probe is adjusted outward to the first data point
location. The wind tunnel air velocity is adjusted to the
appropriate velocity as monitored by the pitot tube and
micromanometer. The tunnel velocity is checked and cor-
rected for each data point. For non-oscillatory profiles
the membrane is kept level with the plate surface.

The locations for the data points of each profile
are determined in the following way. Table 4.1 gives the
theoretical laminar boundary layer thickness (δ) as
defined by 99% of the free stream velocity. The boundary
layer thickness for the appropriate plate location and
free stream velocity is divided by ten and the first data
point location is taken at approximately 10% of the
boundary layer thickness. In addition two or three points
are taken at the same interval beyond the boundary layer
to insure that the free stream has been reached. A
final point is taken at least 3/4-inches from the plate
to insure that the other free stream measurements are

34

Table 4.1

Boundary Layer Thickness As A Function of Free-Stream Velocity

and Distance From Leading Edge According to Blasius (2)

u_∞ ft./sec.	x In.	δ in. 2	4	6	8	10	12	14	16	18	20	22	24	26	28	30
	20	.070	.099	.121	.140	.157	.171	.185	.198	.210	.222	.232	.243	.253	.262	.271
	30	.057	.081	.099	.114	.128	.140	.151	.162	.172	.181	.190	.198	.206	.214	.222
	40	.050	.071	.086	.099	.111	.121	.131	.140	.149	.157	.164	.172	.179	.185	.192

correct. Some profiles measured are in the transition
zone and therefore require more data points than the thir-
teen or fourteen above. The procedure is similar in that
equidistant points are taken receding from the plate until
the free stream velocity is reached and checked as above.

At each data point the following procedure is
carried out:

a) the probe is adjusted to the appropriate distance
normal to the plate,

b) the air stream temperature is checked and recorded,

c) if the air stream temperature has deviated more than
0.5° Fahrenheit from the value at the previous data point
then the hot-wire cold resistance is rechecked,

d) the hot-wire is balanced with a resistance ratio of 1.6,

e) the hot-wire current is read and recorded with the
galvanometer,

f) if the oscillator is operating then the motor speed is read
and recorded from the electronic counter,

g) the hot-wire current is rechecked.

The oscillating profile is always measured immediately
after the non-oscillating profile measurement thus insuring
the most accurate possible comparison. Quantitative
measurement with the hot-wire anemometer is an art that
requires much experience before the best results can be
consistently obtained.

The raw data are in terms of wire current in milli-
amperes. From the hot-wire calibration curve the velocities

may be read. The velocity and the geometric position of

the hot-wire are reduced to non-dimensional form as,

$$\frac{u}{u_\infty} = F(\eta) = F\left(y\sqrt{\frac{u_\infty}{\nu x}}\right)$$

(4.2)

where η is the Blasius similarity parameter and ν

equals 0.16373×10^{-3} feet per second squared, the kinematic

viscosity of air. The values of $\frac{u}{u_\infty}$ are plotted

versus η.

The static pressure gradient along the surface of the

plate is checked with an aluminum flat plate of similar

configuration to the test plate (Figure 4.2). The plate

for the pressure check contains static pressure taps two

inches apart along the length of the plate. With the tunnel

in operation and the plate at a minus $\frac{1}{2}°$-angle of attack, the

static pressure at each tap is compared with the ambient

barometric pressure utilizing the micromanometer. The

changes in the pressure difference read on the micromanometer

are introduced into the following expression which is

derived from Bernoulli's equation along a streamline.

$$dV = -\frac{g_0 C}{\rho_a V} dP_s$$

(4.3)

where $\rho_a = .075$ Lb$_f$/ft^3

V is in feet per second

P is in inches of mercury

C is the conversion factor 70.727 lb$_f$/ft^2/"Hg. The static

pressure at the plate surface must be assumed equal

to the static pressure in the streamlines just beyond the
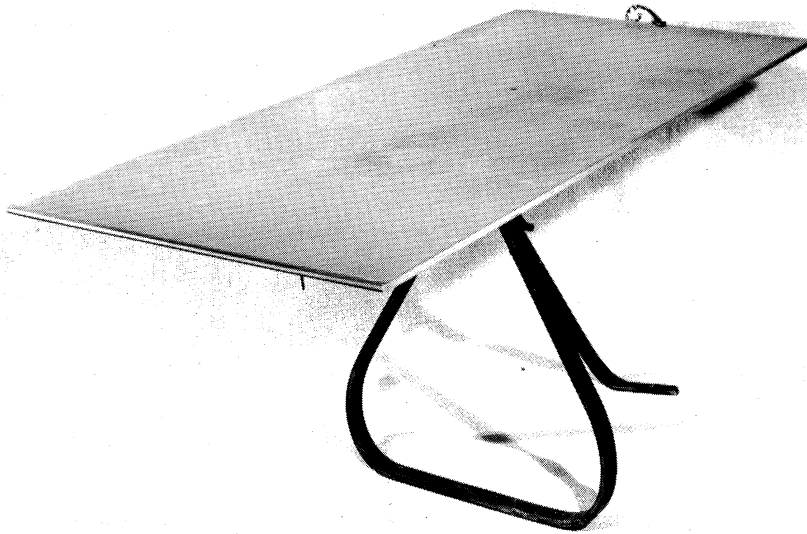
Figure 4.2   Plate for static pressure check

The fourth term may be differentiated with respect to ξ and set equal to zero to obtain,

$$-\lambda_{\delta} \left(53.749\right) F_{3}\left(X'\right)\left(1 - 9\xi^{2} + 8\xi^{3}\right) = 0$$

$$\text{or} \quad \left(1 - 9\xi^{2} + 8\xi^{3}\right) = 0 \tag{4.4}$$

The root of interest in this equation is $\xi = 0.422$ which is the location of the maximum or minimum effect as determined by the sign of $F_{3}(X')$. Thus, the largest absolute effect may be expected at about 42% of the boundary layer thickness or $\eta = 2.1$.

On the basis of this analysis the following procedure is followed. The probe is located at a given value of x and y corresponding to $\eta = 2.1$. The wind tunnel is operated at the appropriate velocity and the hot-wire current balanced with the oscillating membrane turned off. The hot-wire current is measured. Immediately thereafter the oscillating membrane is turned on and the wire current rebalanced and remeasured. This procedure is repeated for various frequencies, velocities and locations on the plate starting with x = 4-inches downstream to x = 22-inches (Table 4.2)

Table 4.2

Frequency and Probe Location for Mean

Velocity Change at η = 2.1

x inches		4	6	8	10	11	12	14	16	18	19.5
U_∞ = 40 ft sec	Freq. c.p.s.	40 50 56 108	40 50 56 108	40 50 56 108	40 50 56 108	40 50 56 108	40 50 56 108	40 50 56 108	40 50 56 108	40 50 56 --	40 50 56 --
U_∞ = 20 ft. sec.	Freq. c.p.s.	40 50 56 108	40 50 56 108	40 50 56 108	40 50 56 108	40 50 56 108	40 50 56 108	40 50 56 108	40 50 56 108	40 50 56 108	40 50 56 108

CHAPTER V

Uncertainty Analysis

This chapter concerns both the inaccuracies associated with the actual construction of the test apparatus and the uncertainties involved in the measurement procedure for the profile data points. A single sample analysis (14) for uncertainties will be applied to the procedure for the reduction of data.

The micromanometer reading accuracy for the dynamic head is estimated at $\pm$ 0.001 inches of water. The micromanometer accuracy for static pressure measurement is also $\pm$ 0.001 inches of water. The result of the mercury thermometer calibration in an ice bath was 32.7 $^{\circ}$F. The 0.7°F is assumed to hold over the entire range of the thermometer and is taken into account in obtaining the raw data for the calibration curves. The reading accuracy of the thermometer is $\pm$ 0.1°F.

The uncertainty of the calibration points may be ascertained with a single sample uncertainty analysis. The uncertainty interval for each result may be computed with the following expression,

$$b_F = \sqrt{\left(\frac{\partial F}{\partial d_1} b_1\right)^2 + \left(\frac{\partial F}{\partial d_2} b_2\right)^2 \cdots \left(\frac{\partial F}{\partial d_N} b_N\right)^2} \qquad (5.1)$$

where F is the function used to compute the result from the raw data, d_i is a measured variable and b_i is the uncertainty of the ith variable. Equation 4.1 rearranged

into the following form is used to compute the velocity,

$$V = \sqrt{\frac{2(P_o - P_s)g_o T_s R}{P_s}}$$

(5.2)

Equation 5.2 is substituted into equation 5.1 and the
resulting expression divided through by equation 5.2 to give
the following expression,

$$\frac{b_V}{V} = \left[\left(\frac{1}{2} \frac{b_{(P_o - P_s)}}{P_o - P_s}\right)^2 + \left(\frac{1}{2} \frac{b_{(P_s)}}{P_s}\right)^2 + \left(\frac{1}{2} \frac{b_{(T_s)}}{T_s}\right)^2\right]^{1/2}$$

(5.3)

Table 5.1 indicates the uncertainty interval for various
velocities.

The geometric position of the hot wire is accurate
to ± 0.050 inches in x and ±0.005 inches normal
to the plate. The hot-wire current is measured to an
accuracy of $\frac{1}{4}$-milliampere by balancing the galvanometer.
Table 5.2 indicates the percentage inaccuracy as a
function of velocity as read from the calibration curve
for a hot-wire resistance ratio of 1.6. The raw cali-
bration data of the hot-wire is applied directly to
the calibration curve.

Since the oscillating drive is a moving mechanical
device, play was present when the linkage was first assembled
due to inaccuracies in the manufacture of the parts.
After completion of all the tests for this investigation,
wear of the moving parts had increased the play. A
fair estimate of the inaccuracy in the oscillating

amplitude is $\pm$ 0.005 inches which is 10% of the 0.050

inches amplitude of oscillation used in this investigation.

Angular play of the eccentric gear in the gear box never

exceeded 5° with respect to the motor pinion when the

gear box was used for the lower frequencies. The

oscillating frequency always remained within $\pm$ 3%

of the desired frequency.

Extraneous vibrations are produced in the whole test

plate from the tunnel test section wall to which the

test plate is attached. Tunnel wall vibration originates

from two sources. A slight rotating unbalance in the

wind tunnel fan produces vibrations along the entire wind

tunnel. This effect is minimized by conducting all

experimental tests at wind tunnel velocities which

minimize the effect. When the oscillating drive

mechanism is operating the reaction force of the

reciprocating masses is transmitted to the tunnel test

section wall and thence to the plate. The amplitude of the

vibrations produced in the whole plate by the above effects

always remained less than 5% of the amplitude of the oscil-

lating membrane.

The uncertainty of the profile curve results may be

ascertained with a single sample uncertainty analysis. The

position of the probe is calculated in terms of the Blasius(2)

non-dimensional similarity parameter,

$$\eta = y \sqrt{\frac{U_\infty}{\nu x}}$$

$$(5.4)$$

The expression for η may be substituted into equation 5.1 and the resulting expression divided by η to obtain

$$\frac{b_\eta}{\eta} = \sqrt{\frac{b_y^2}{y^2} + \frac{1}{4}\frac{b_{u_\infty}^2}{u_\infty^2} + \frac{1}{4}\frac{b_x^2}{x^2}} \qquad (5.5)$$

Table 5.3 indicates the uncertainty interval for a typical η at a velocity of 20 feet per second and x = 8 inches.

The uncertainty interval in the non-dimensional velocity $u' = u/u_\infty$ may be determined, also by substituting into equation 5.1 and dividing through by u' to obtain,

$$\frac{b_{u'}}{u'} = \sqrt{\frac{b_u^2}{u^2} + \frac{b_{u_\infty}^2}{u_\infty^2}} \qquad (5.6)$$

Table 5.4 indicates the uncertainty for typical dimensionless velocities.

Table 5.1

Calibration Velocity Uncertainty

V	10 ft/sec	20 ft/sec	30 ft/sec	40 ft/sec
b_V	$\pm.283$	$\pm.148$	$\pm.102$	$\pm.078$

Table 5.2

Hot Wire Calibration Uncertainty

V	10 ft/sec	20 ft/sec	30 ft/sec	40 ft/sec
$\frac{\Delta V}{\%}$	±2.5	±2.5	±1.65	±1.25

Table 5.3

Uncertainty for u_∞ = 20 ft/sec
and $\varkappa$ = 8 inches

η	1.037	2.075	3.111	4.150	5.187
b_η	$\pm.178$	$\pm.192$	$\pm.213$	$\pm.240$	$\pm.270$

Table 5.4

Dimensionless Velocity Uncertainty

u'	1.00	.75	.50	.25
$b_{u'}$	$\pm.0354$	$\pm.0313$	$\pm.0280$	$\pm.0258$

CHAPTER VI

Results of Measurements

The results of this investigation may be divided
into six categories.

A. Static pressure on the plate as a
function of x.

B. Comparison of the non-oscillating laminar
flow profiles with the Blasius (2) solution.

C. Tests for locations of interest in
oscillating flow.

D. Comparison of non-oscillating and oscillating
profiles at the same velocities and geometric locations.

E. Comparison of oscillating profiles as a
function of x at constant frequency and flow velocity.

F. Comparison of oscillating profiles as a
function of frequency with x and flow velocity constant.

The first and second categories concern the fidelity
with which the physical system approximates the theoretical
model. The final four categories concern the effect pro-
duced by the oscillating disturbance. All results found in
this study are for free stream velocities of 20 or 40
feet per second.

6.1 Static pressure on the plate as a function of x.

The static pressure data from the static taps of the
flat plate constructed for the pressure gradient check are
reduced with equation 4.3, divided by the free stream velocity.

46

The percentage change is plotted as a function of distance along the plate surface from the leading edge. The resulting velocity gradient is assumed to occur midway between the pressure taps. Figure 6.1 is the plot for tunnel velocities of 20 feet per second and 40 feet per second. It may be noted that the maximum velocity gradient is slightly larger than 1% at 40 feet per second and always less than 1% at 20 feet per second. Thus, the assumption of a zero free stream velocity gradient is valid.

6.2 Comparison of the non-oscillating laminar flow profiles with the Blasius(2) solution.

A better check of the actual laminar flow velocity profiles along the plate as compared with the theory by Blasius(2) is afforded in Figures 6.2 through 6.10. The solid curve is the Blasius solution. The figures indicate that the measured profiles at the values of x as shown closely approximate the theory for both the 20 and 40 feet per second free stream velocities. Therefore, the physical system constructed quite closely approximates the theory for laminar boundary layer flow with no artificially induced disturbances in the boundary layer and for zero pressure gradient. Of course, random instantaneous disturbances are always present in the free stream and boundary layer as observed on the oscilloscope.
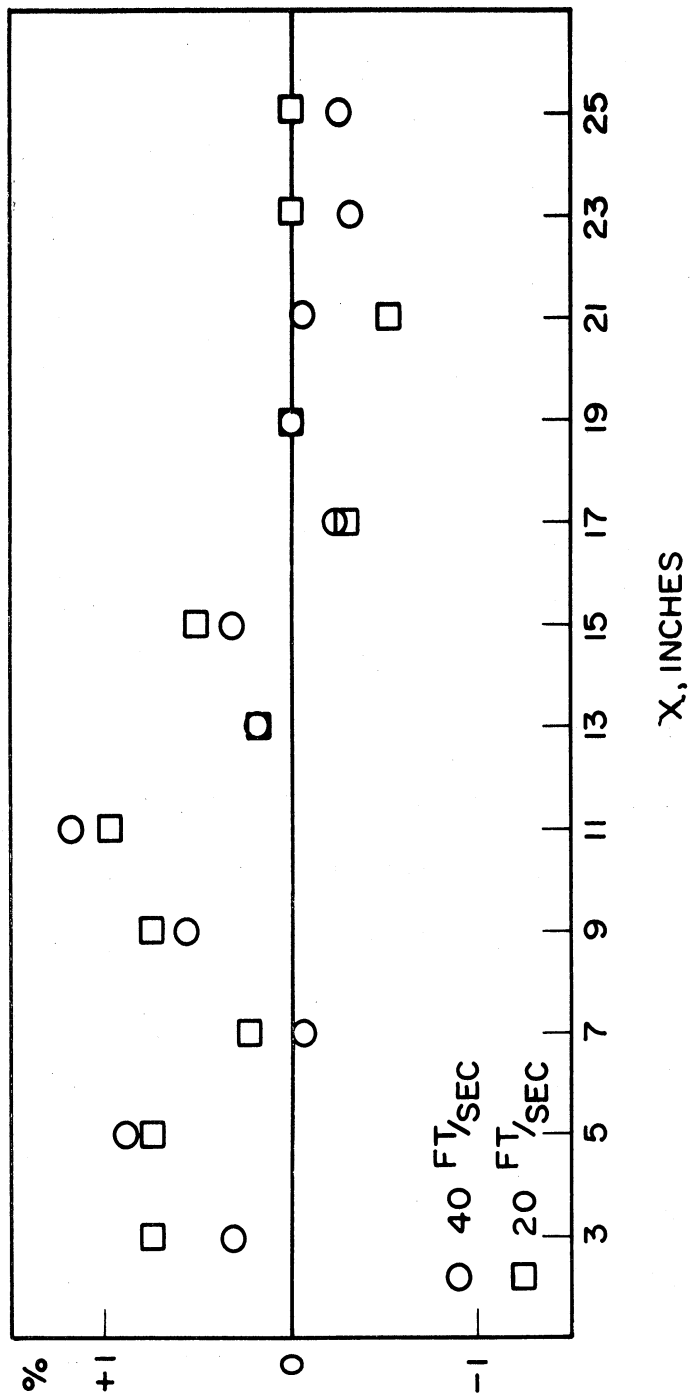
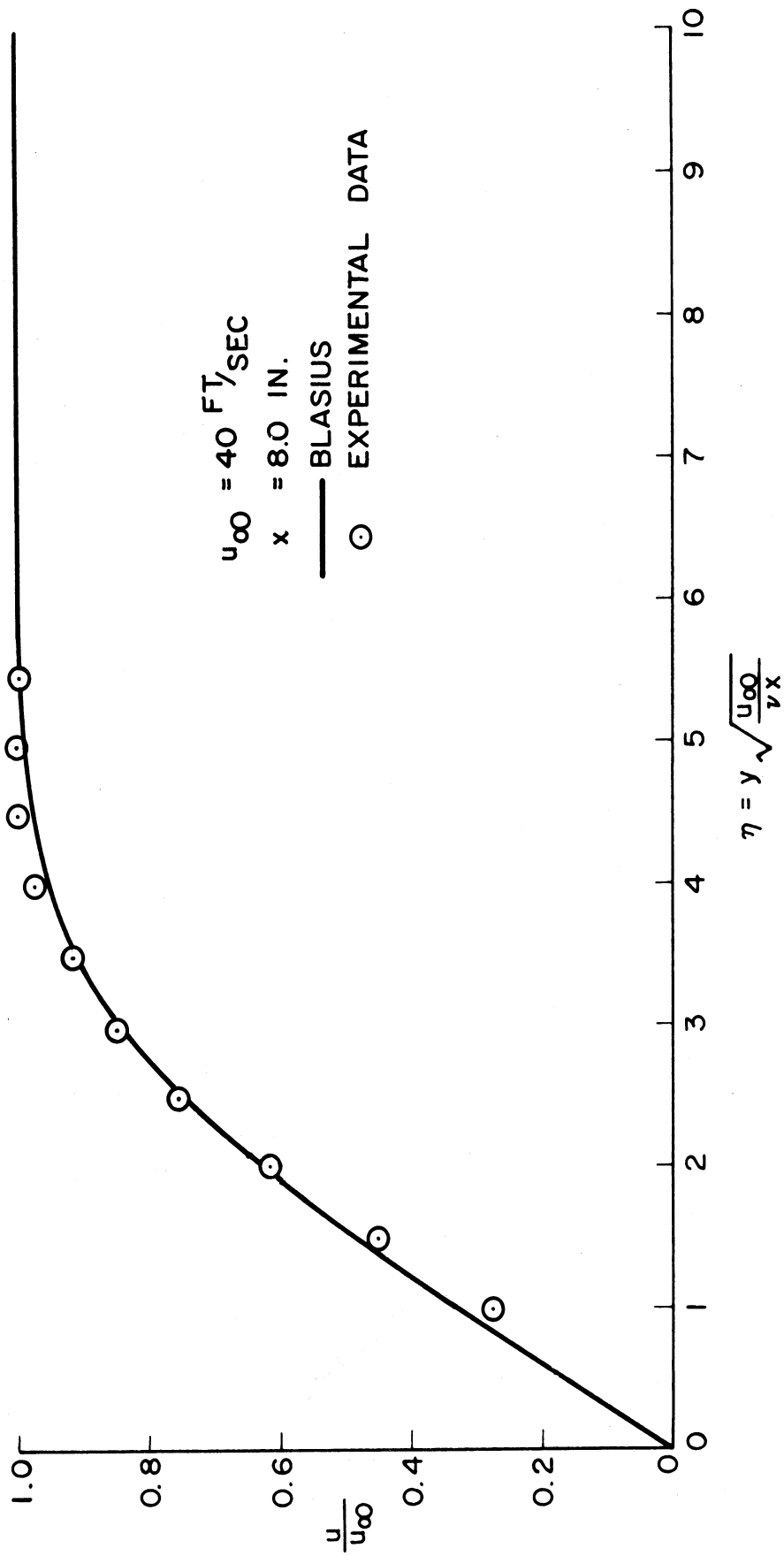Figure 6.1 Percentage change in free stream velocity as a function of x.

Figure 6.2 Steady experimental profile compared to
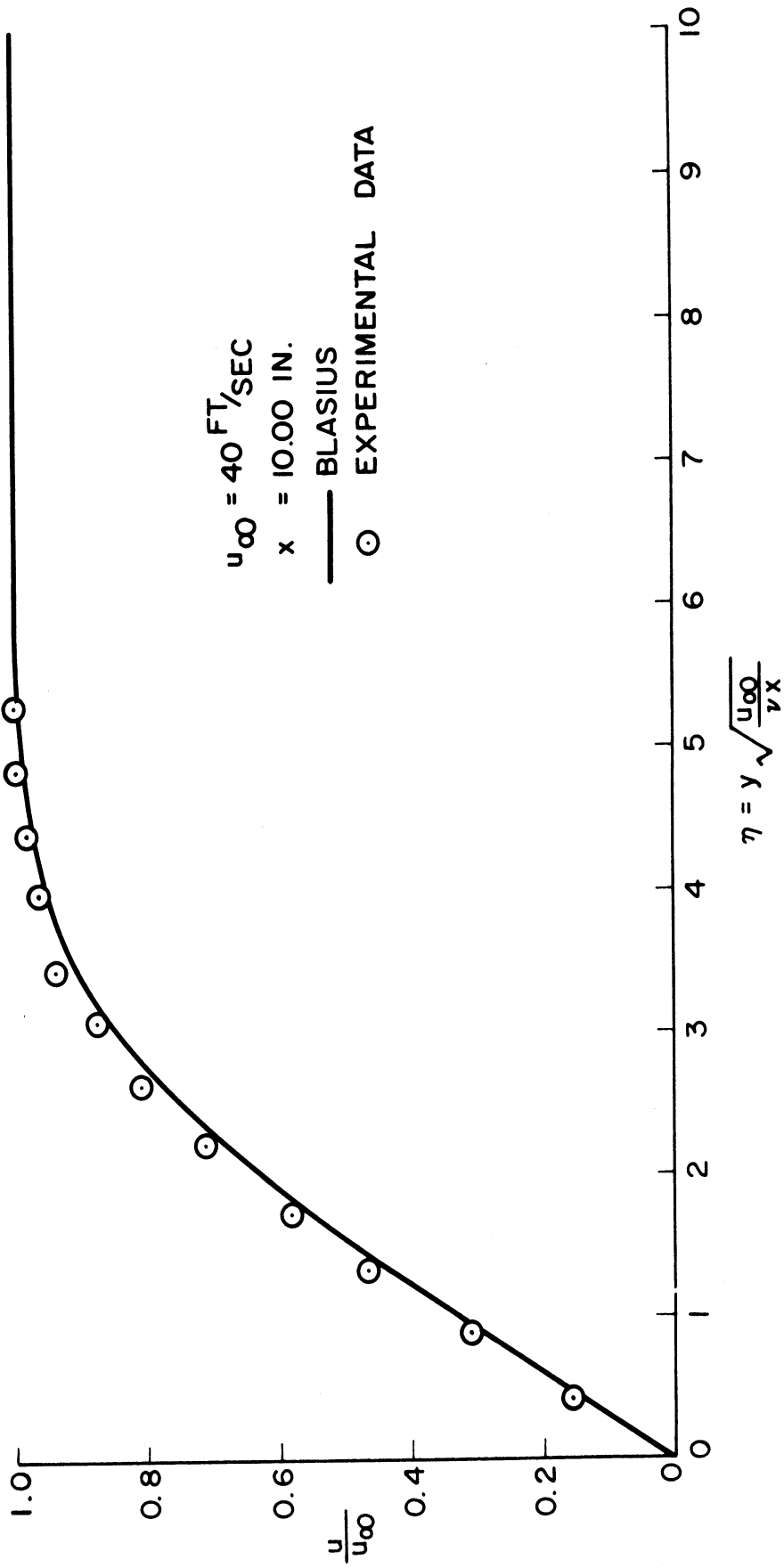Blasius ($x = 8$, $u_\infty = 40$)

Figure 6.3 Steady experimental profile compared to Blasius (x = 10, u_∞ = 40)
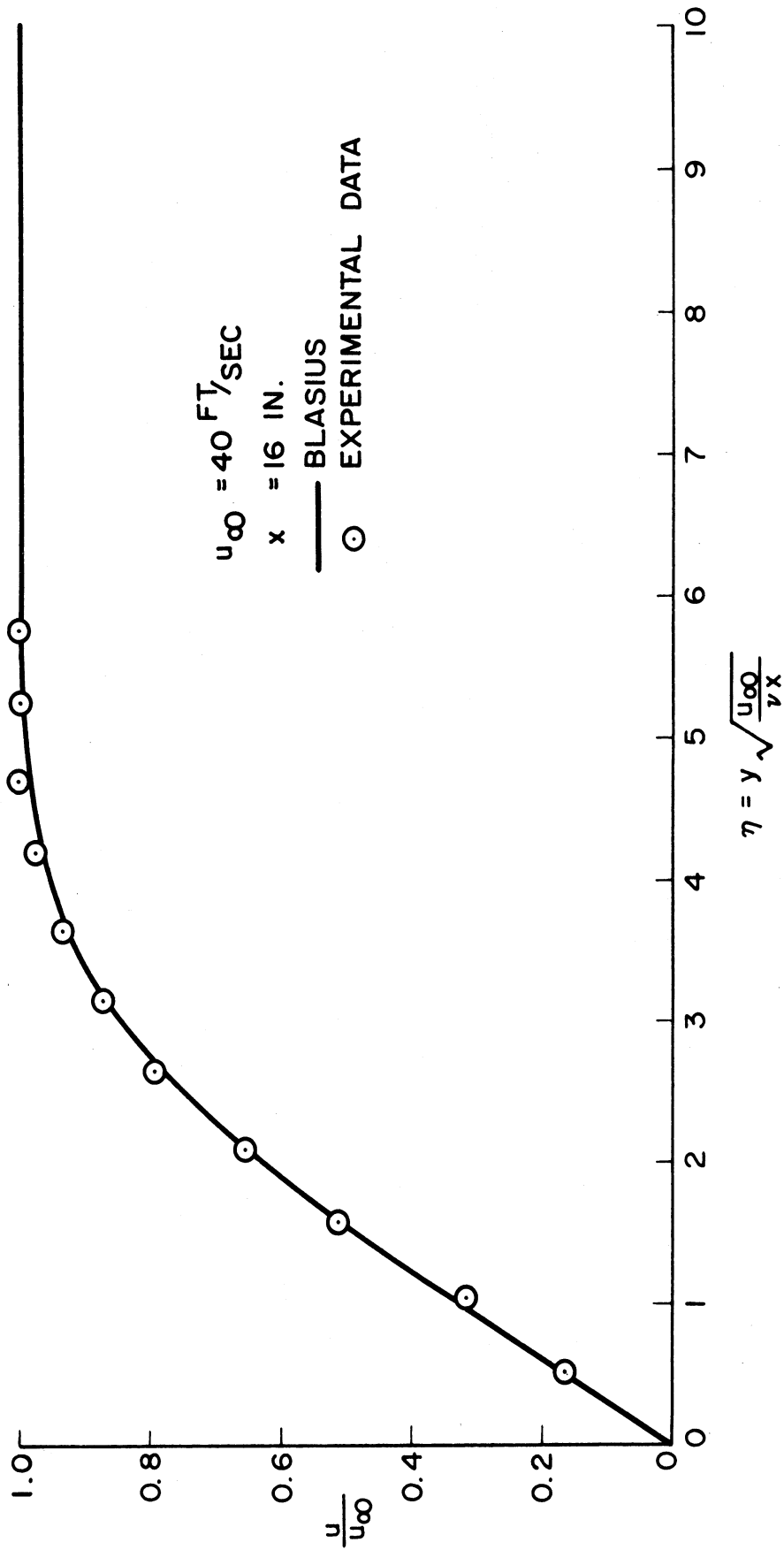
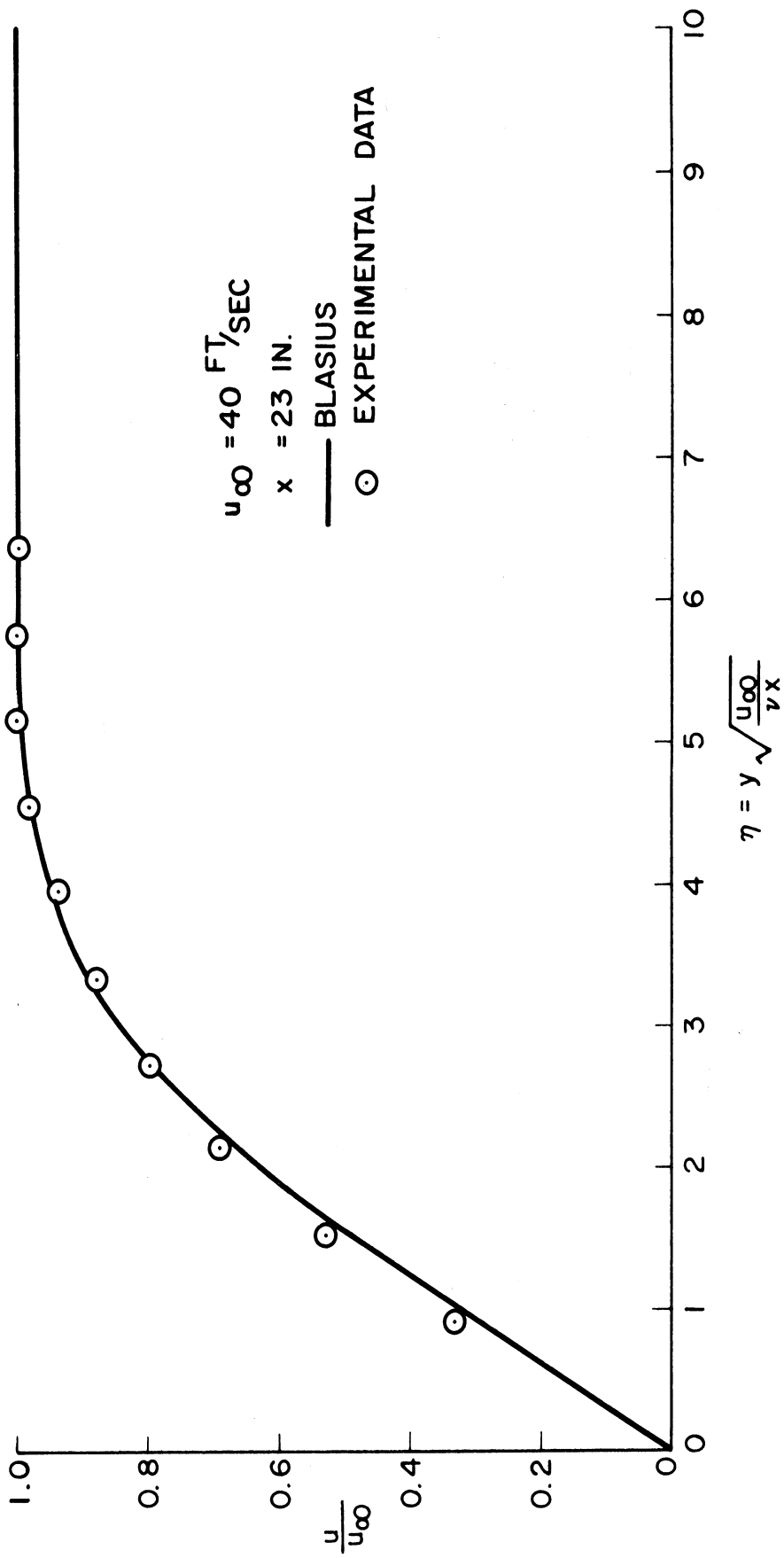Figure 6.4 Steady experimental profile compared to Blasius (x = 16, u_∞ = 40)

Figure 6.5 Steady experimental profile compared to Blasius ($x = 23$, $u_\infty = 40$)
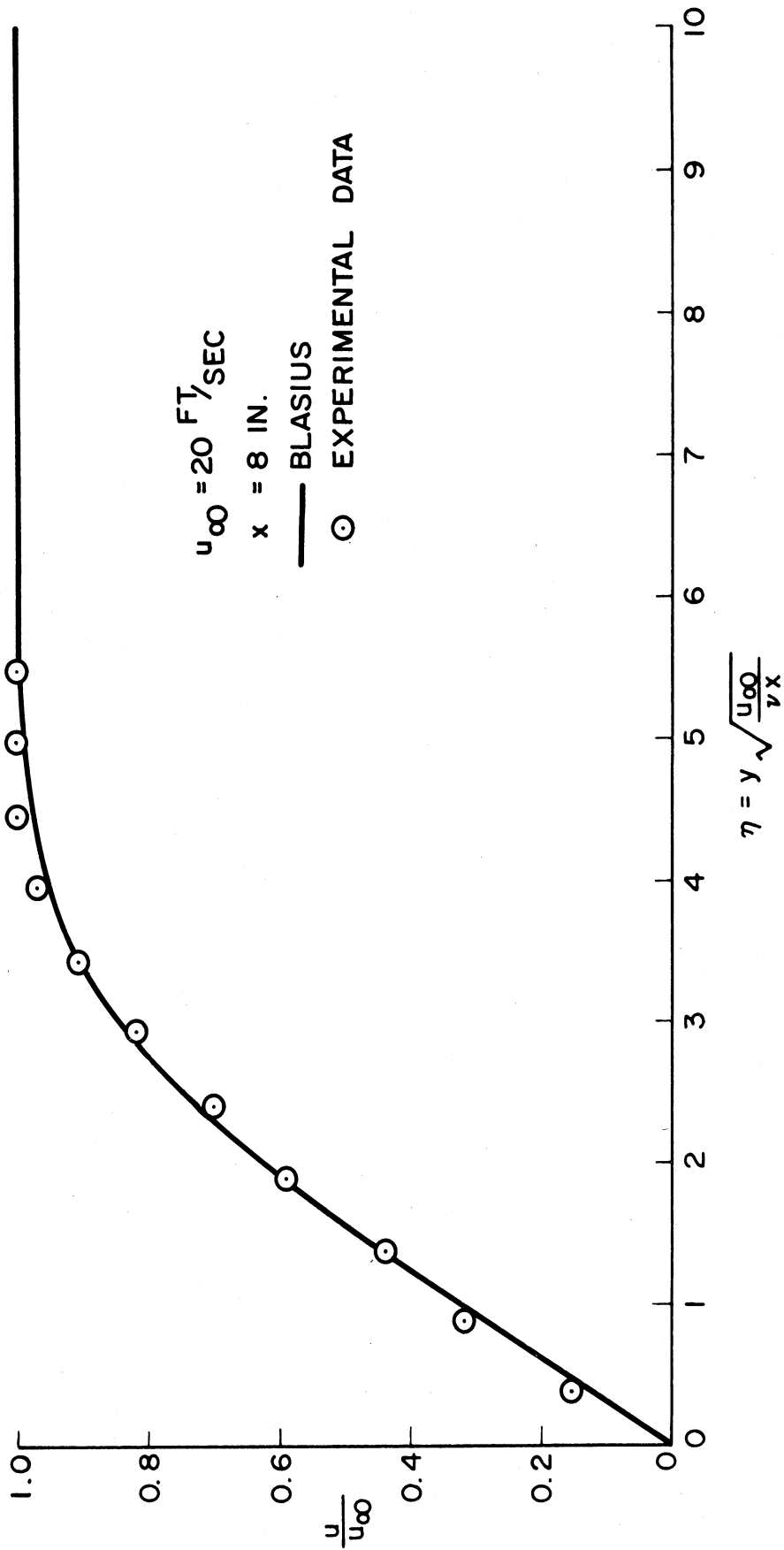
Figure 6.6 Steady experimental profile compared to
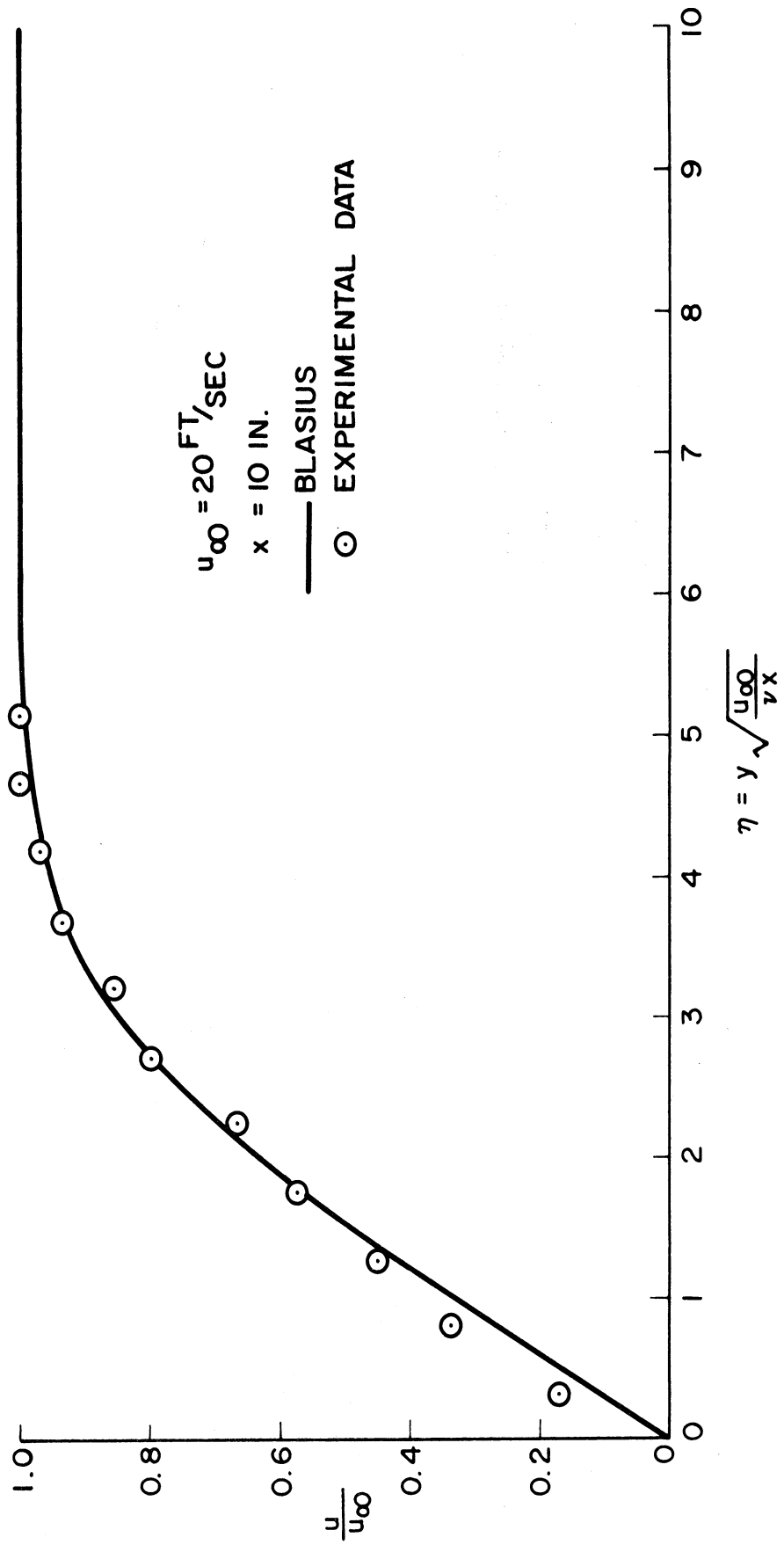Blasius (x = 8, u_∞ =20)

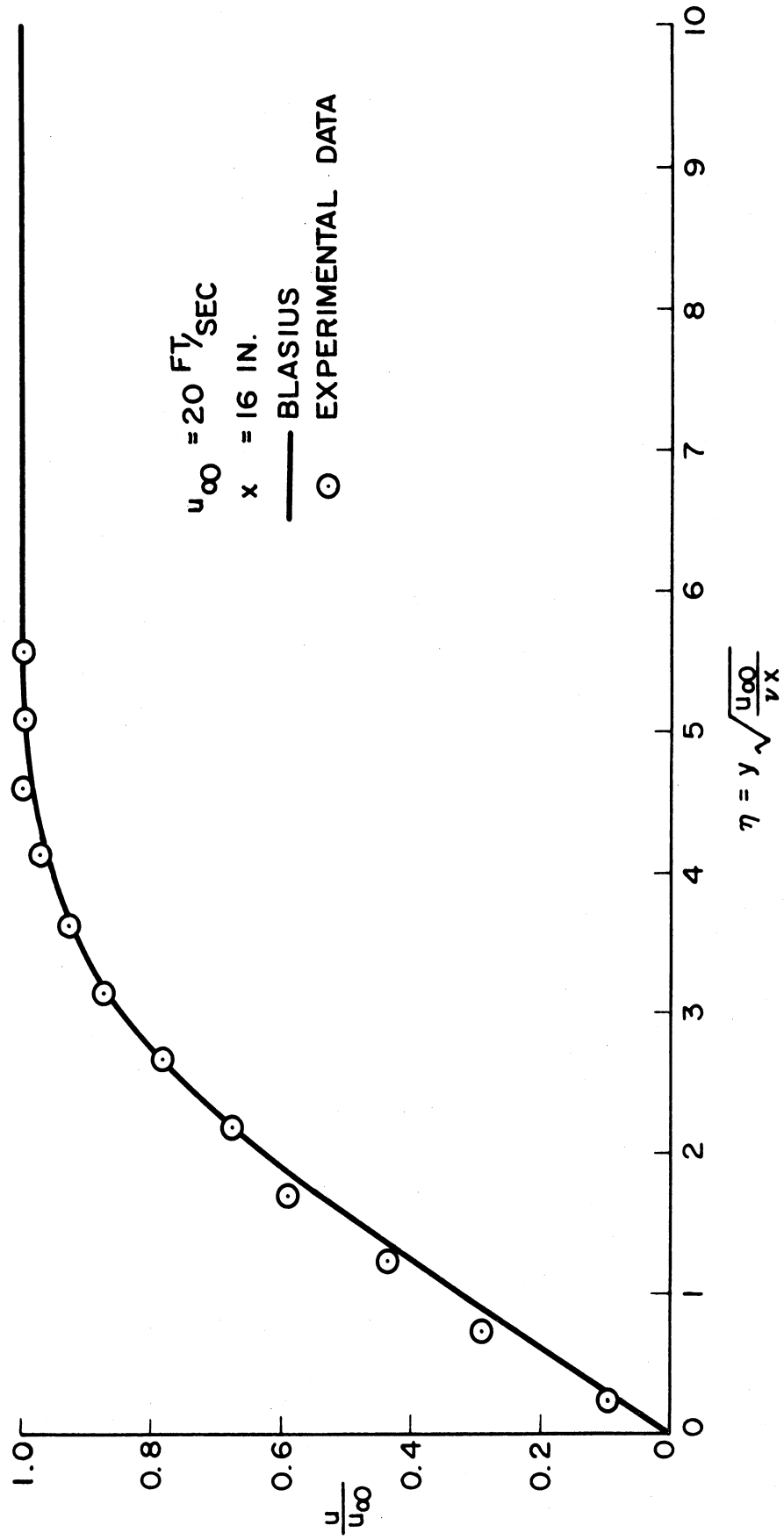Figure 6.7 Steady experimental profile compared to
Blasius (x = 10, u_∞ =20)

Figure 6.8 Steady experimental profile compared to
Blasius (x = 16, u_∞ =20)

$u_\infty = 20 \ ^{FT}/_{SEC}$

$x = 23$ IN.

—— BLASIUS

⊙ EXPERIMENTAL DATA

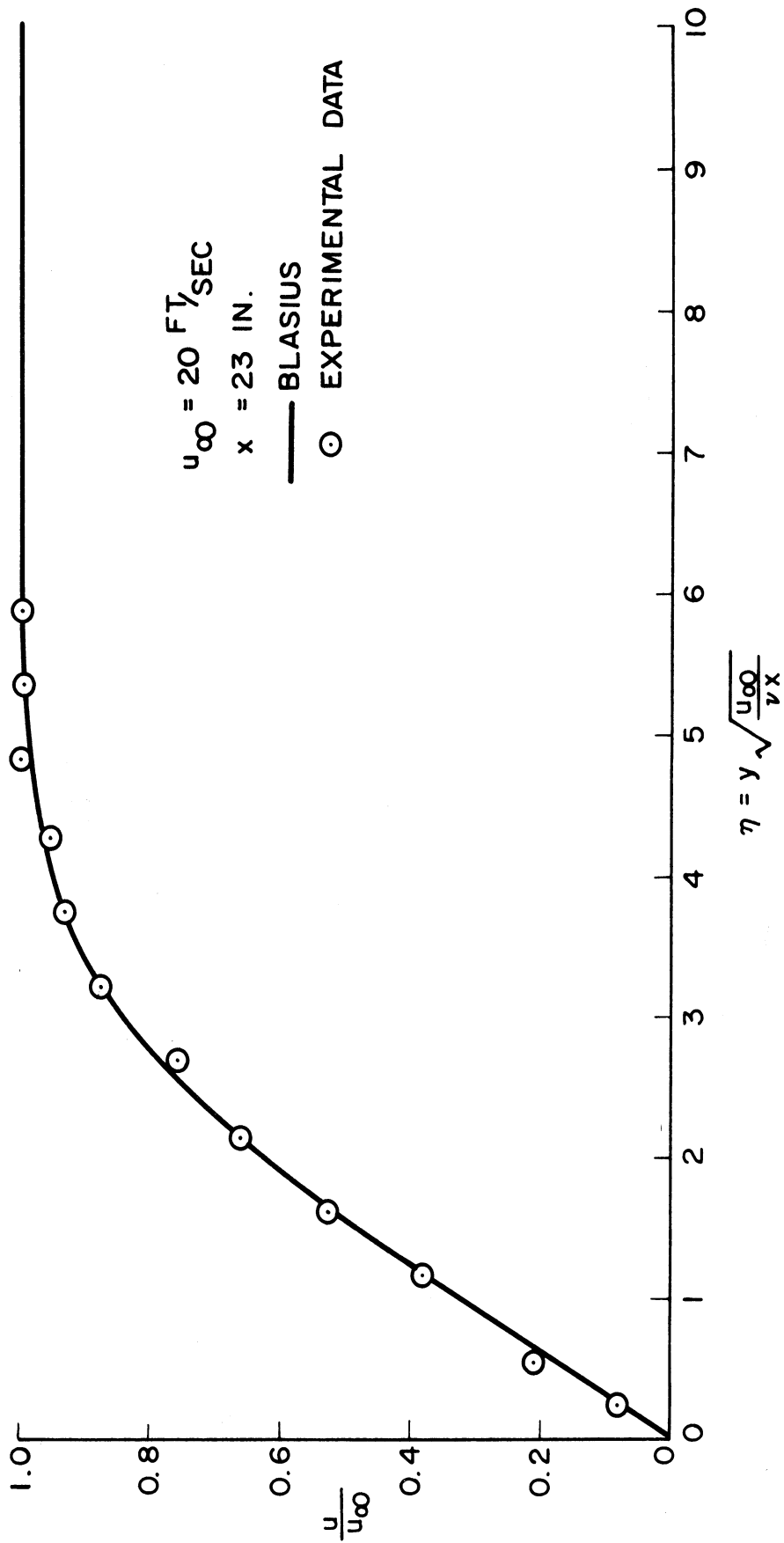$\eta = y \sqrt{\dfrac{u_\infty}{\nu x}}$

Figure 6.9   Steady experimental profile compared to Blasius ($x = 23$, $u_\infty = 20$)
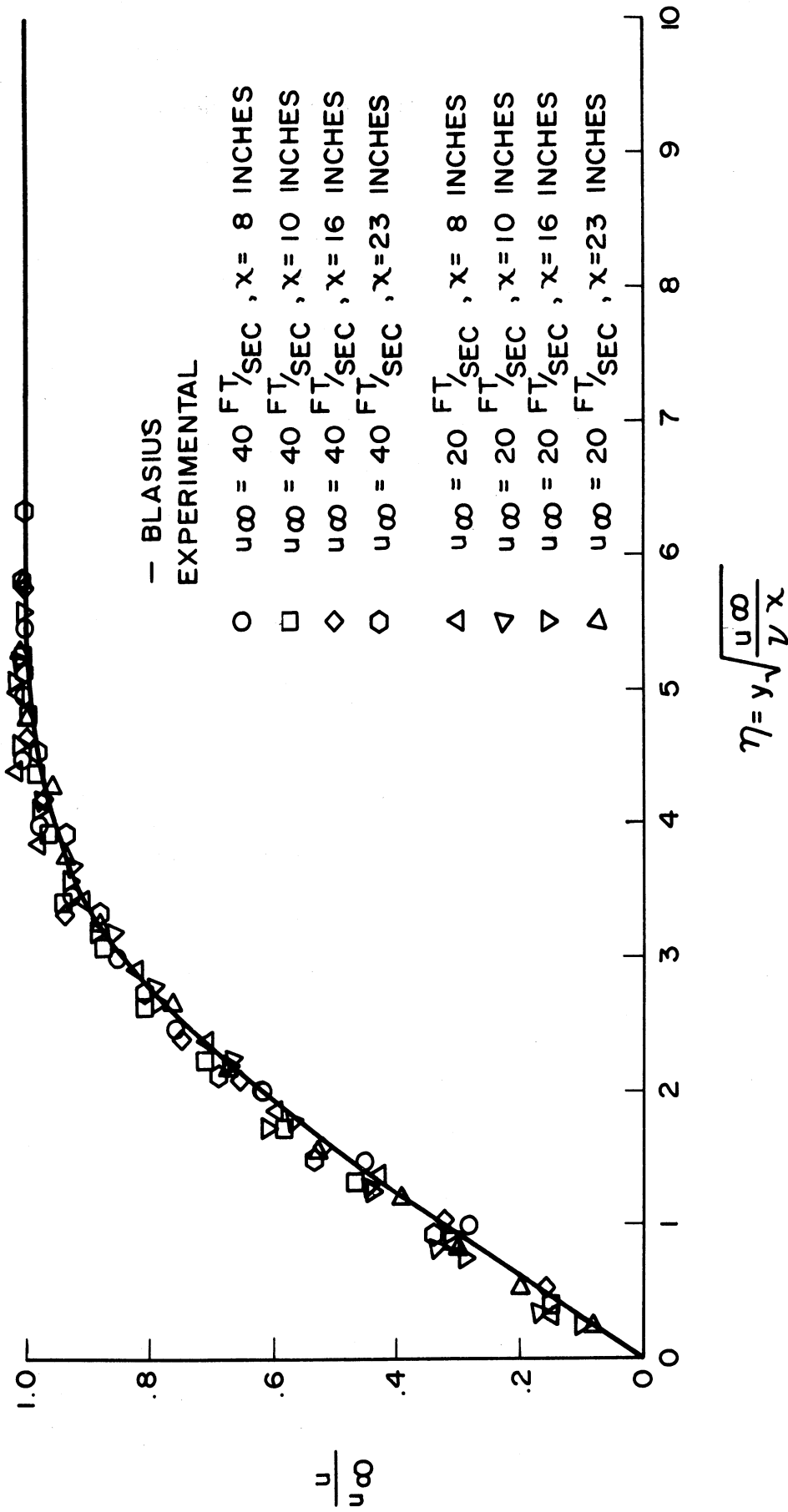
Figure 6.10 Composite of steady experimental profiles

6.3 Tests for locations of interest in oscillating flow.

All oscillating data was obtained with a membrane amplitude of $\pm$ 0.050 inches. The membrane centerline is 9-inches from the leading edge. For a free stream velocity of 20 feet per second the theoretical laminar boundary layer thickness is 0.149 inches. Therefore, the oscillating amplitude is 33% of the boundary layer thickness. For a free stream velocity of 40 feet per second the boundary layer thickness is 0.105 inches and therefore the oscillating amplitude is 48%. Hence, the disturbance is a finite disturbance in amplitude.

Figures 6.11 and 6.12 indicate the results of the measurements made to determine the locations of interest on the plate. The measurements were made at 2-inch intervals of x except immediately downstream of the oscillating membrane where the measurements were made one inch apart. The last position was at 19.5 inches because of mechanical difficulties underneath the plate. The location of the probe from the surface of the plate always corresponded to a value of η of 2.1. The data are plotted as the change in mean velocity due to the oscillating disturbance as a percentage of the free stream velocity versus plate location x. The positive percentages indicate an increase in velocity. The lines at $\pm$ 2.5% indicate the accuracy band of the hot wire anemometer. The centerline of the oscillating membrane is the location 9-inches from the leading edge, as shown.
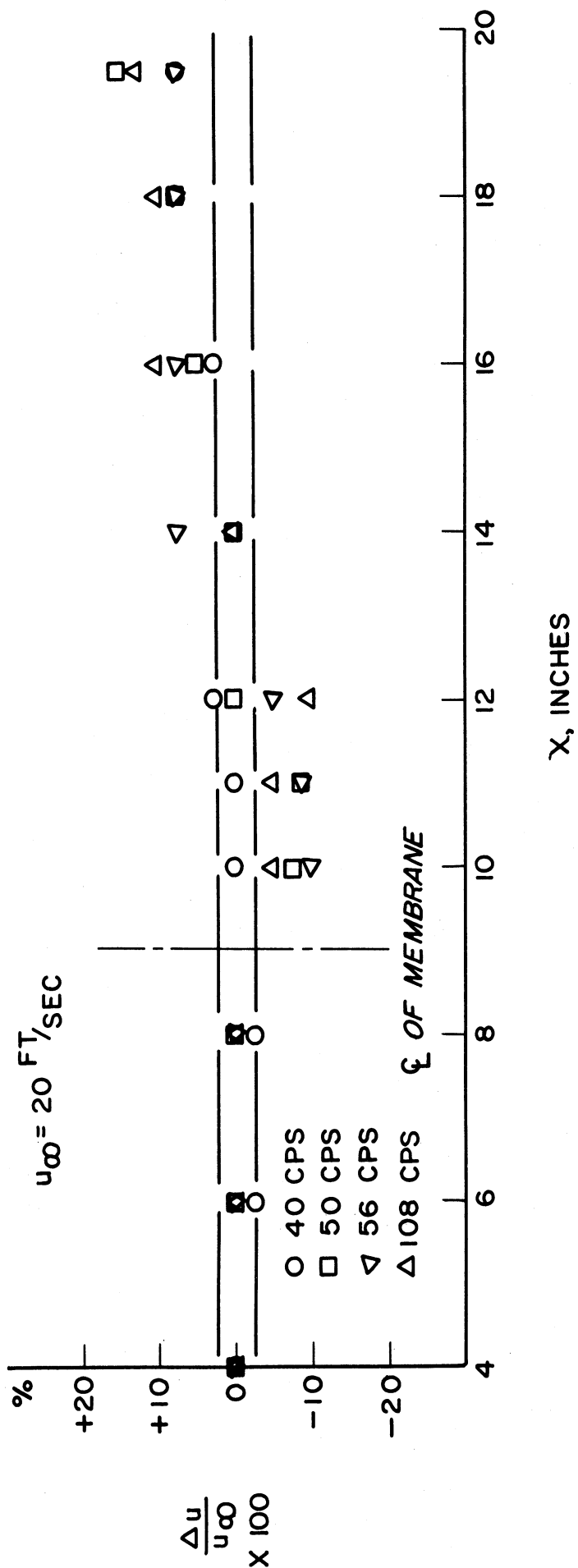
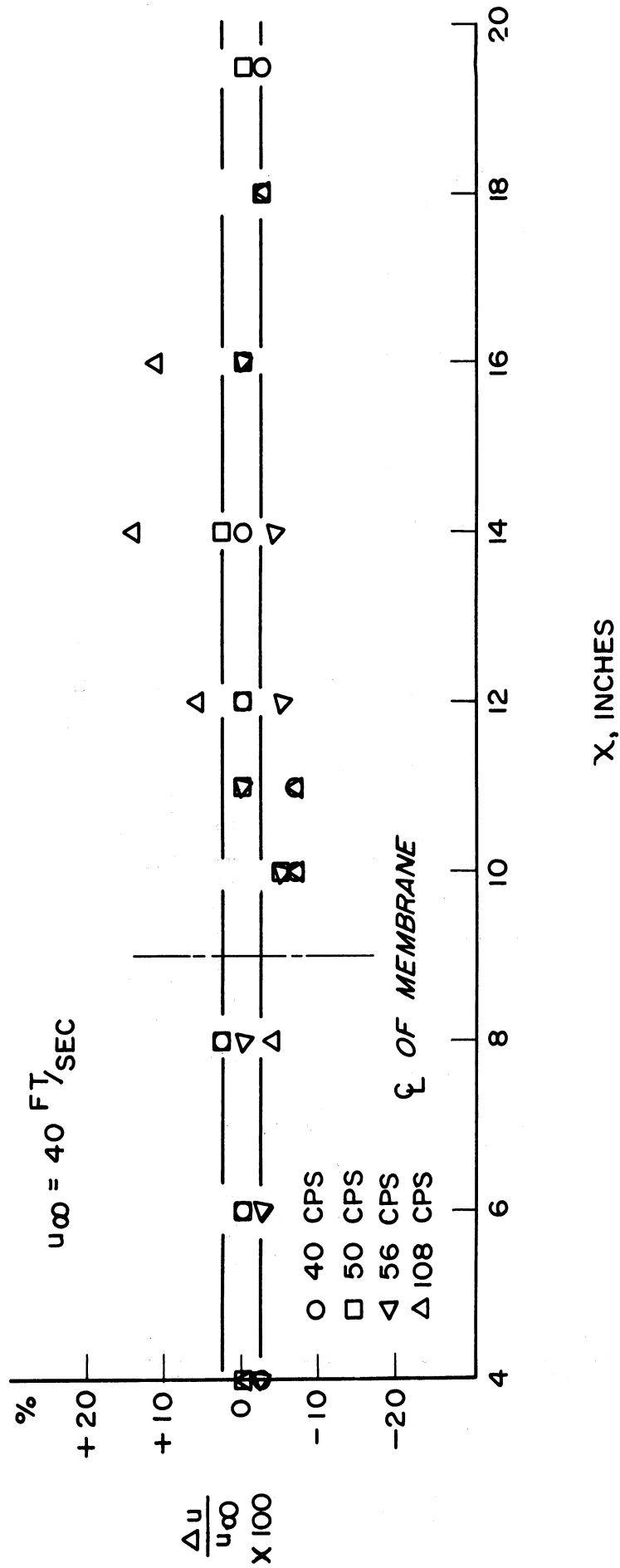Figure 6.11 Mean velocity change at $\eta = 2.1$ due to oscillation ($u_\infty = 20$)

Figure 6.12 Mean velocity change at $\eta = 2.1$
due to oscillation ($u_\infty = 40$)

Figure 6.11 for 20 feet per second indicates that
there is no significant effect upstream of the membrane
for any of the frequencies checked. Immediately downstream
for frequencies of 50 cps and above a definite decrease in
the velocity is to be noted. At 14-inches and beyond
there is a definite increase in the velocity. The instant-
aneous hot-wire signal on the oscilloscope indicated turbu-
lence spots at locations 16-inches and downstream.

Figure 6.12 for 40 feet per second also indicates no
significant effect upstream of the membrane except for one
point at 108 cps and 8-inches. Downstream of the membrane the
effect at the lower frequencies is less discernable.
At 108 cps, however, a definite decrease occurs immediately
downstream with an increase at 12-inches and thereafter.
Turbulent spots were noted on the oscilloscope from
locations 14-inches downstream at a frequency of 108 cps.

In reference to the Tollmien-Schlichting stability
theory (64) the disturbances of this investigation lie
entirely within the damping region to the left and below
the neutral curve. The neutral curve applies to disturbances
of vanishingly small amplitude whereas this investigation
concerns large amplitude disturbances.

6.4 Comparison of non-oscillating with oscillating profiles
at the same velocities and geometric locations.

Figures 6.13 through 6.49 compare the mean value
profile for oscillating flow with the profile for non-
oscillating flow. Figures 6.13 through 6.17 are for a

free stream velocity of 40 feet per second and an oscillating
frequency of 15 cps. There is no significant difference in
the profiles except those at x = 9.63 and x = 10-inches
which exhibit a consistent decrease in velocity.

Figures 6.18 through 6.21 are at 40 feet per second and
50 cps. There is no significant change at x = 8-inches.
However, at x = 10-inches there is a consistent decrease
in velocity. At x = 16-inches there is an increase in
velocity near the wall and a decrease in velocity near the
edge of the boundary layer. This oscillating profile
exhibits an increase in the boundary layer thickness.
However, no turbulent spots were noted on the oscillo-
scopes. The profile at x = 23-inches is a definite
transition profile with turbulent spots observed on the
oscilloscope.

Figures 6.22 through 6.26 are at 40 feet per second
and 75 cps. Again no significant change is noted at
x = 8 inches. However, at x = 9.63-inches a consistent
decrease in velocity is noted and at x = 10-inches a large
decrease in velocity is apparent in combination with a
thickening of the boundary layer. No turbulent spots were
noted on the oscilloscope at this location. However, at
x = 16-inches the flow has gone into transition with
attendent turbulent spots. The flow is further into
transition at x = 23-inches.

Figures 6.27 through 6.31 are at 40 feet per second and 100 cps. No significant change is noted at x = 8-inches. At x = 10-inches a consistent decrease in velocity can be noted and at x = 12-inches, the velocity increases near the wall and then decreases as the edge of the boundary layer is approached. No turbulent spots were observed on the oscilloscope at this location. However, at x = 16-inches the velocity increases over a larger portion of the boundary layer and the boundary layer is thicker. A few beginning turbulent spots were noted on the oscilloscope. At x = 23-inches transition flow has again occurred.

No boundary layer separation was noted at either x = 9.63-inches or x = 10-inches. x = 9.63-inches is the downstream edge of the oscillating membrane.

Figures 6.32 through 6.36 are for a velocity of 20 feet per second and a frequency of 15 cps. There is no significant change in the profiles except at x = 23-inches where the oscillating profile is consistently decreased.

Figures 6.37 through 6.40 are for 20 feet per second and 50 cps. There is no significant change in the profiles at x = 8 or x = 10-inches. At x = 16-inches the velocity increases near the wall and near the edge of the boundary layer but does not increase in the central portion of the boundary layer. Apparently this profile occurs just upstream of the location where the velocity profile is fully increased. No turbulent spots were present on the oscilloscope. At x = 23-inches a transition profile occurs with turbulent spots appearing on the oscilloscope.
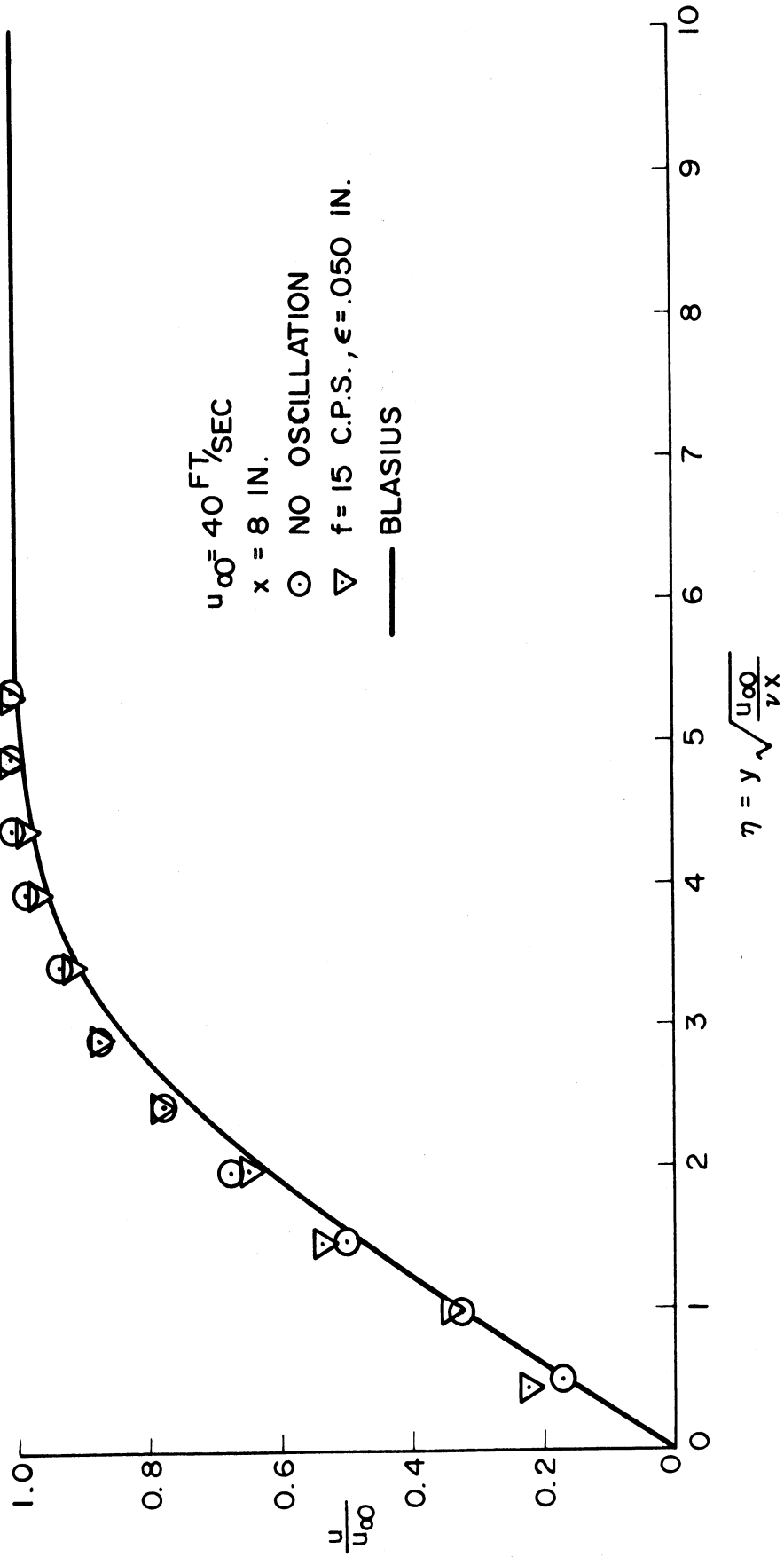
Figure 6.13 Comparison of velocity profiles with and without oscillation ($u_\infty = 40$, $x=8$, $f=15$)

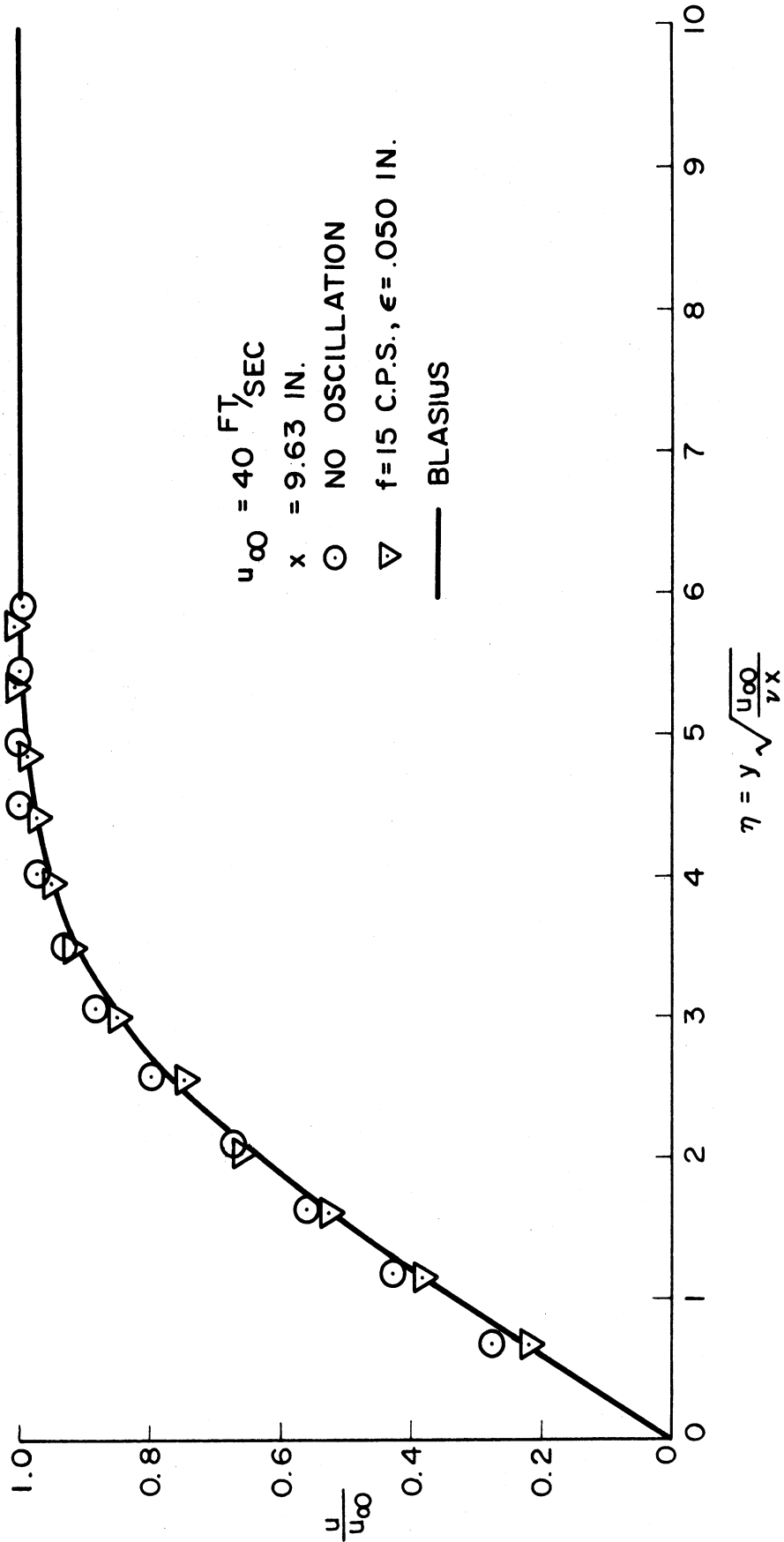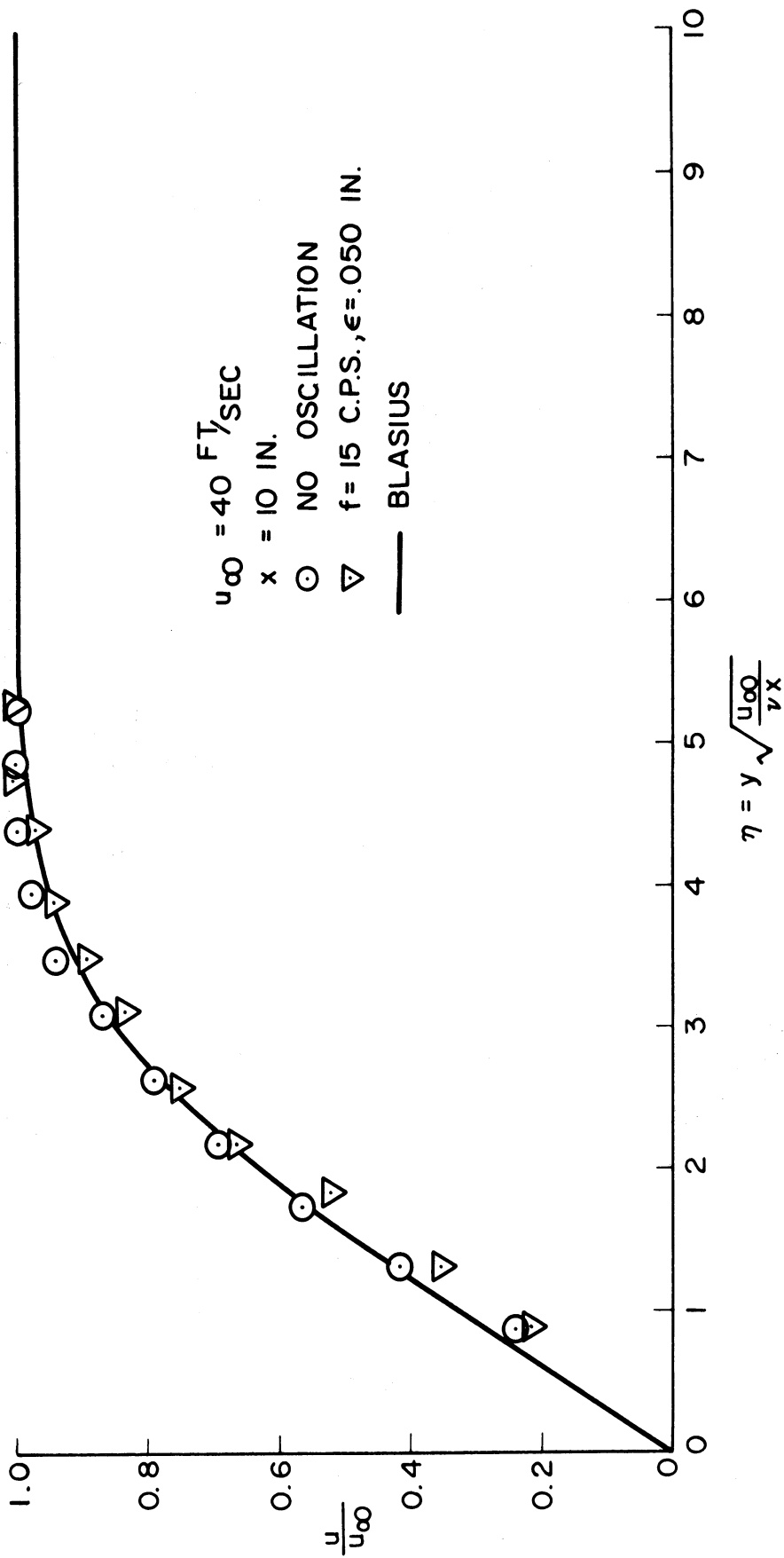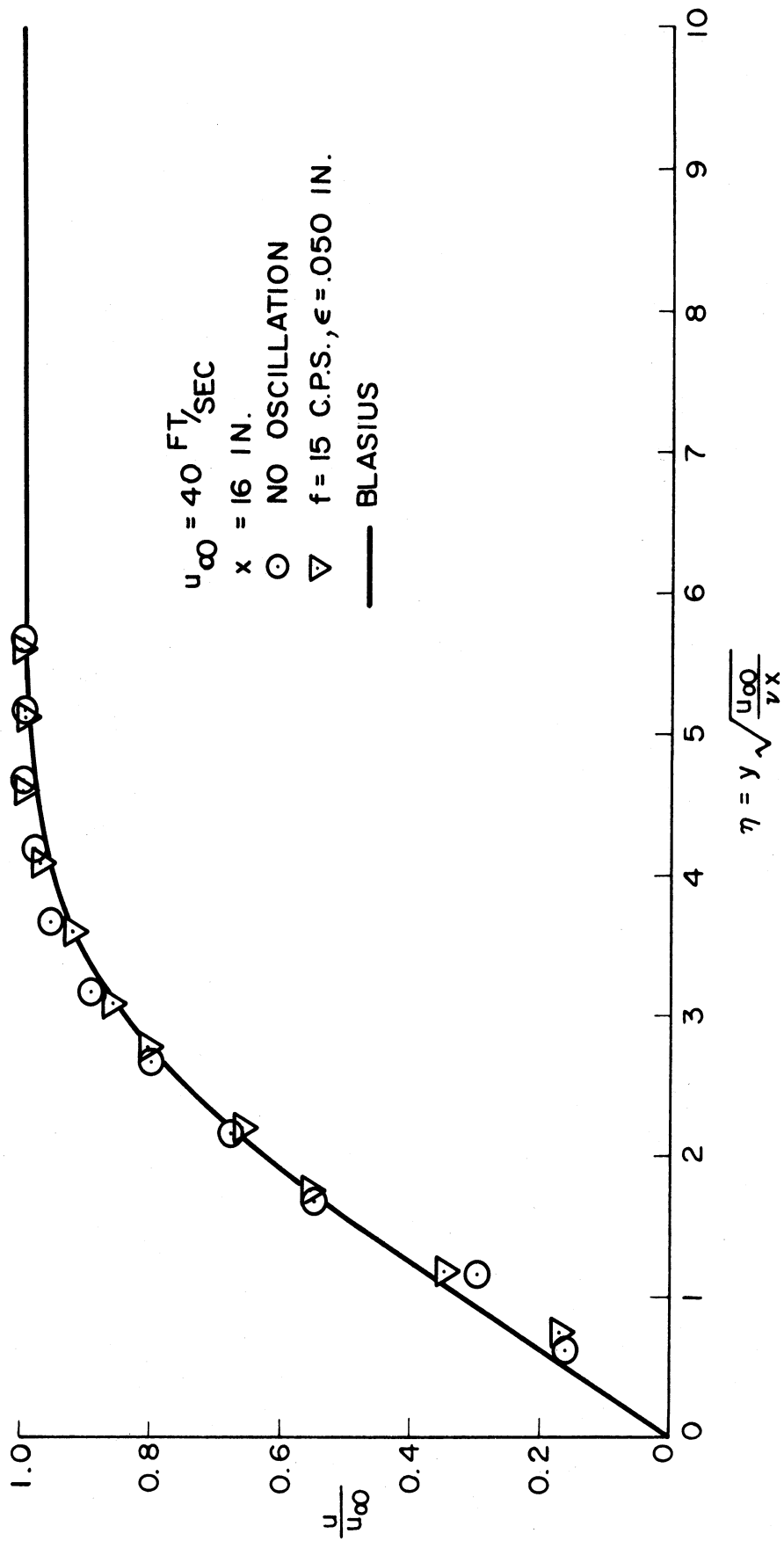Figure 6.14 Comparison of velocity profiles with and without oscillation (u_∞ =40, x=9.63, f=15)

$u_\infty = 40 \; {}^{FT}\!/_{SEC}$

$x = 10$ IN.

⊙   NO OSCILLATION

▽ $f = 15$ C.P.S., $\epsilon = .050$ IN.

——   BLASIUS

$\eta = y \sqrt{\dfrac{u_\infty}{\nu x}}$

$\dfrac{u}{u_\infty}$

Figure 6.15   Comparison of velocity profiles with and without oscillation ($u_\infty = 40$, $x = 10$, $f = 15$)

$u_\infty = 40 \, {}^{FT}\!/_{SEC}$

$x = 16$ IN.

⊙ NO OSCILLATION

▷ $f = 15$ C.P.S., $\epsilon = .050$ IN.

──── BLASIUS

$\eta = y \sqrt{\dfrac{u_\infty}{\nu x}}$

$\dfrac{u}{u_\infty}$

Figure 6.16 Comparison of velocity profiles with and without oscillation ($u_\infty = 40, x = 16, \, f = 15$)

$u_\infty = 40 \ ^{FT}/_{SEC}$

$x = 23$ IN.

⊙ NO OSCILLATION

▷ $f = 15$ C.P.S., $\epsilon = .050$ IN.

——— BLASIUS

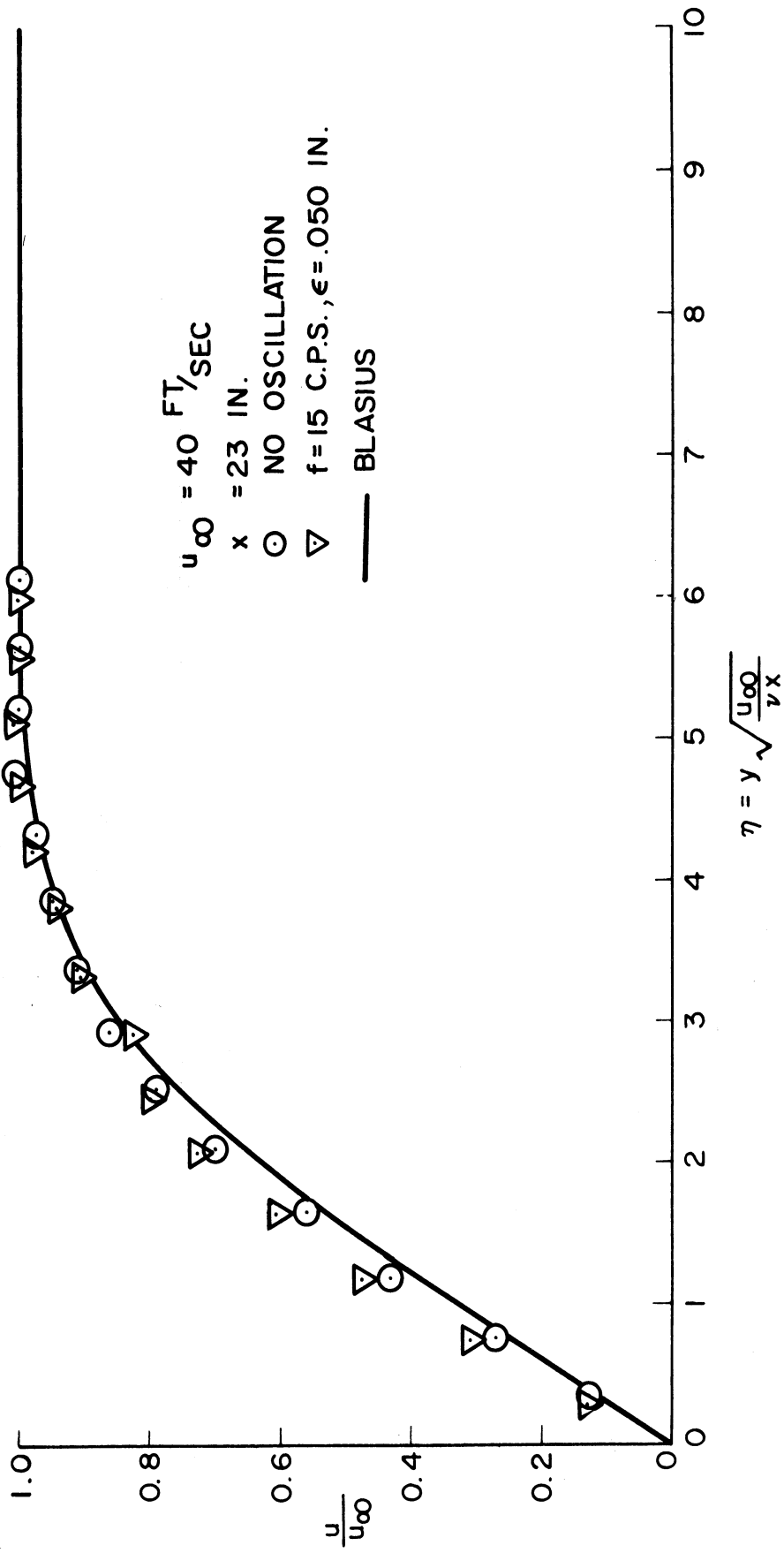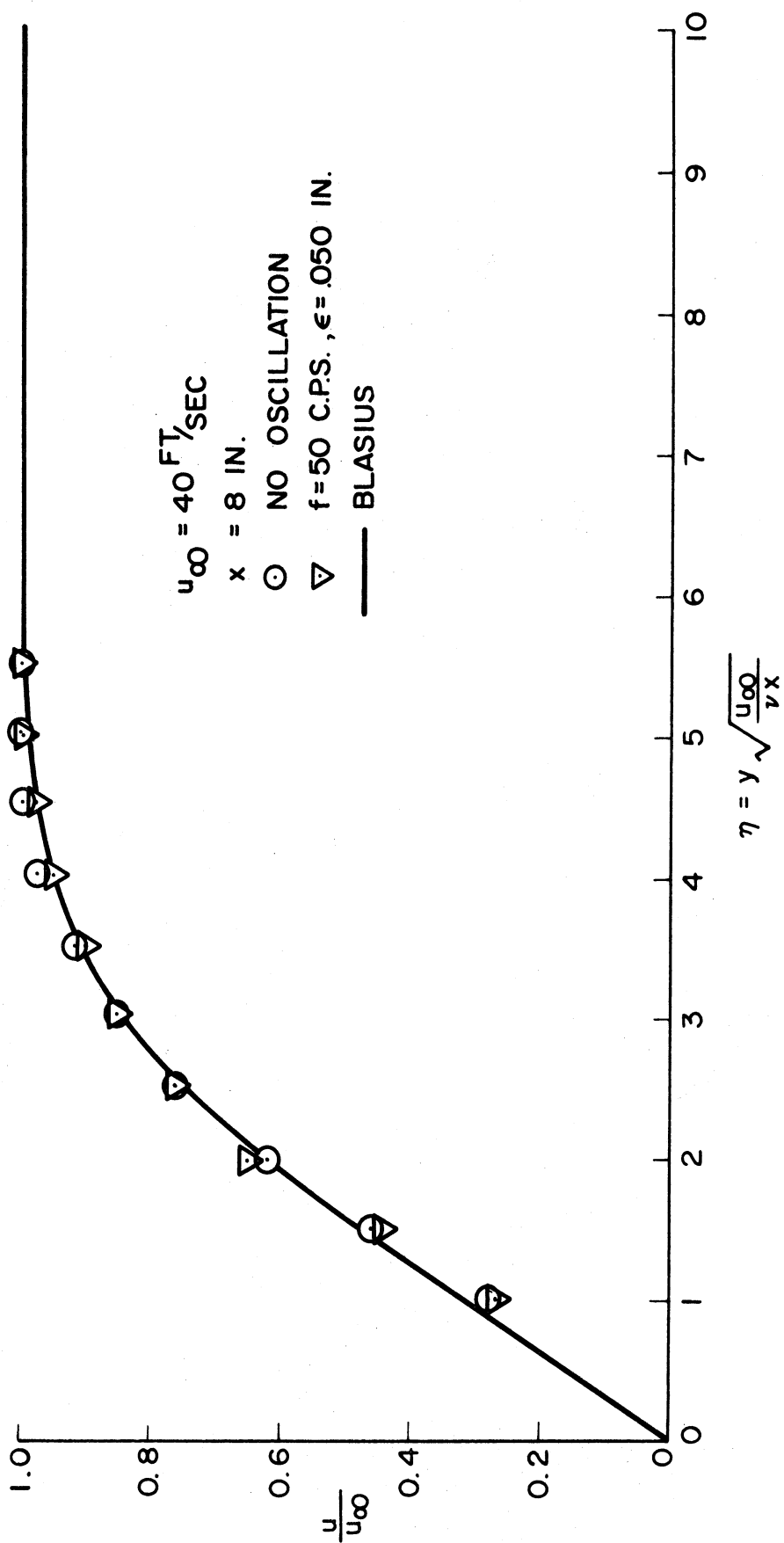$\eta = y \sqrt{\dfrac{u_\infty}{\nu x}}$

$\dfrac{u}{u_\infty}$

Figure 6.17 Comparison of velocity profiles with and
without oscillation ($u_\infty = 40$, $x = 23$, $f = 15$)

Figure 6.18   Comparison of velocity profiles with and without oscillation (u_{∞} =40, x=8, f=50)

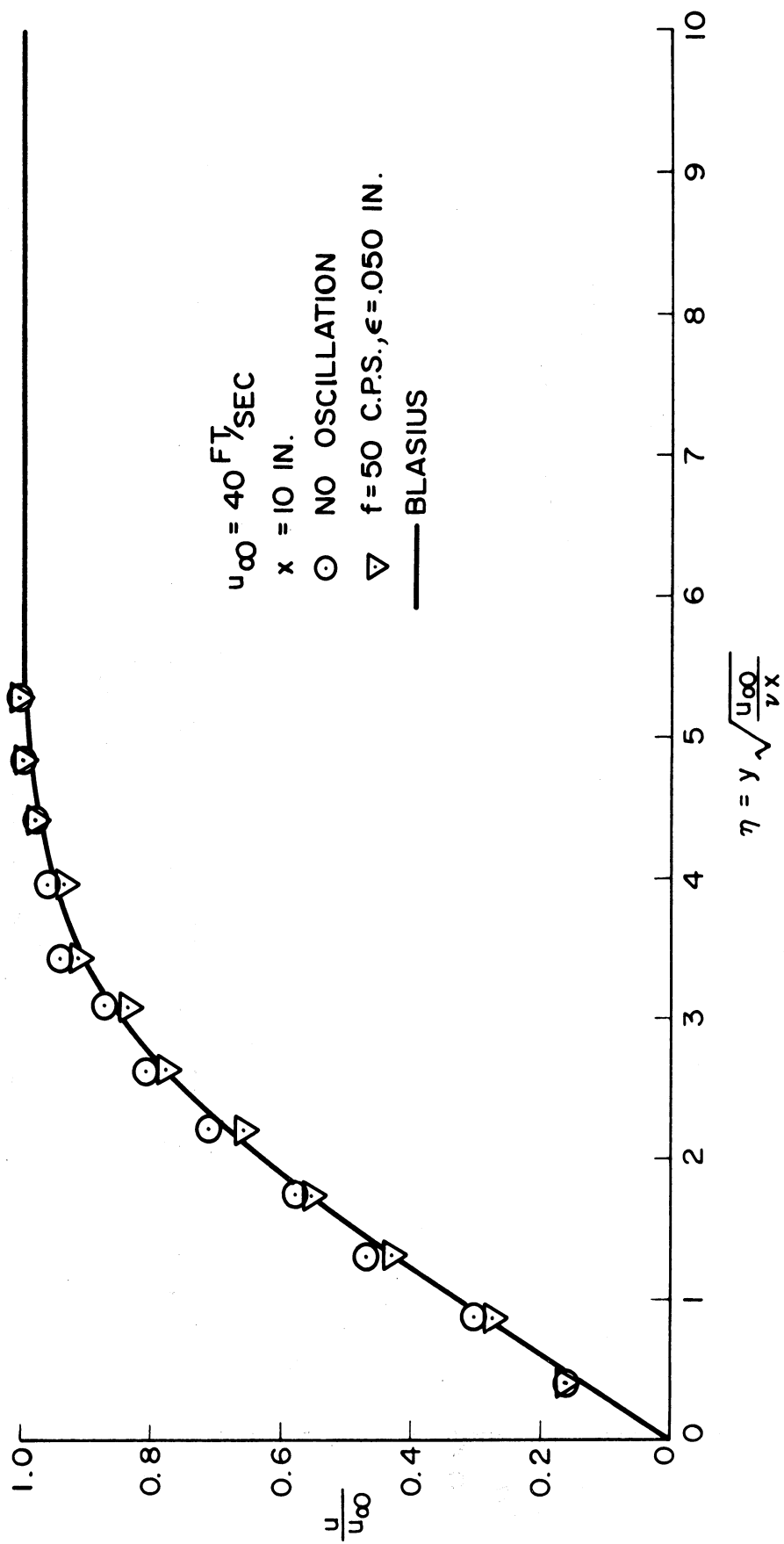Figure 6.19 Comparison of velocity profiles with and without oscillation ($u_\infty = 40$, $x = 10$, $f = 50$)

$$\eta = y\sqrt{\frac{u_\infty}{\nu x}}$$

$u_\infty = 40 \, ^{FT}/_{SEC}$

$x = 16$ IN.

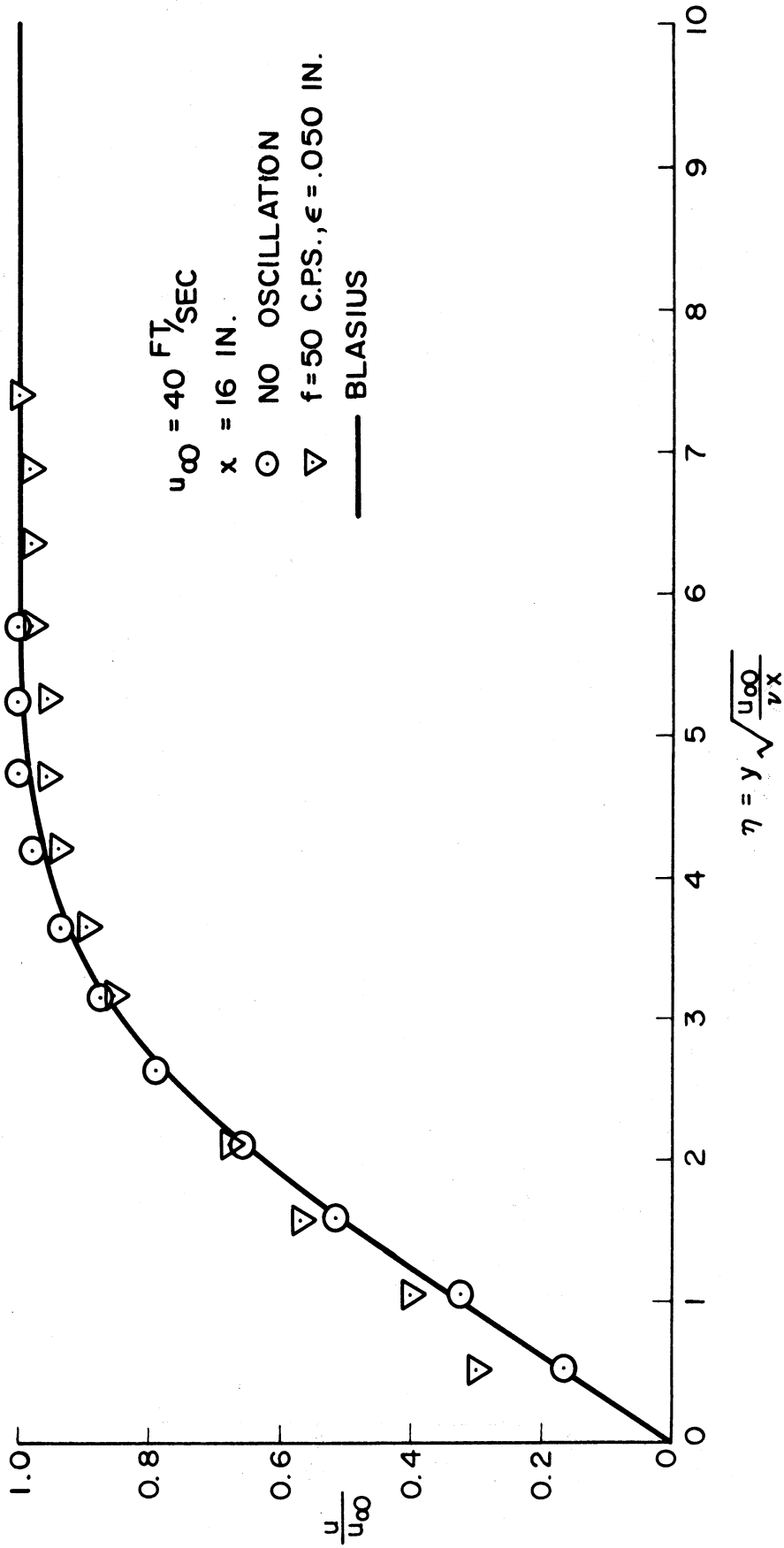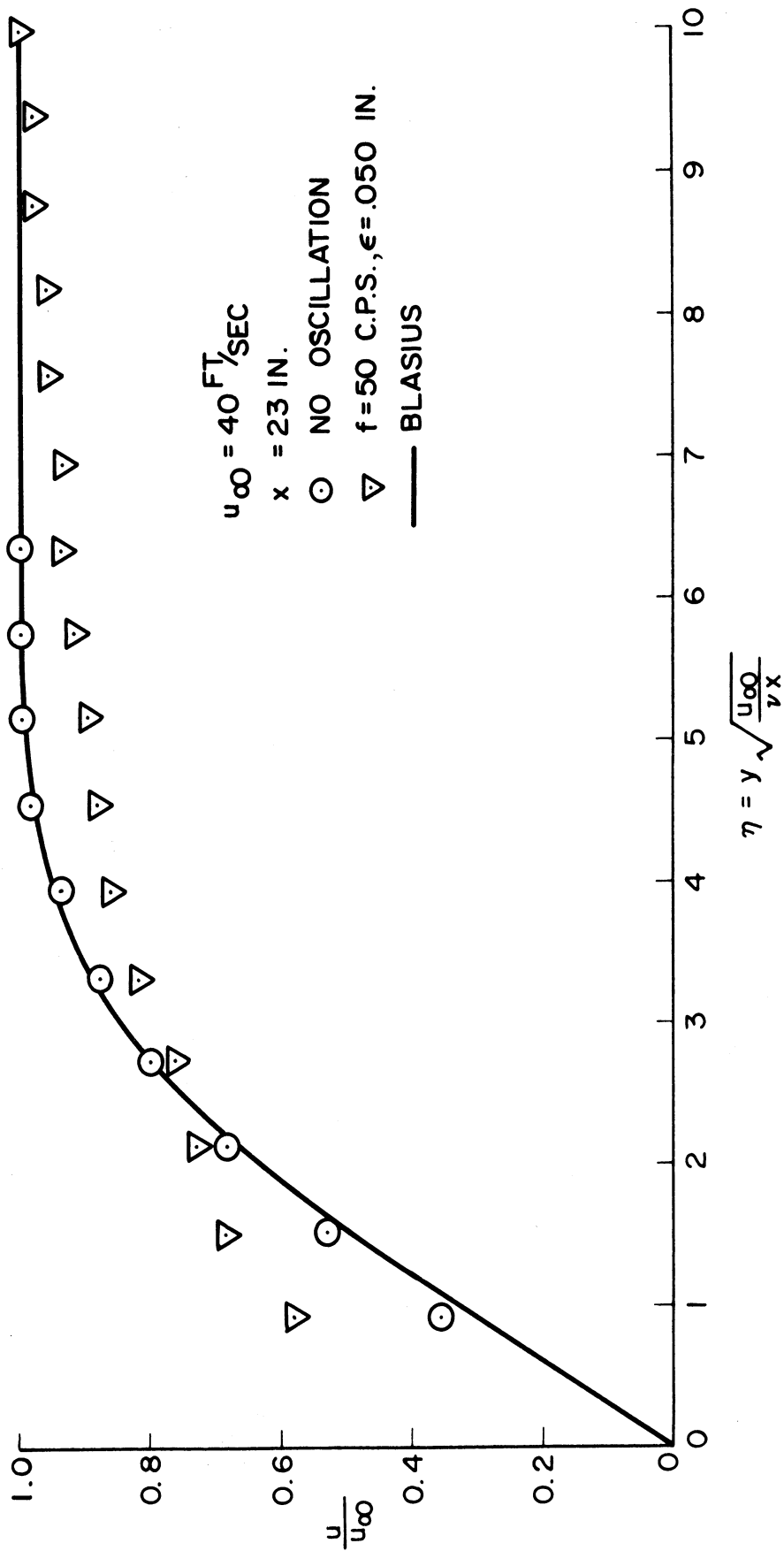⊙ NO OSCILLATION

▷ f=50 C.P.S., ϵ = .050 IN.

—— BLASIUS

Figure 6.20 Comparison of velocity profiles with and without oscillation (u_∞ =40, x=16, f=50)

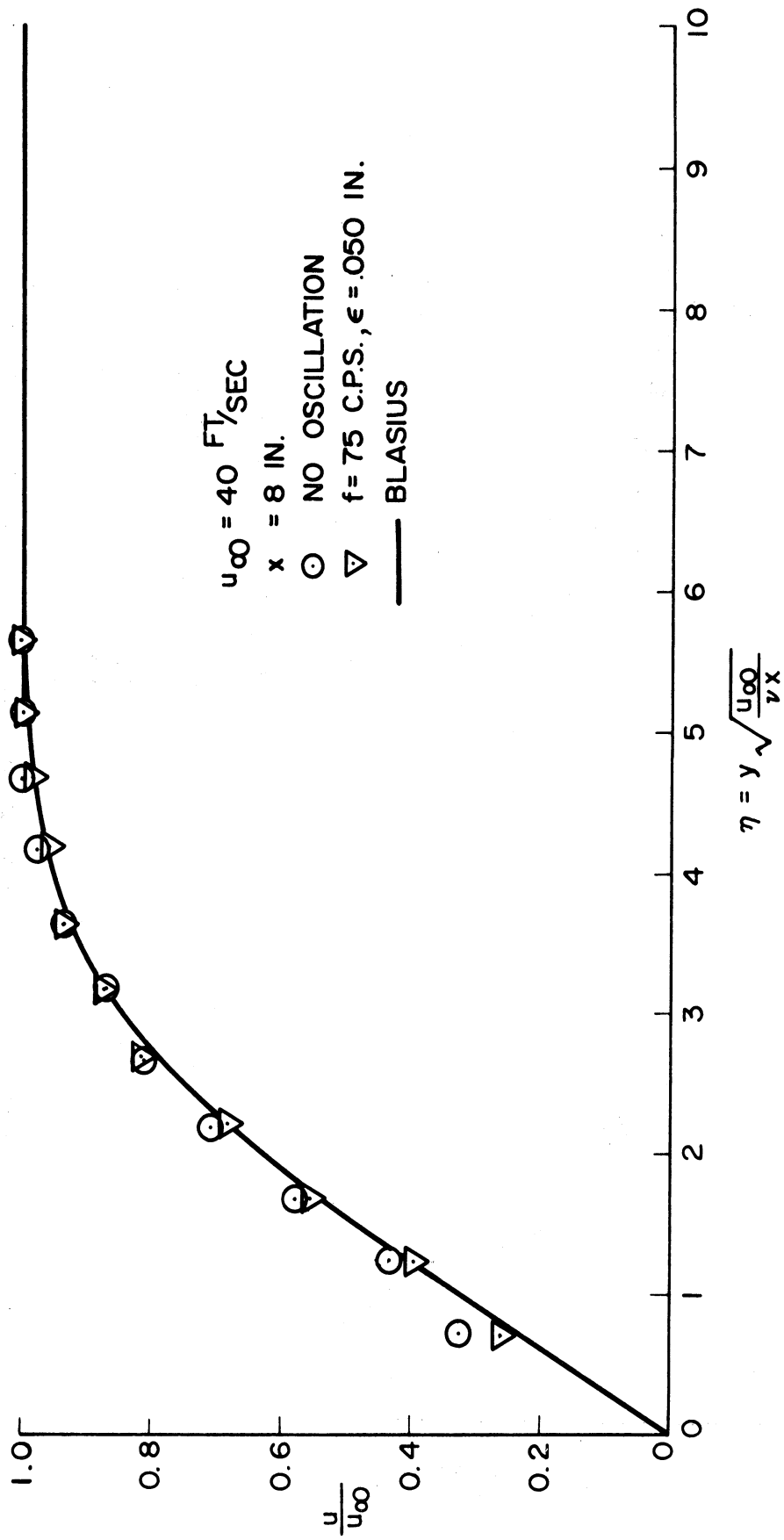Figure 6.21 Comparison of velocity profiles with and without oscillation ($u_\infty = 40$, $x = 23$, $f = 50$)

$u_\infty = 40 \ {}^{FT}\!/_{SEC}$

$x = 8$ IN.

⊙   NO OSCILLATION

▽   f = 75 C.P.S., ϵ = .050 IN.

—— BLASIUS

$\eta = y \sqrt{\dfrac{u_\infty}{\nu x}}$

Figure 6.22   Comparison of velocity profiles with and without oscillation ($u_\infty = 40$, $x=8$, $f=75$)

$u_\infty = 40 \, ^{FT}/_{SEC}$

$x = 9.63$ IN

$\odot$ NO OSCILLATION

$\triangledown$ f=75 C.P.S., $\epsilon = .050$ IN.

—— BLASIUS

$\eta = y \sqrt{\dfrac{u_\infty}{\nu x}}$

$\dfrac{u}{u_\infty}$
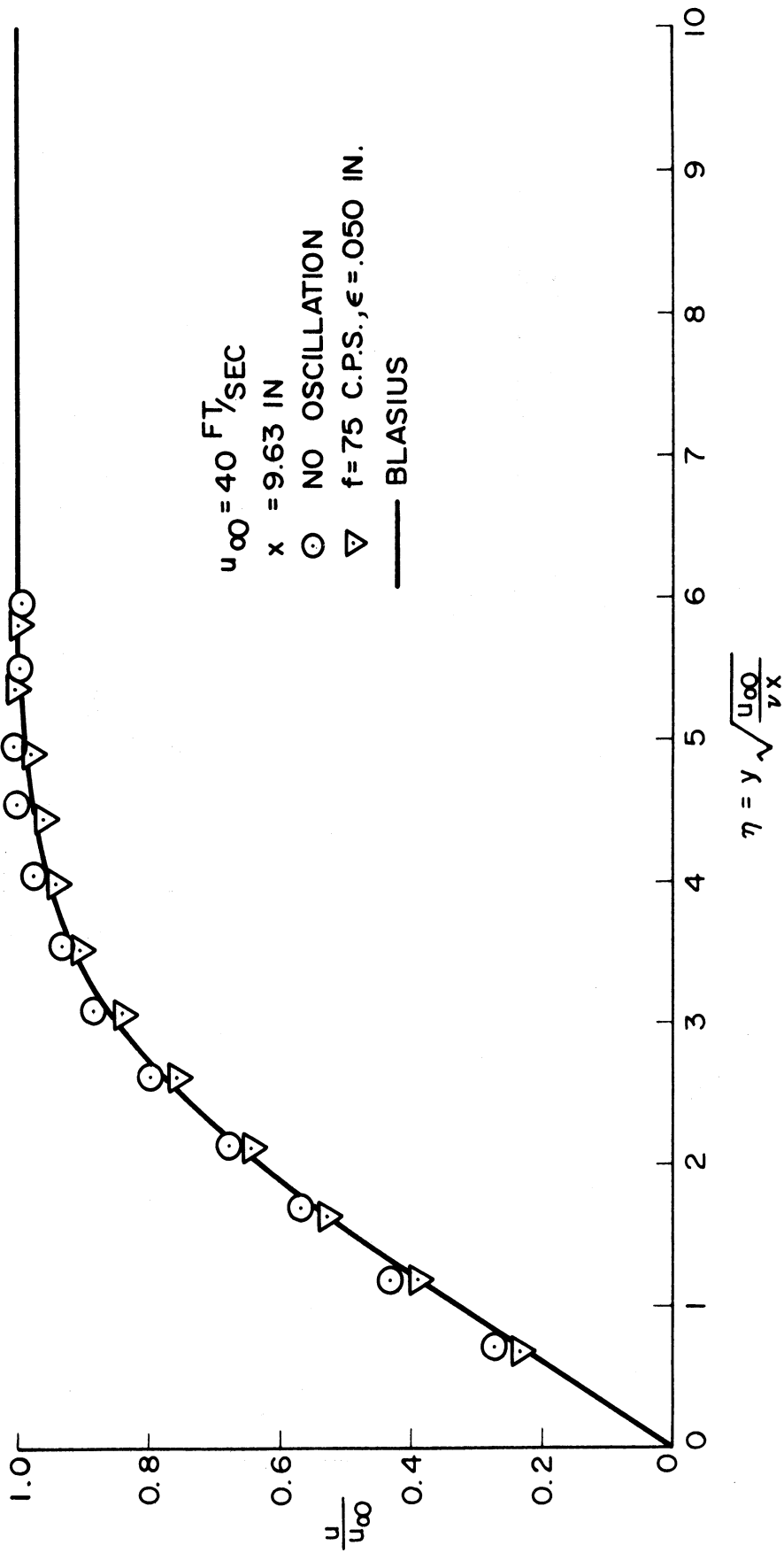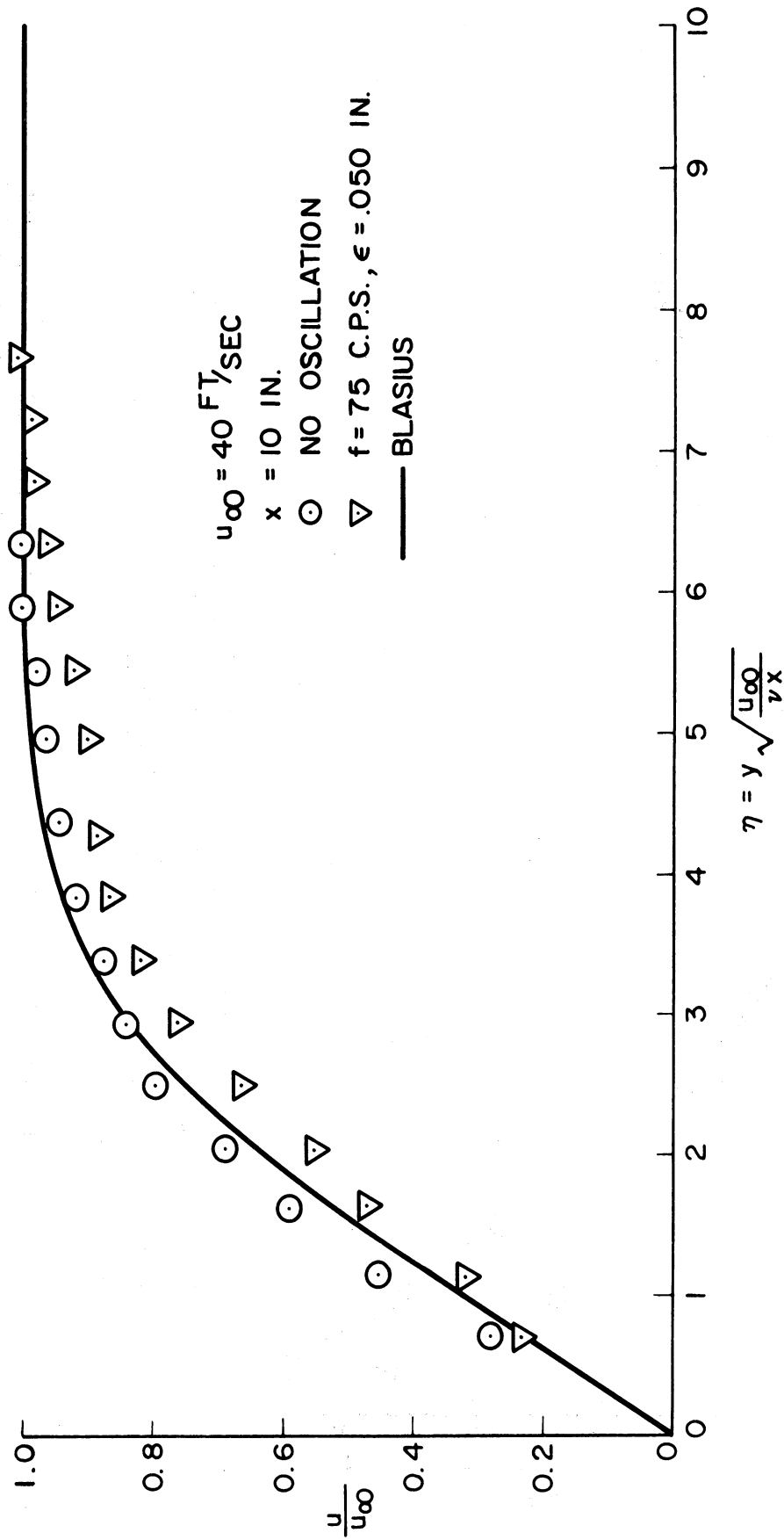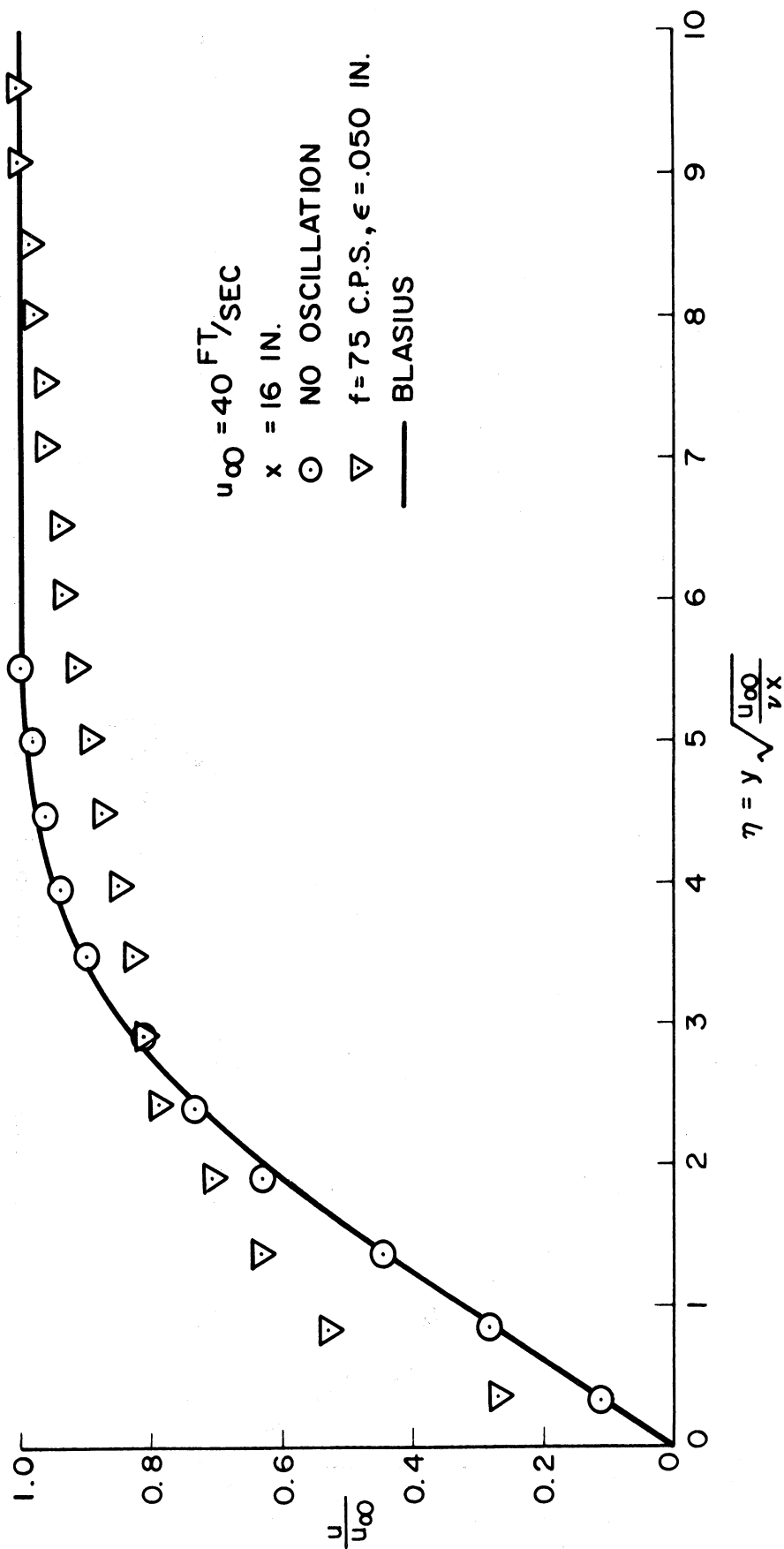
Figure 6.23 Comparison of velocity profiles with and without oscillation ($u_\infty = 40$, $x = 9.63$, $f = 75$)

Figure 6.24 Comparison of velocity profiles with and without oscillation (u∞ =40, x=10, f=75)

$u_\infty = 40 \, {}^{FT}/_{SEC}$

x = 16 IN.

⊙ NO OSCILLATION

▽ f=75 C.P.S., ϵ=.050 IN.

—— BLASIUS

$\eta = y \sqrt{\dfrac{u_\infty}{\nu x}}$

$\dfrac{u}{u_\infty}$

Figure 6.25   Comparison of velocity profiles with and without oscillation (u_∞ =40, x=16, f=75.)

$$\eta = y \sqrt{\frac{u_\infty}{\nu x}}$$

$u_\infty = 40 \, {}^{FT}/_{SEC}$

$x = 23$ IN.

⊙ NO OSCILLATION

▽ f = 75 C.P.S., $\epsilon = .050$ IN

—— BLASIUS

$\frac{u}{u_\infty}$

Figure 6.26 Comparison of velocity profiles with and without oscillation ($u_\infty = 40$, $x = 23$, $f = 75$)

$u_\infty = 40 \; {}^{FT}\!/_{SEC}$

$x = 8$ IN.

⊙   NO OSCILLATION

▽   f = 100 C.P.S., ϵ = .050 IN.
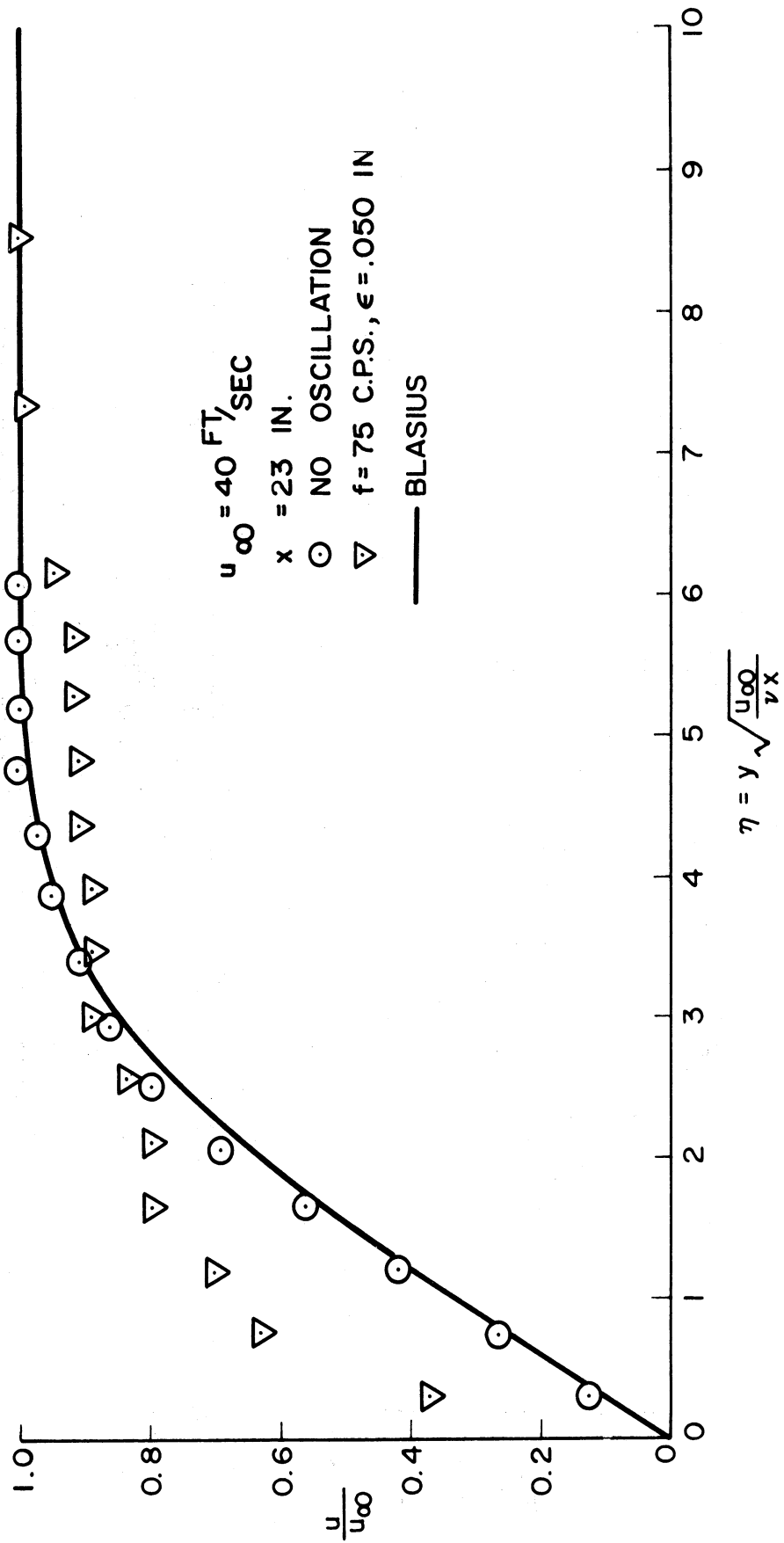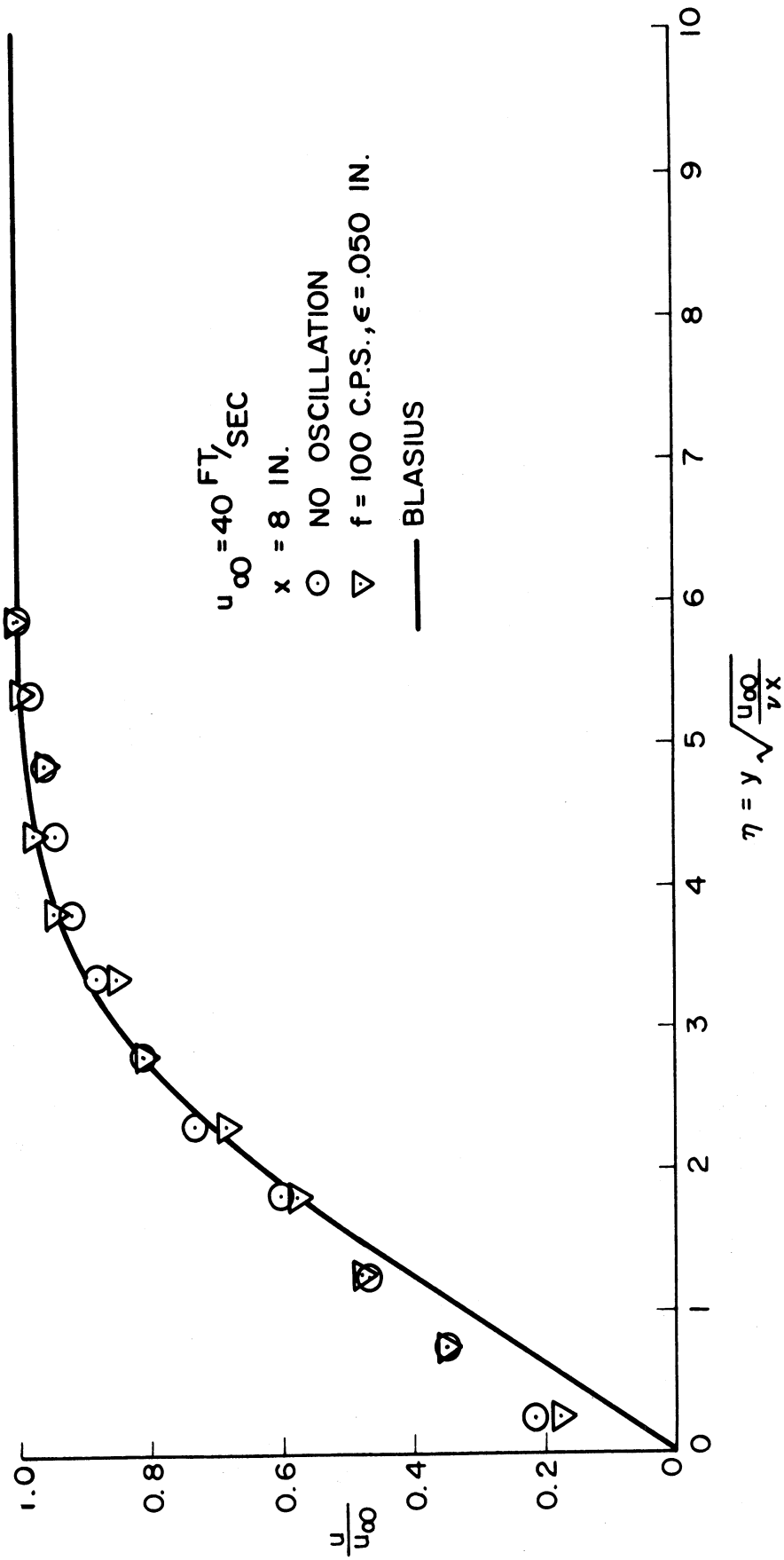
—— BLASIUS

$\eta = y \sqrt{\dfrac{u_\infty}{\nu x}}$

Figure 6.27   Comparison of velocity profiles with and
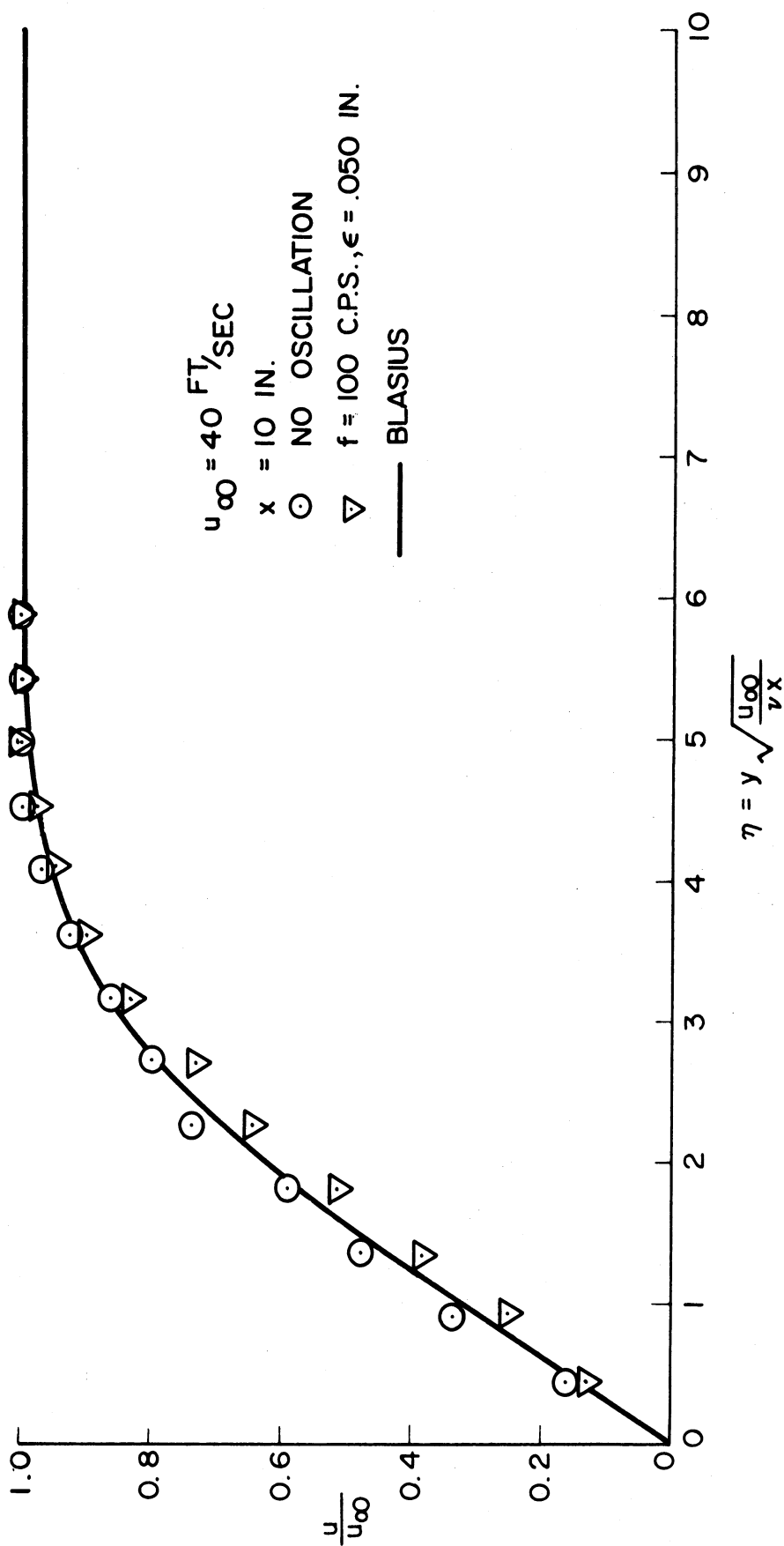without oscillation ($u_\infty = 40$, $x=8$, $f=100$)

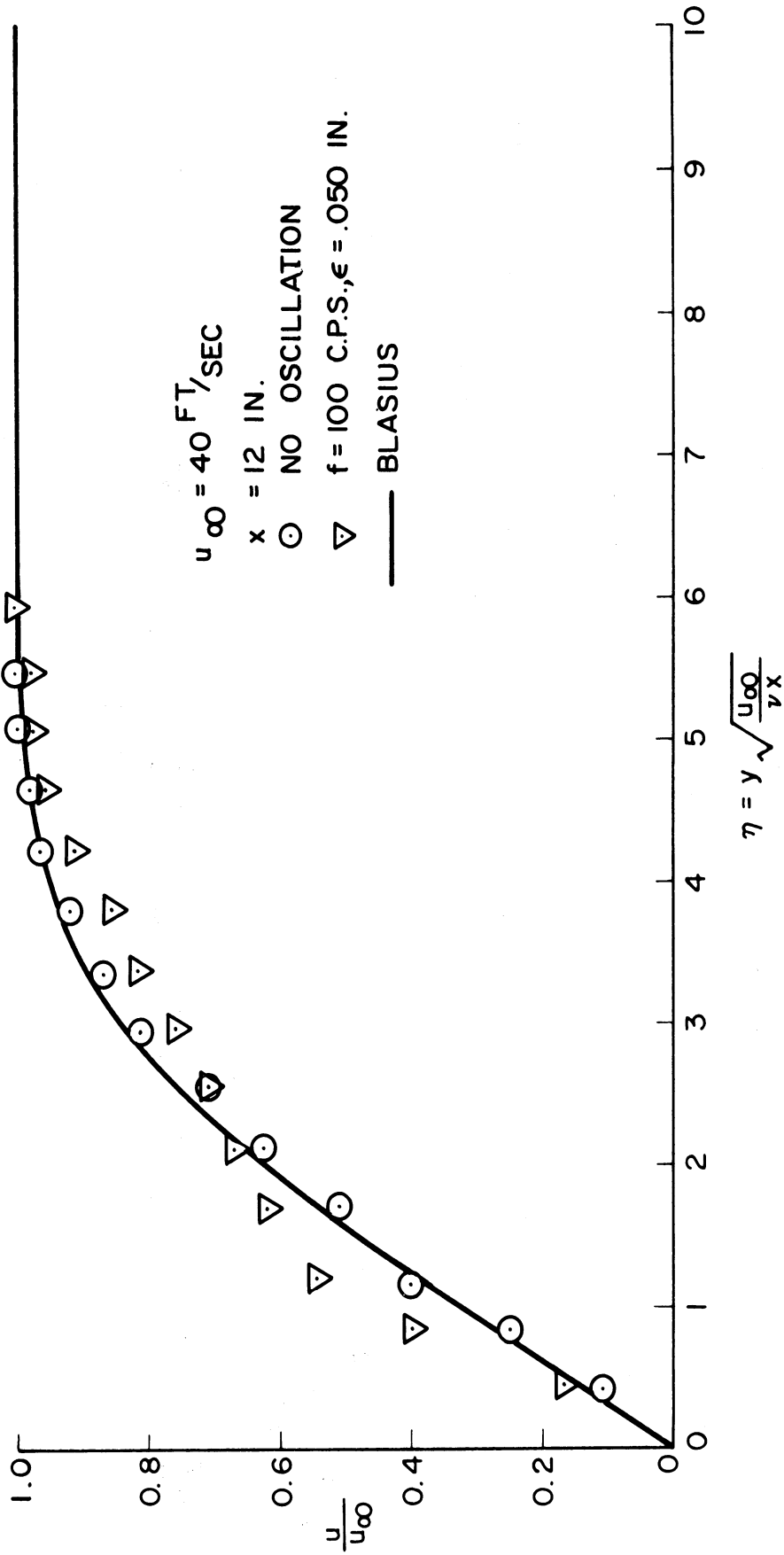Figure 6.28 Comparison of velocity profiles with and without oscillation ($u_\infty = 40$, $x=10$, $f=100$)

Figure 6.29 Comparison of velocity profiles with and without oscillation ($u_\infty = 40$, $x = 12$, $f = 100$)

Figure 6.30 Comparison of velocity profiles with and
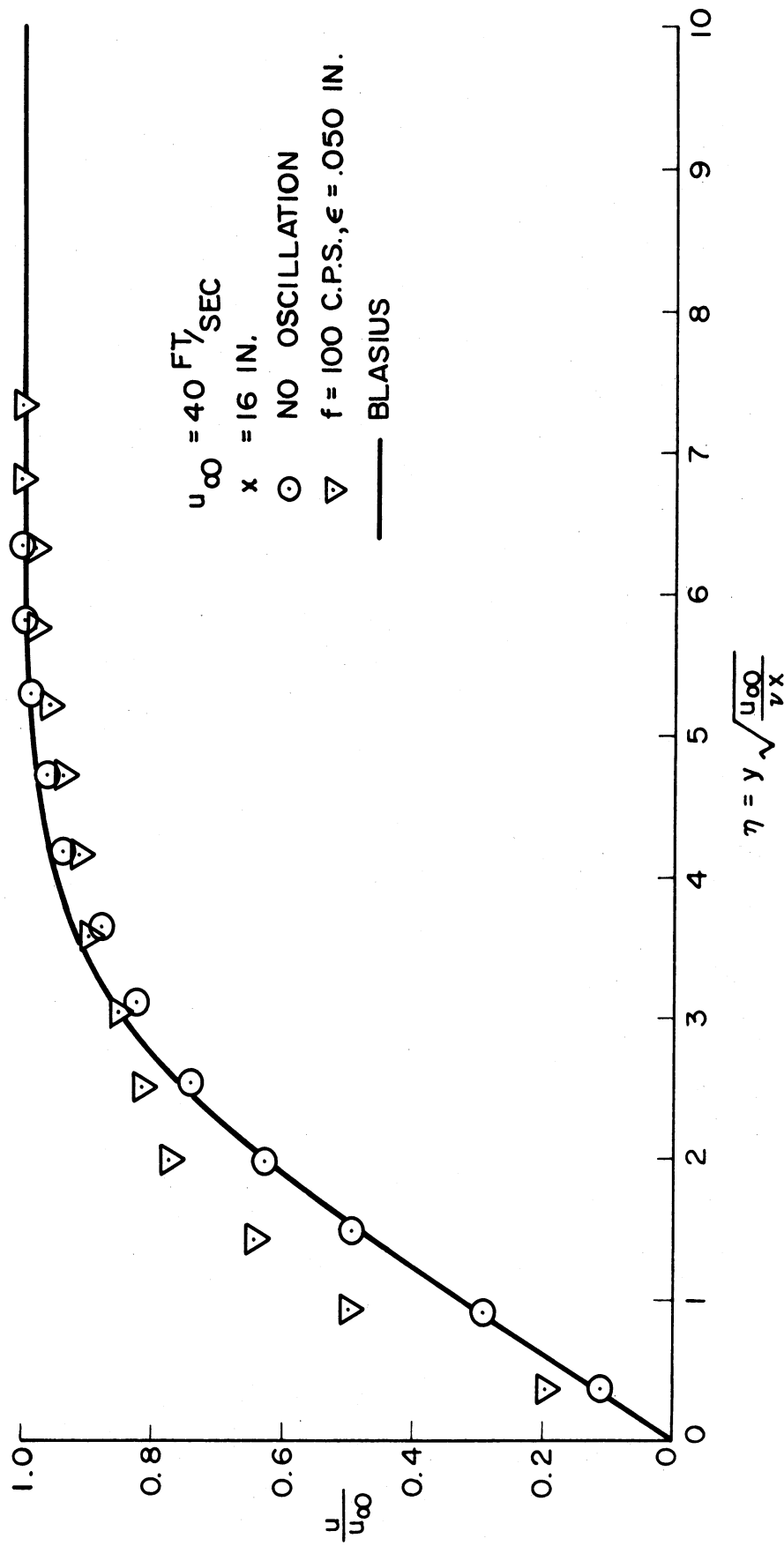without oscillation (u_∞ =40, x=16, f=100)

Figure 6.31   Comparison of velocity profiles with and without oscillation ($u_\infty = 40$, $x=23$, $f=100$)

Figure 6.32 Comparison of velocity profiles with and without oscillation ($u_\infty = 20$, $x=8$, $f=15$)

Figure 6.33 Comparison of velocity profiles with and without oscillation (u_∞ =20, x=9.63, f=15)

Figure 6.34   Comparison of velocity profiles with and
without oscillation ($u_\infty = 20$, $x = 10$, $f = 15$)

$u_{\infty} = 20 \, {}^{FT}\!/_{SEC}$

$x = 16$ IN.

$\odot$ NO OSCILLATION

$\triangledown$ $f = 15$ C.P.S., $\epsilon = .050$ IN.

—— BLASIUS

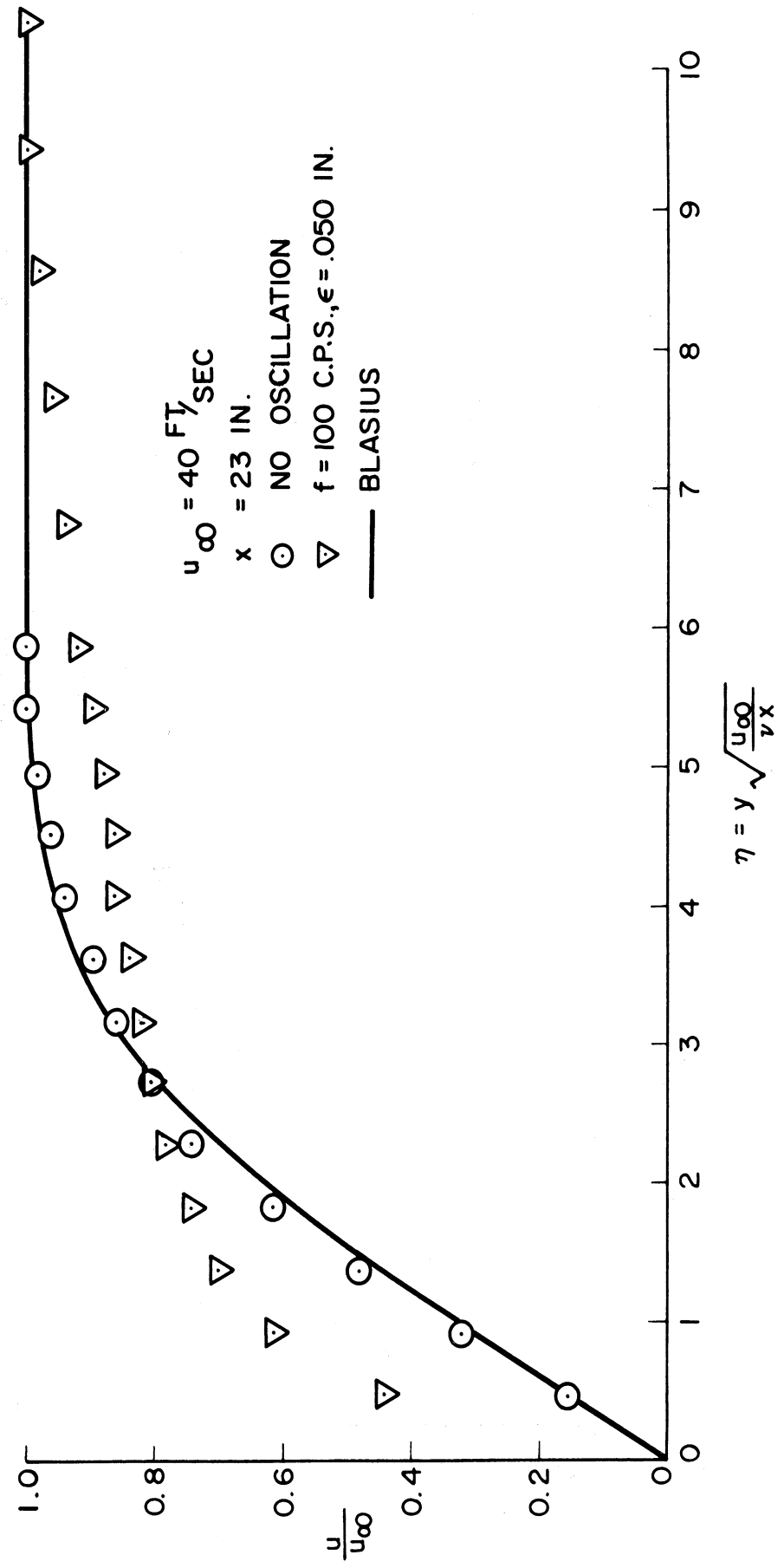$\eta = y \sqrt{\dfrac{u_{\infty}}{\nu x}}$
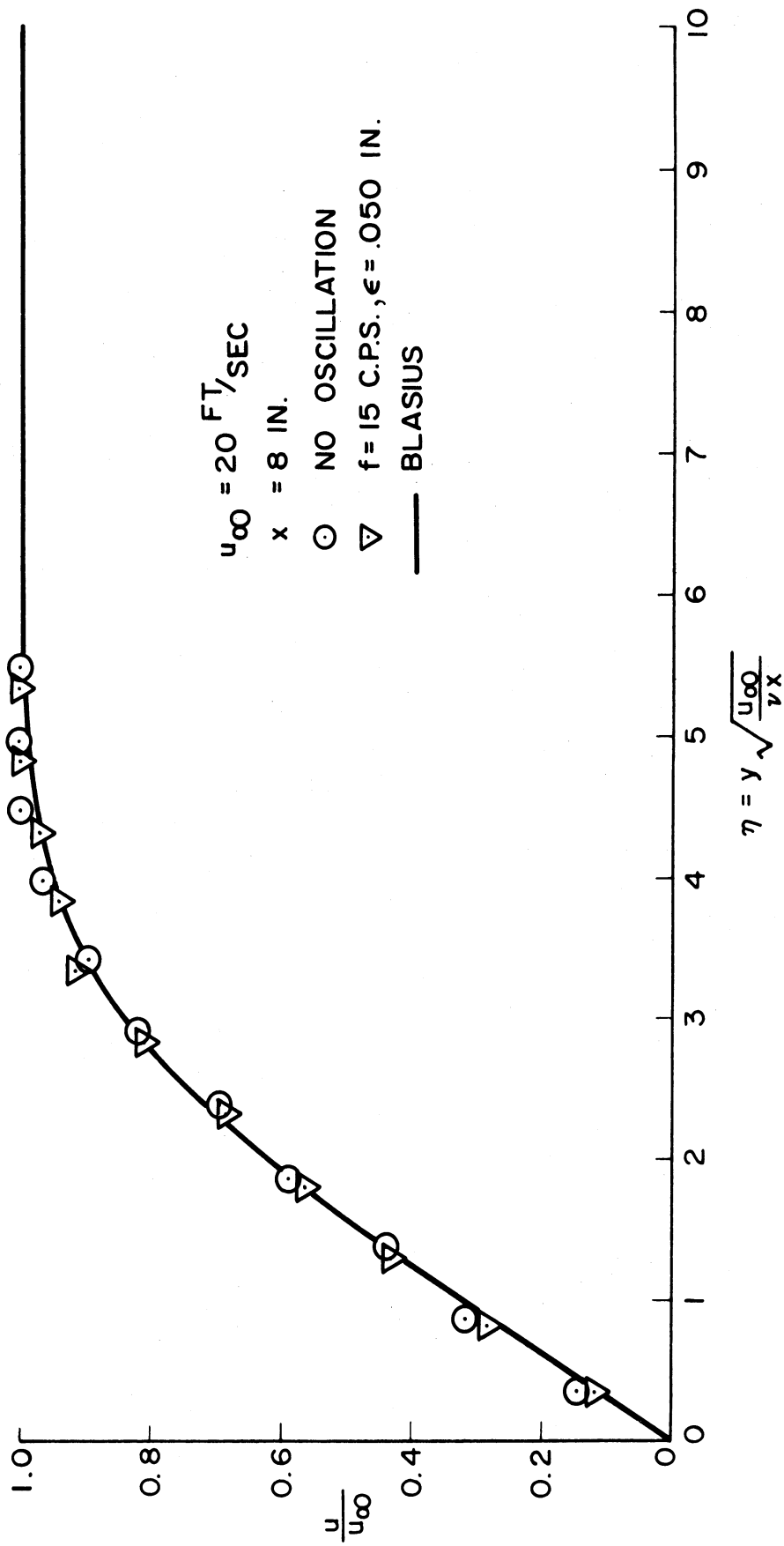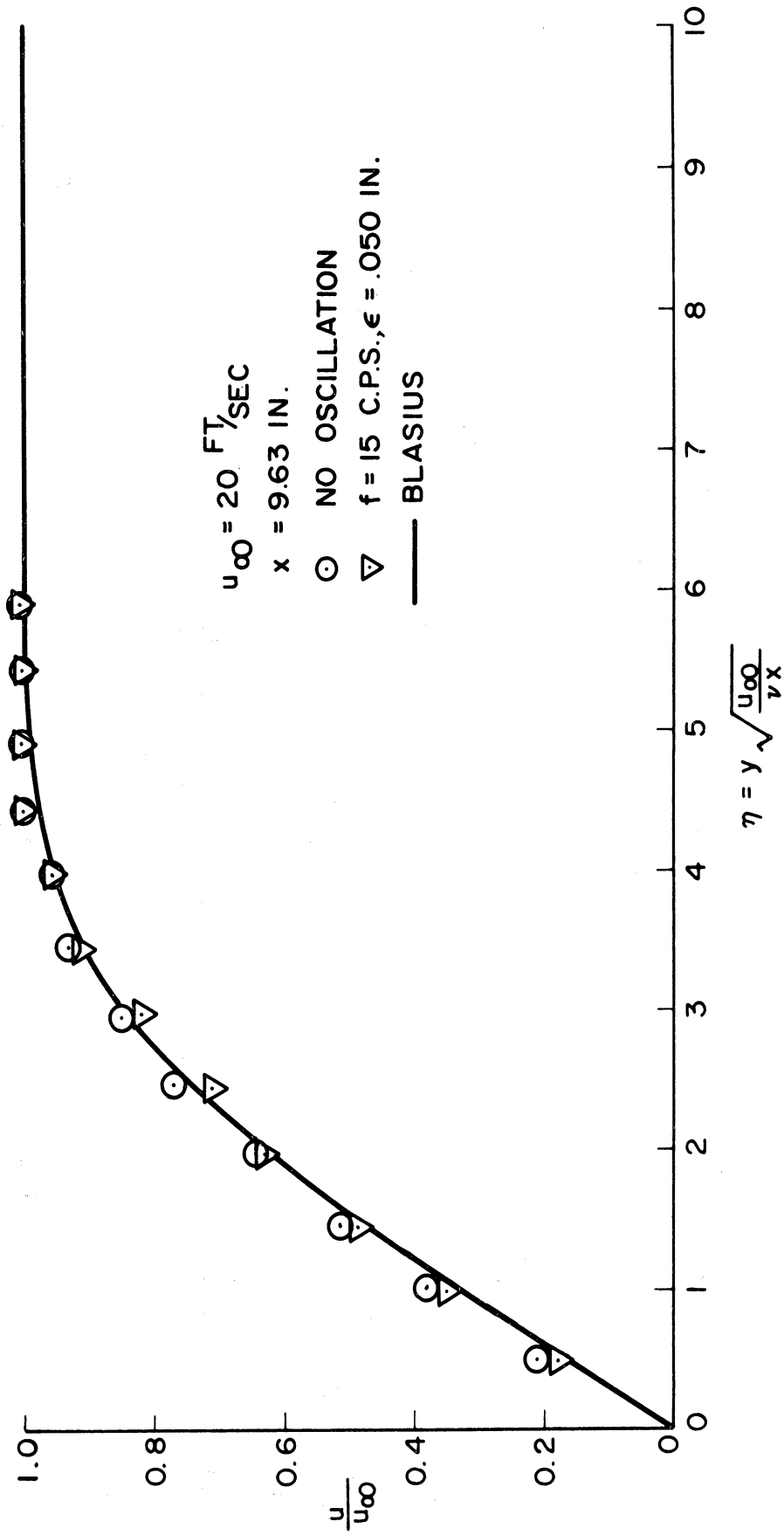
$\dfrac{u}{u_{\infty}}$

Figure 6.35 Comparison of velocity profiles with and without oscillation ($u_{\infty} = 20$, $x = 16$, $f = 15$)

Figure 6.36 Comparison of velocity profiles with and without oscillation ($u_\infty = 20$, x=23, f=15)

Figure 6.37 Comparison of velocity profiles with and without oscillation ($u_\infty = 20$, $x=8$, $f=50$)

$$\eta = y \sqrt{\frac{u_\infty}{\nu x}}$$

$u_\infty = 20 \; {}^{FT}\!/_{SEC}$

$x = 10 \; IN.$

$\odot$ NO OSCILLATION

$\triangledown$ f=50 C.P.S., ϵ = .050 IN.

—— BLASIUS

Figure 6.38 Comparison of velocity profiles with and without oscillation (u_∞=20, x=10, f=50)

$u_\infty = 20 \, {}^{FT}/_{SEC}$

$x = 16$ IN.

$\odot$ NO OSCILLATION

$\triangleright$ $f = 50$ C.P.S., $\epsilon = .050$ IN.

—— BLASIUS

$\eta = y \sqrt{\dfrac{u_\infty}{\nu x}}$

$\dfrac{u}{u_\infty}$

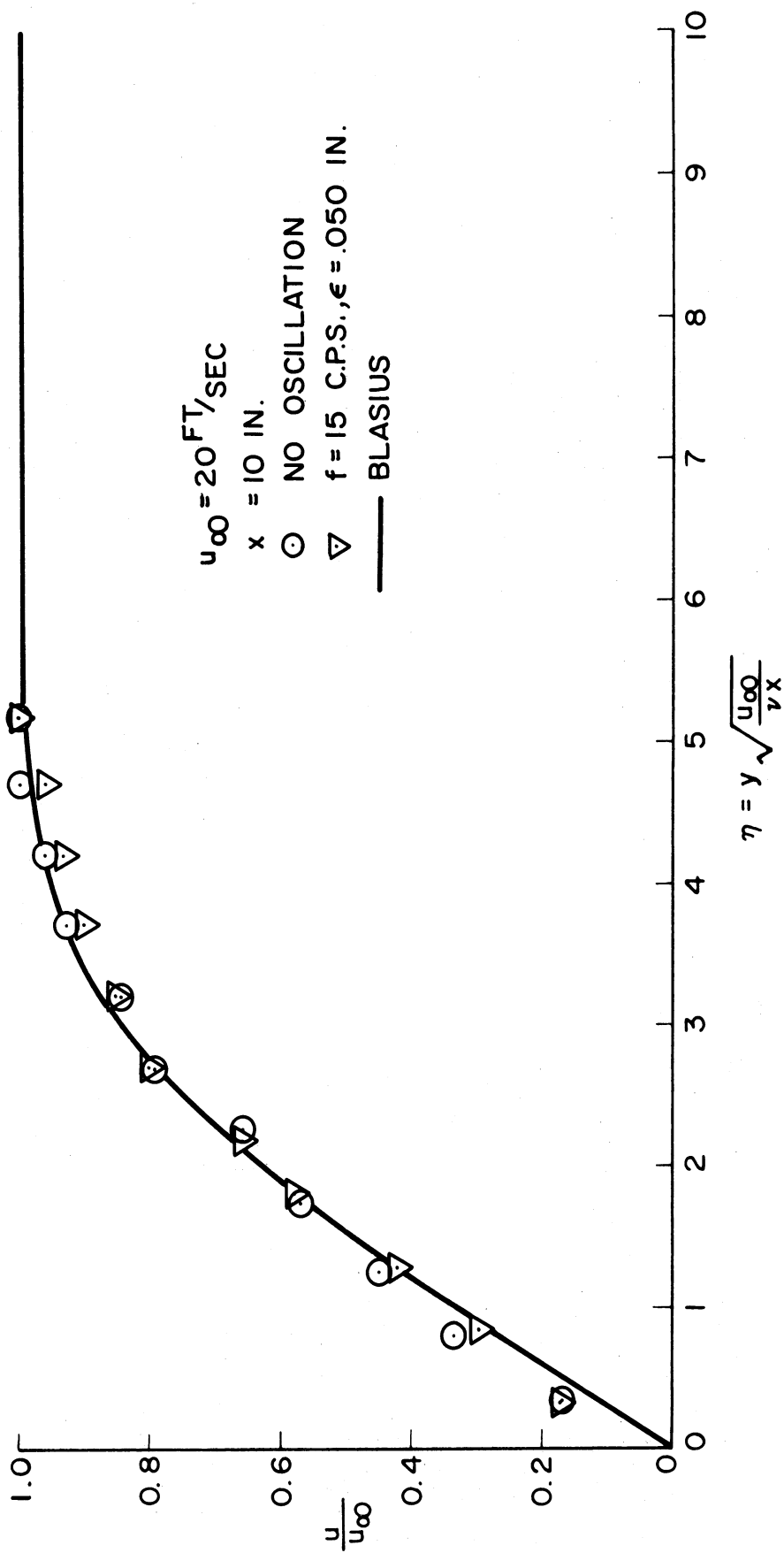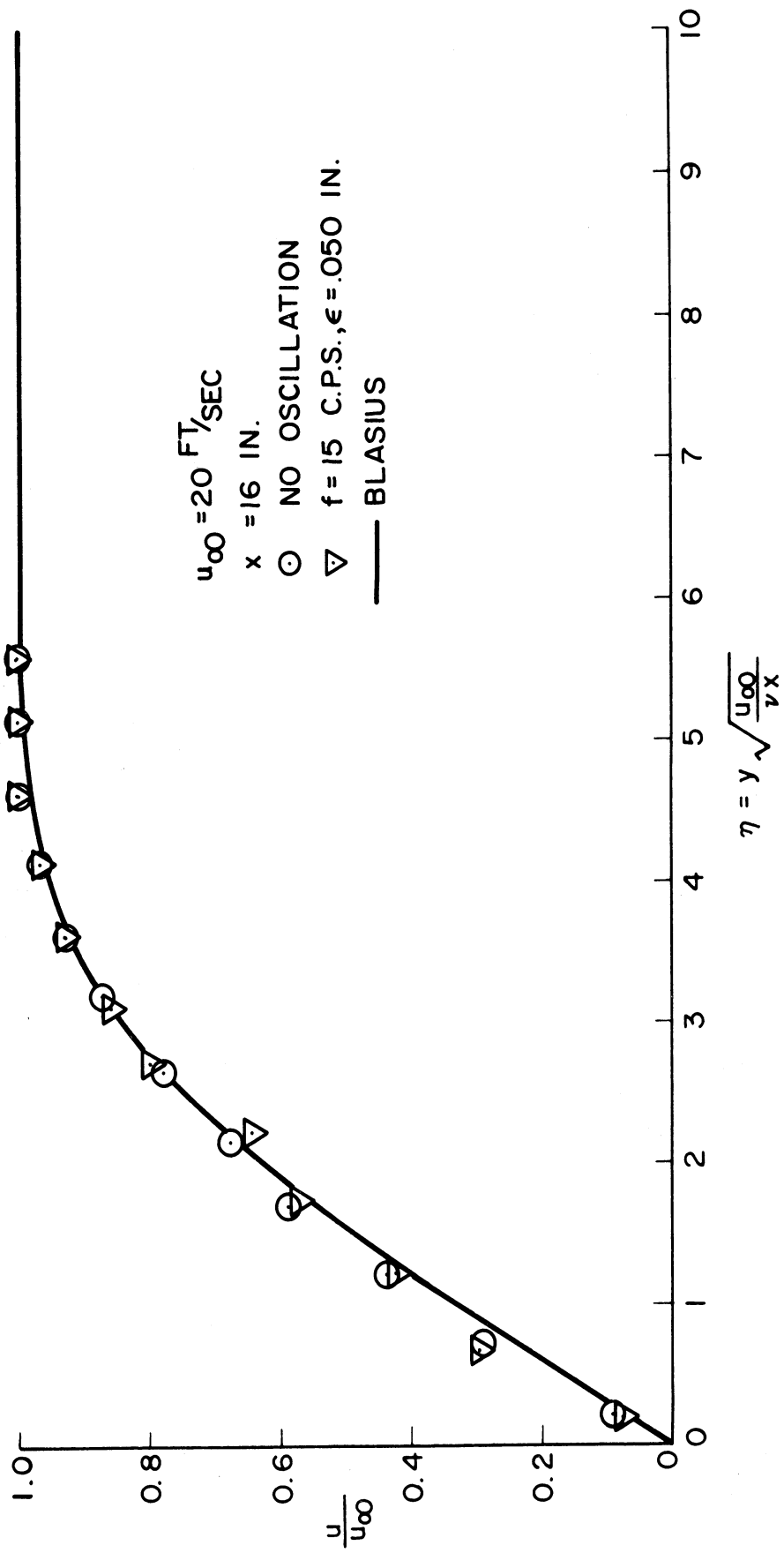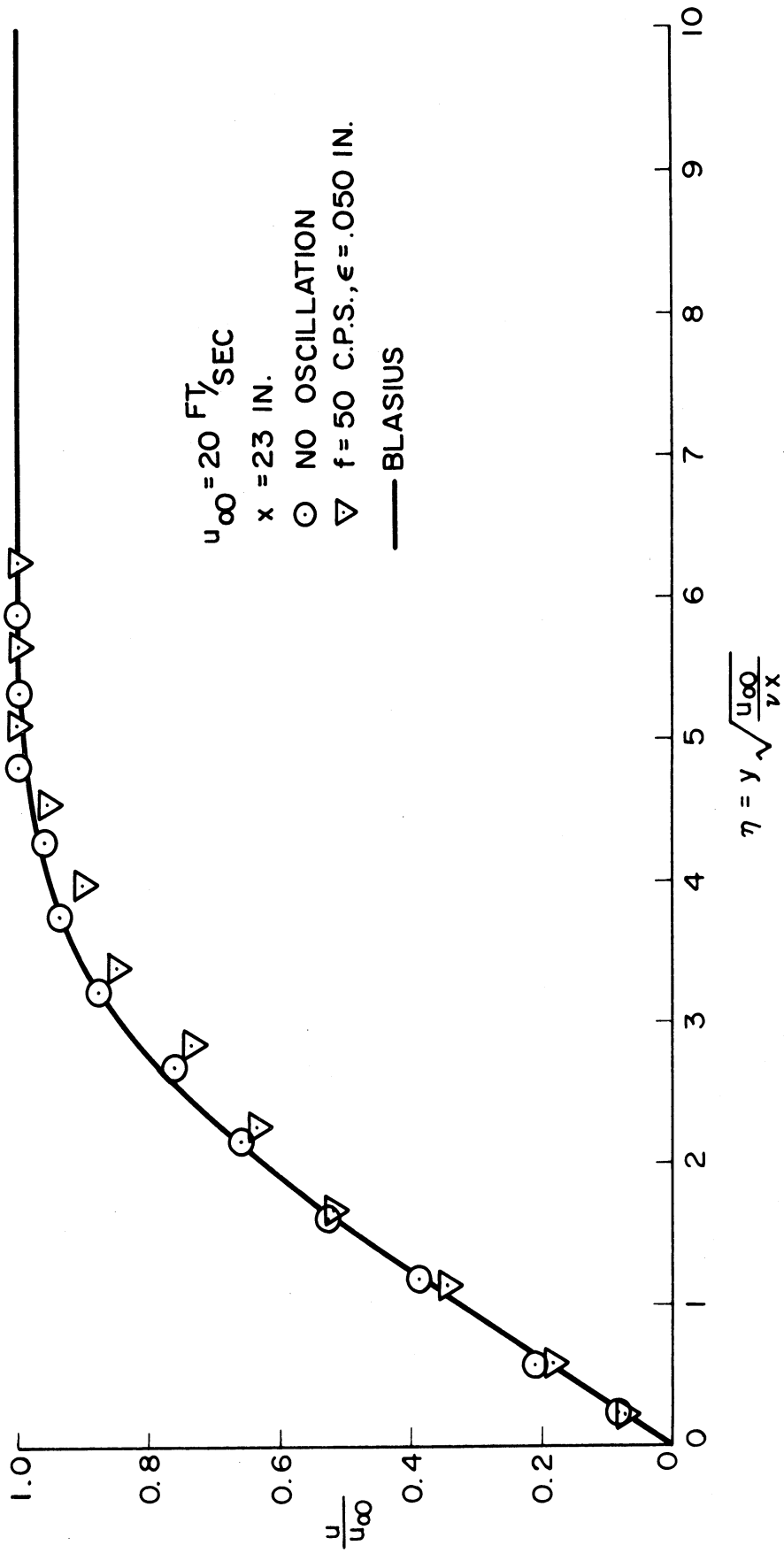Figure 6.39   Comparison of velocity profiles with and without oscillation ($u_\infty = 20$, $x = 16$, $f = 50$)

Figure 6.40 Comparison of velocity profiles with and without oscillation ($u_\infty = 20$, $x = 23$, $f = 50$)
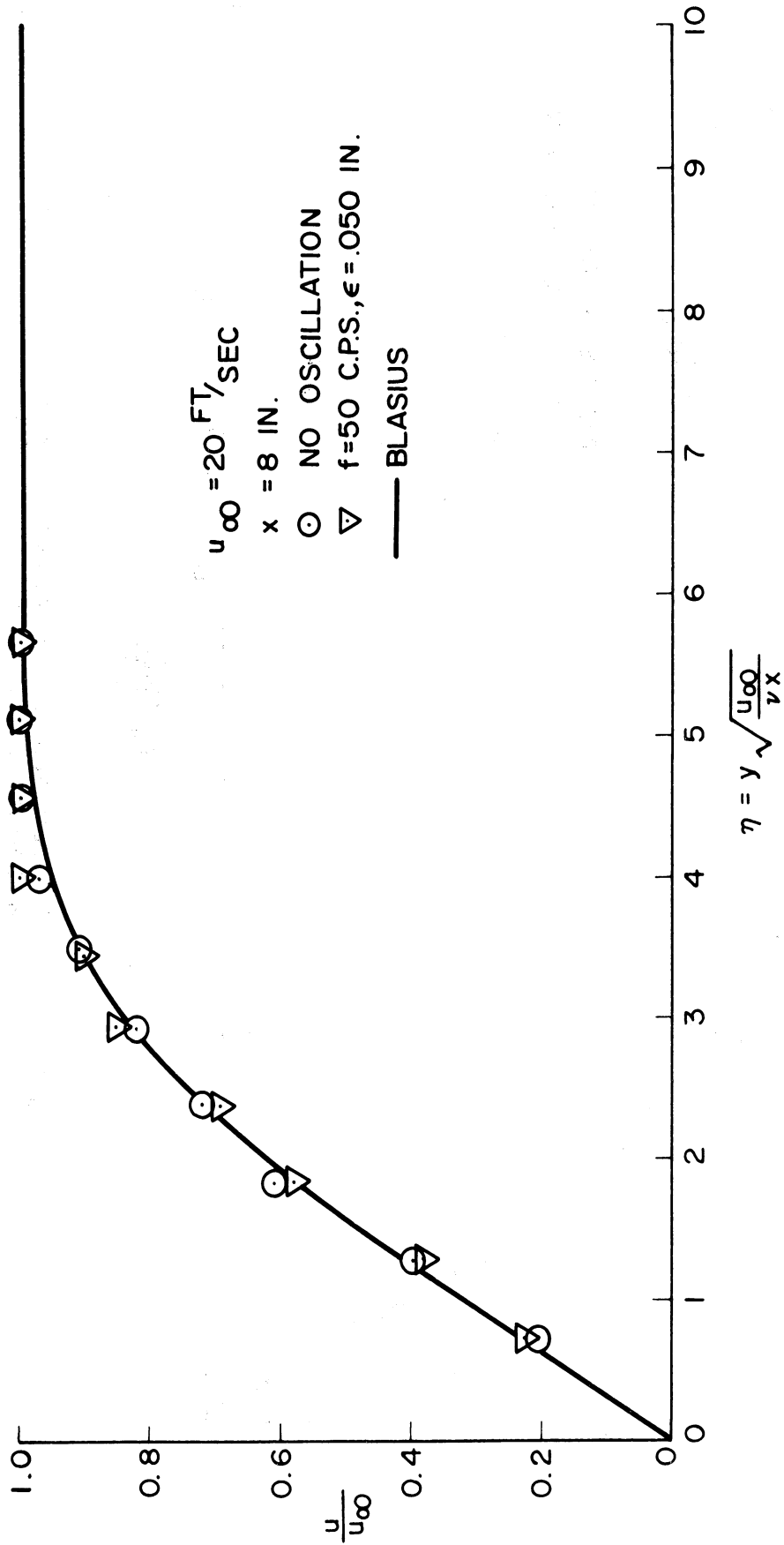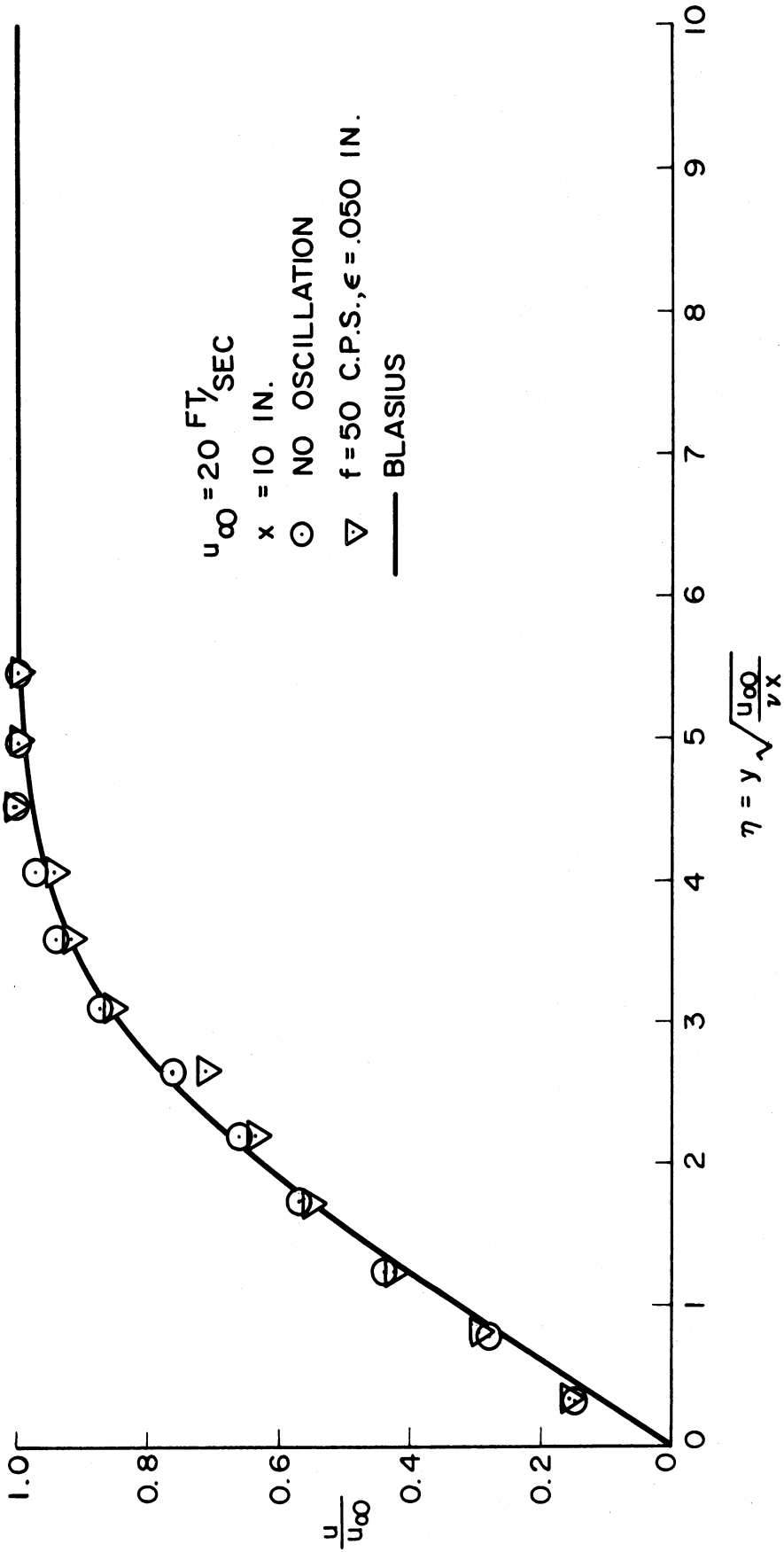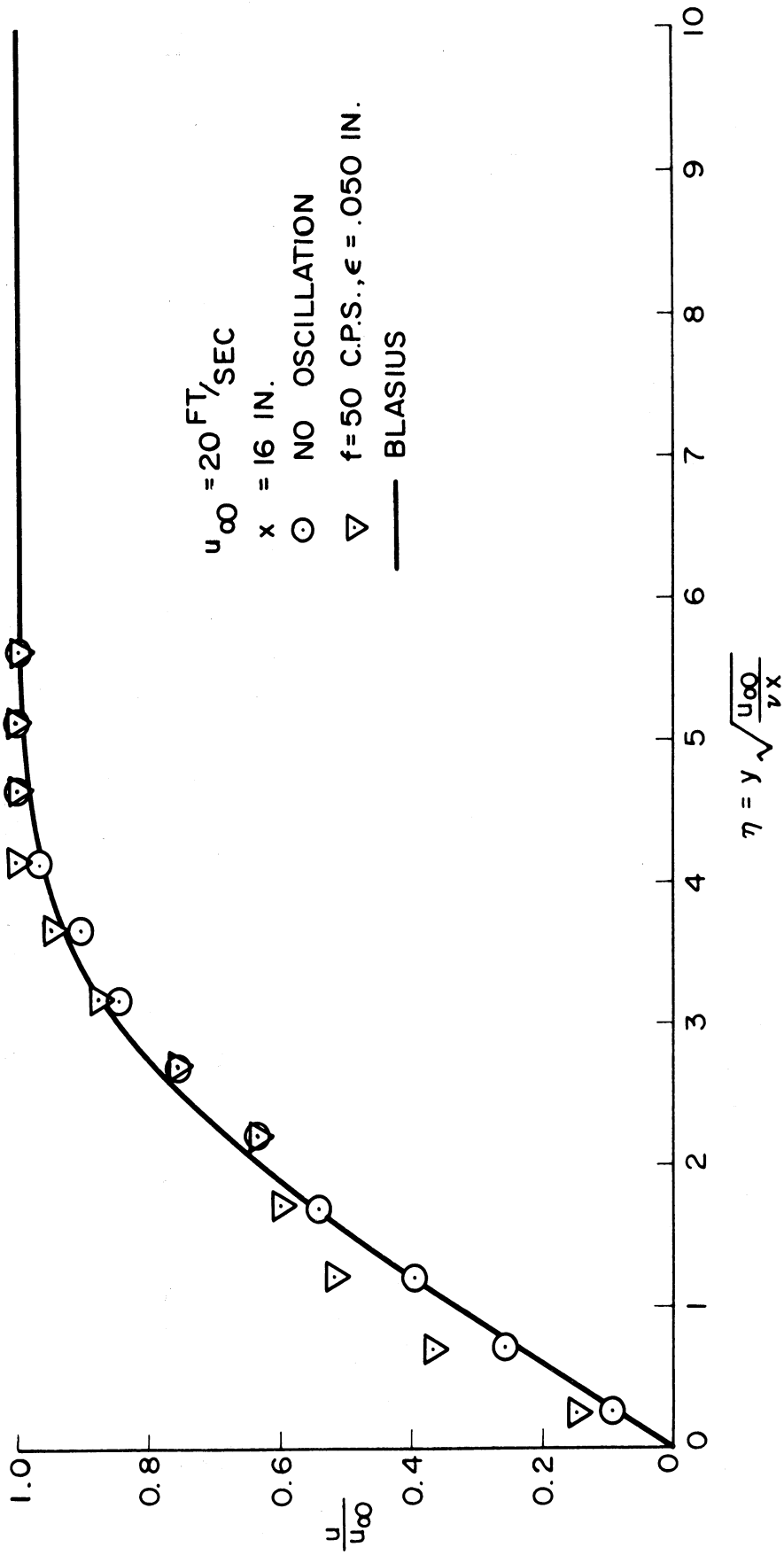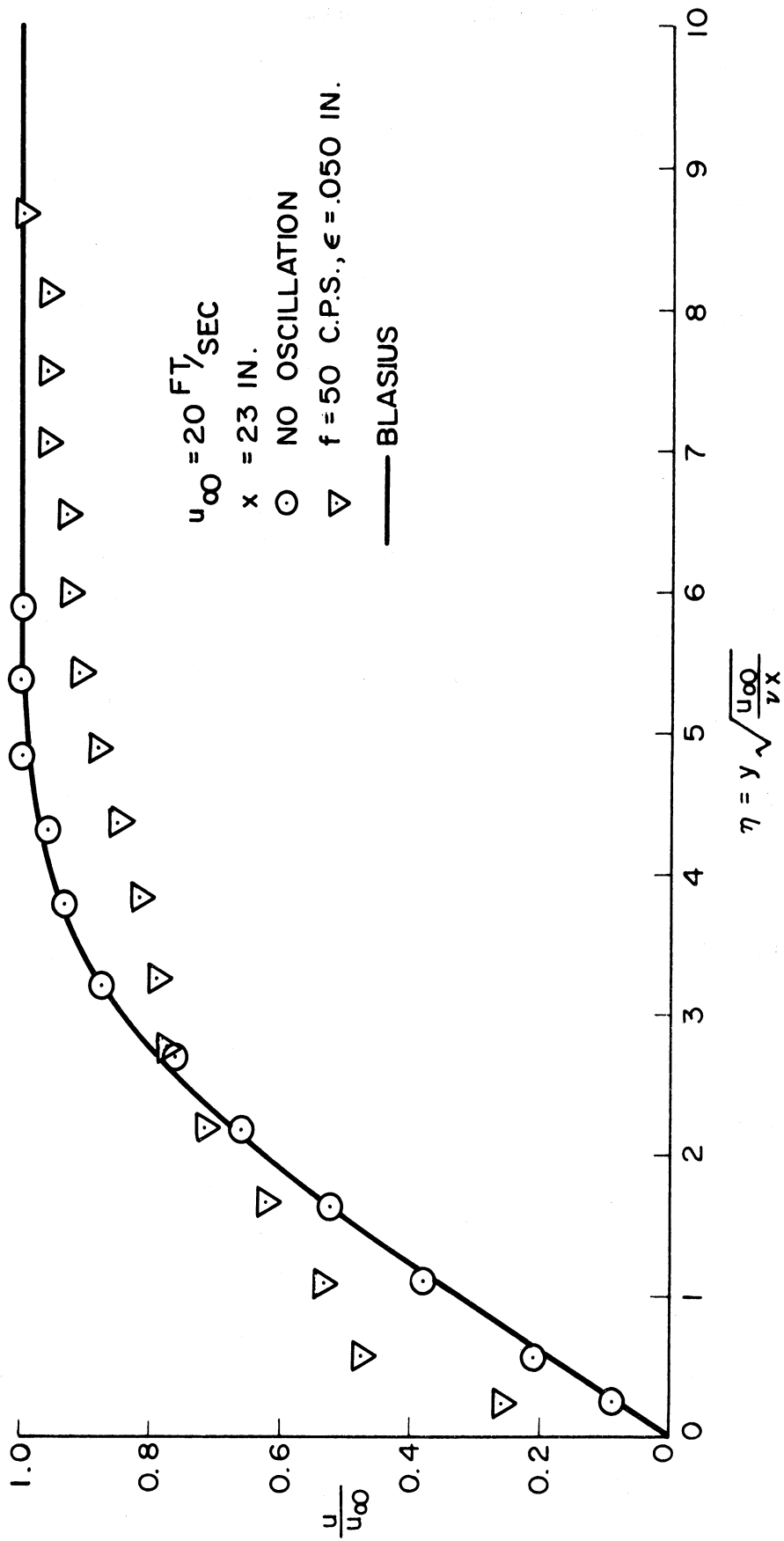
Figures 6.41 through 6.45 pertain to 20 feet per second and 75 cps. At x = 8 and x = 9.63-inches there is no significant change in velocity. At x = 10-inches the velocity consistently decreases. At x = 16-inches the velocity is consistently increased throughout the boundary layer. No turbulent spots are present on the oscilloscope. A transition profile occurs at x = 23-inches.

Figures 6.46 through 6.49 are for 20 feet per second and 100 cps. There is no significant change in the profile at x = 8-inches. At x = 10-inches the velocity is consistently lower. At x = 16-inches the profile increases in velocity near the wall and decreases near the boundary layer edge. A transition profile occurs at x = 23-inches.

6.5 Comparison of the time-averaged oscillating profiles for various values of x.

Figures 6.50 through 6.57 are a comparison of the oscillating profiles as a function of x with frequency and velocity held constant. All profiles of this comparison are at x values of 8, 10, 16 and 23-inches. Figures 6.50 through 6.53 are at a free stream velocity of 40 feet per second. Figure 6.50 indicates that at a frequency of 15 cps all four profiles follow the theoretical Blasius (2) solution closely. At 50 cps in Figure 6.51 the profiles at x = 8 and 10-inches follow the Blasius profile closely but at x = 16-inches an increase in velocity near the wall and a decrease in velocity near the edge of the boundary

layer are apparent. The boundary layer also thickens in
this profile. At x = 23-inches the transition profile
occurs.

Figure 6.52 at 75 cps more clearly indicates the pro-
gress of the phenomenon. At x = 8-inches the profile
closely approximates the Blasius (2) profile whereas at
x = 10-inches the velocity is seen to decrease and the
boundary layer thicken. The profiles at x = 16 and 23-
inches are both transition profiles.

Figure 6.53 at 100 cps clearly illustrates the phenomenon.
The profile at x = 8-inches is close to the Blasius profile.
At x = 10-inches the decrease in velocity is apparent. At
x = 16-inches the increase in velocity near the wall and
the thickening of the boundary layer is apparent. At x = 23-
inches transition has already occurred.

The thickening of the boundary layer while the flow is
still laminar may be explained as a similar effect to that
which occurs with a stationary bulge in the plate surface.
A stationary bulge will cause an acceleration and sub-
sequent deceleration in a laminar boundary layer.

Figures 6.54 through 6.57 are at a free stream velocity
of 20 feet per second. Figure 6.54 shows that at 15 cps
all the profiles except x = 23-inches follow the Blasius
profile closely. The profile at x = 23-inches tends to
decrease in velocity. Figure 6.55 at 50 cps indicates that
the profiles at x = 8 and 10-inches follow the Blasius
profile but at x = 16-inches the profile begins its
increase in velocity leading to the transition velocity of
x = 23-inches.

Figure 6.56 at 75 cps presents the clearest picture
of the phenomenon. Again the profile at x = 8-inches follows
the Blasius profile. At x = 10-inches the velocity decrease
is clearly shown. At x = 16-inches the velocity increase
over the entire profile in the laminar boundary layer is
apparent. Finally at x = 23-inches the transition range
has been entered.

Figure 6-57 at 100 cps again indicates the phenomenon.
The profile at x = 8-inches follows Blasius. The profile
at x = 10-inches shows the decrease in velocity. The
profile at x = 16-inches indicates the increase in velocity
near the wall and the decrease in velocity near the boundary
layer edge. This profile apparently occurs after the fully
increased velocity profile and just before the transition
zone at x = 23-inches.

The experimental results just presented indicate that
the analytic solution of Na (56) is qualitatively valid
downstream of the membrane. The solution by Na indicates
a decrease in the velocity profile and then a subsequent
increase in the profile. The analytic solution cannot
give any indication of the onset of transition but the
experimental evidence shows transition occurs just down-
stream of the profile where all velocities exceed the
Blasius profile. The assumption in the analytic solution (56)
that no separation exists downstream from the membrane
is shown to be valid by the experimental laminar flow profiles
at x = 9.63 and 10-inches.

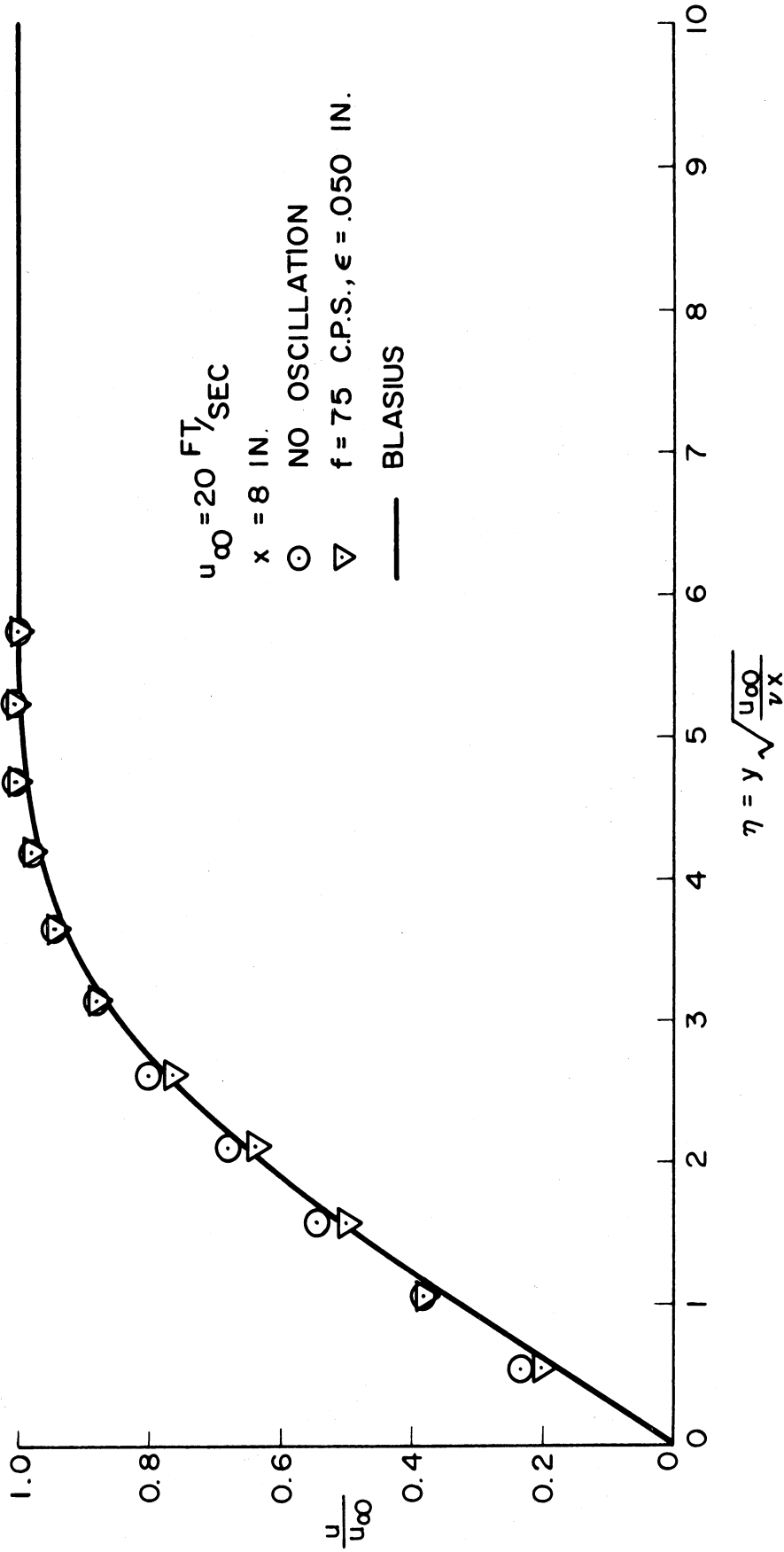Figure 6.41 Comparison of velocity profiles with and without oscillation ($u_\infty = 20$, $x=8$, $f=75$)

Figure 6.42 Comparison of velocity profiles with and without oscillation ($u_\infty = 20$, $x=9.63$, $f=75$)

Figure 6.43 Comparison of velocity profiles with and without oscillation ($u_\infty =20$, x=10, f=75)

Figure 6.44 Comparison of velocity profiles with and without oscillation ($u_\infty = 20$, x=16, f=75)

$\eta = y \sqrt{\dfrac{u_\infty}{\nu x}}$

$u_\infty = 20 \ ^{FT}/_{SEC}$
x = 23 IN.
⊙ NO OSCILLATION
▽ f = 75 C.P.S., ε = .050 IN.
── BLASIUS

Figure 6.45   Comparison of velocity profiles with and without oscillation (u_∞ =20, x=23, f=75)
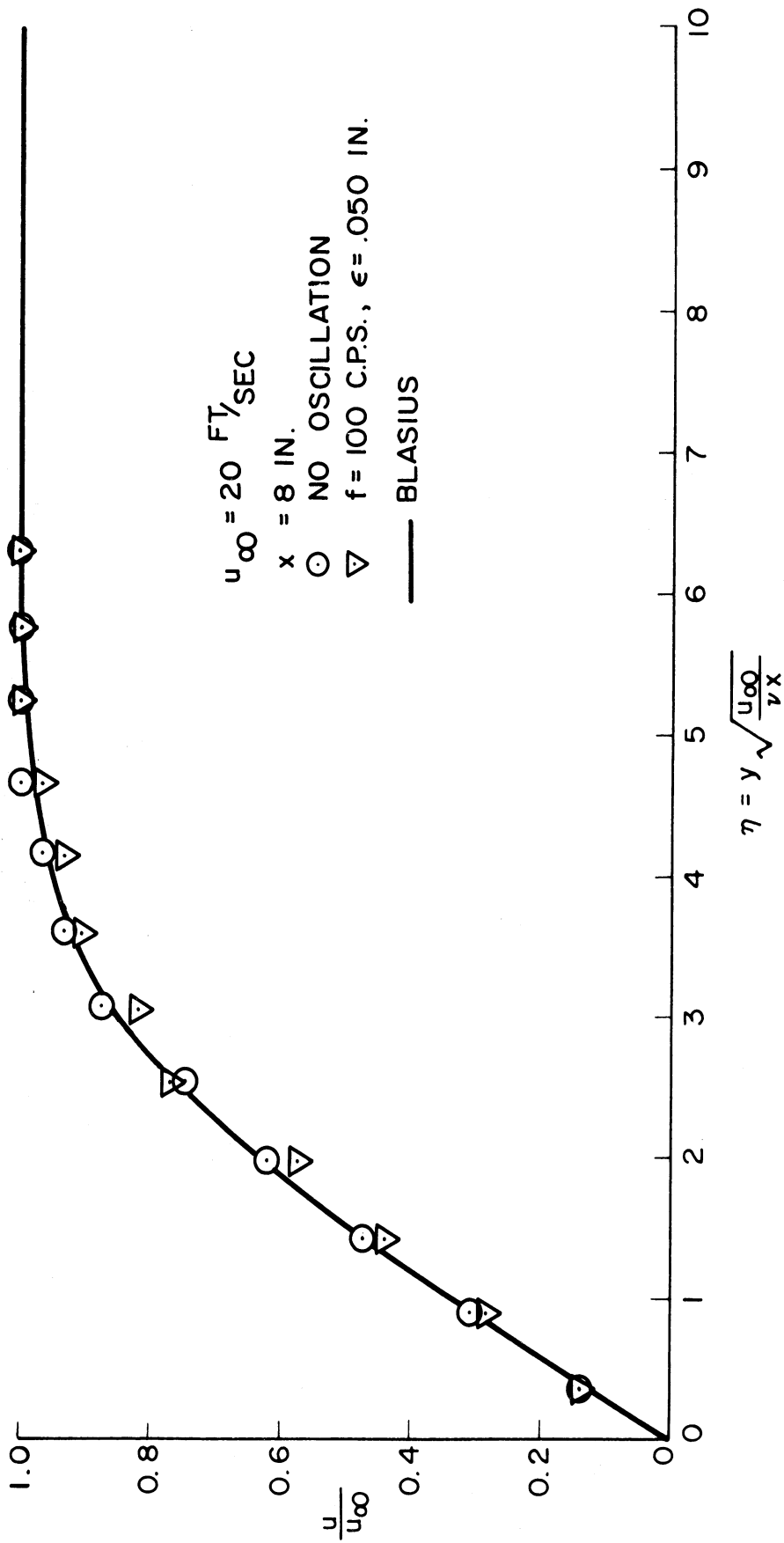
Figure 6.46   Comparison of velocity profiles with and
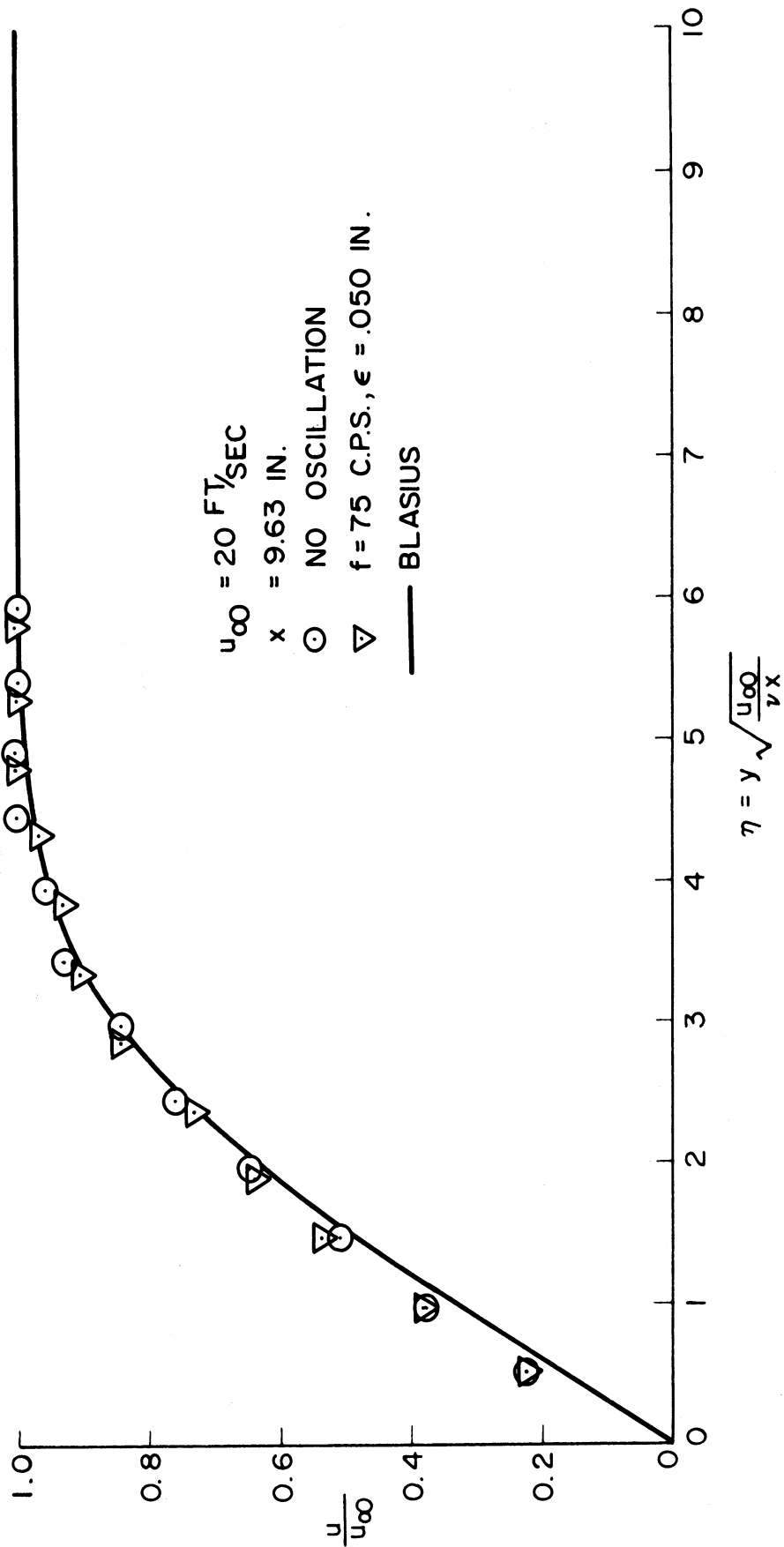without oscillation (u_∞ =20, x=8, f=100)
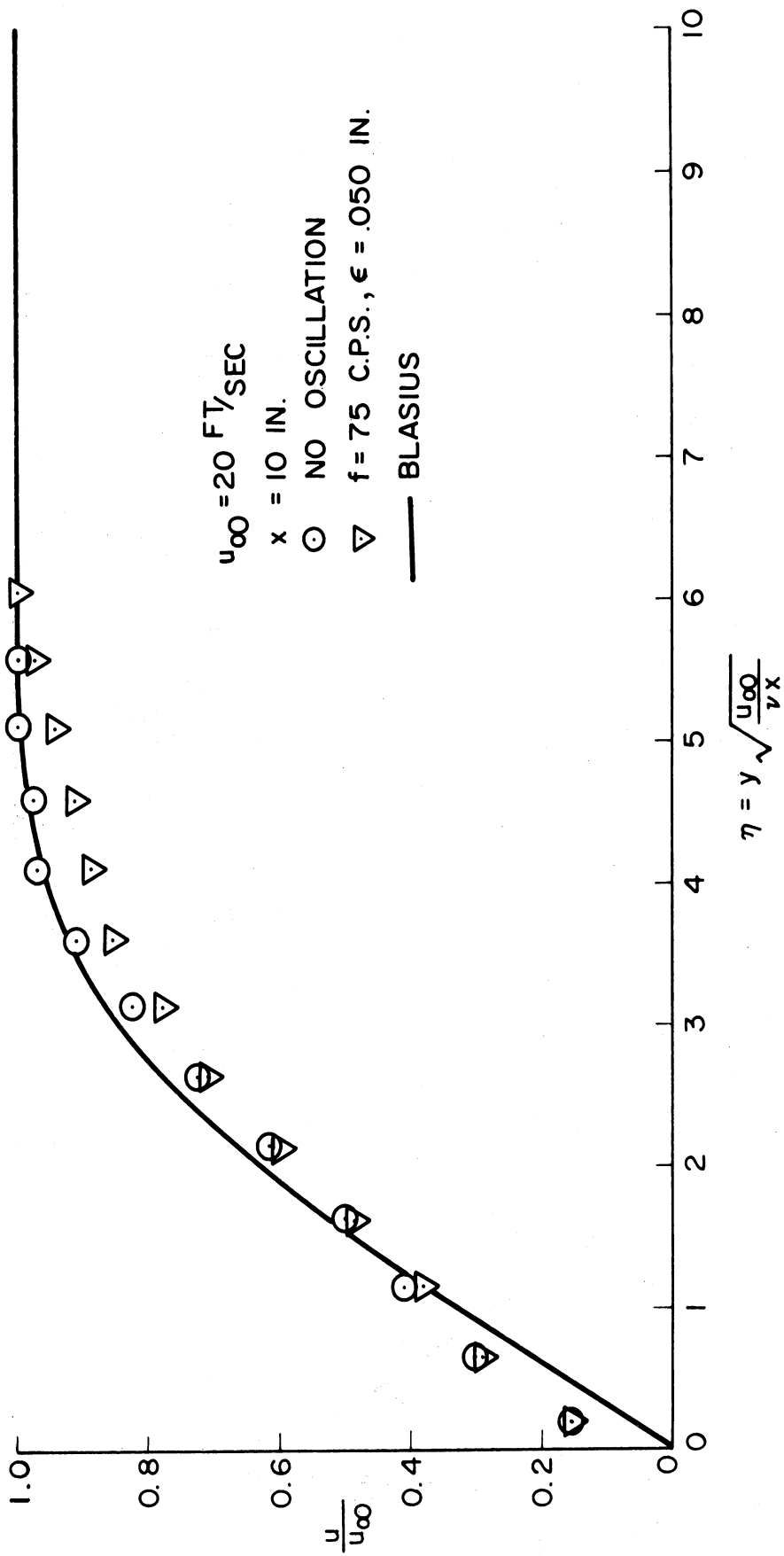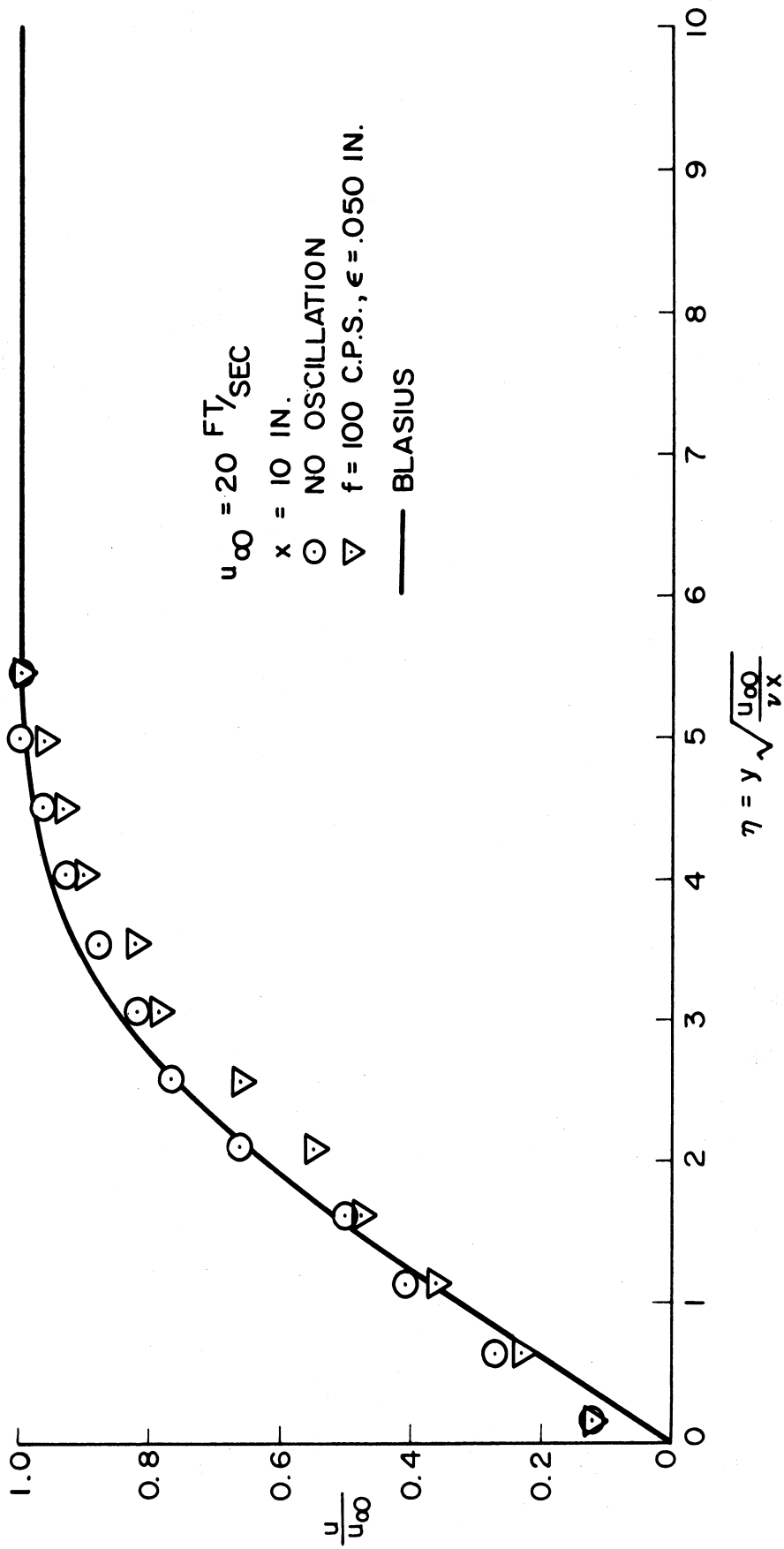
Figure 6.47 Comparison of velocity profiles with and without oscillation ($u_\infty = 20$, $x=10$, $f=100$)
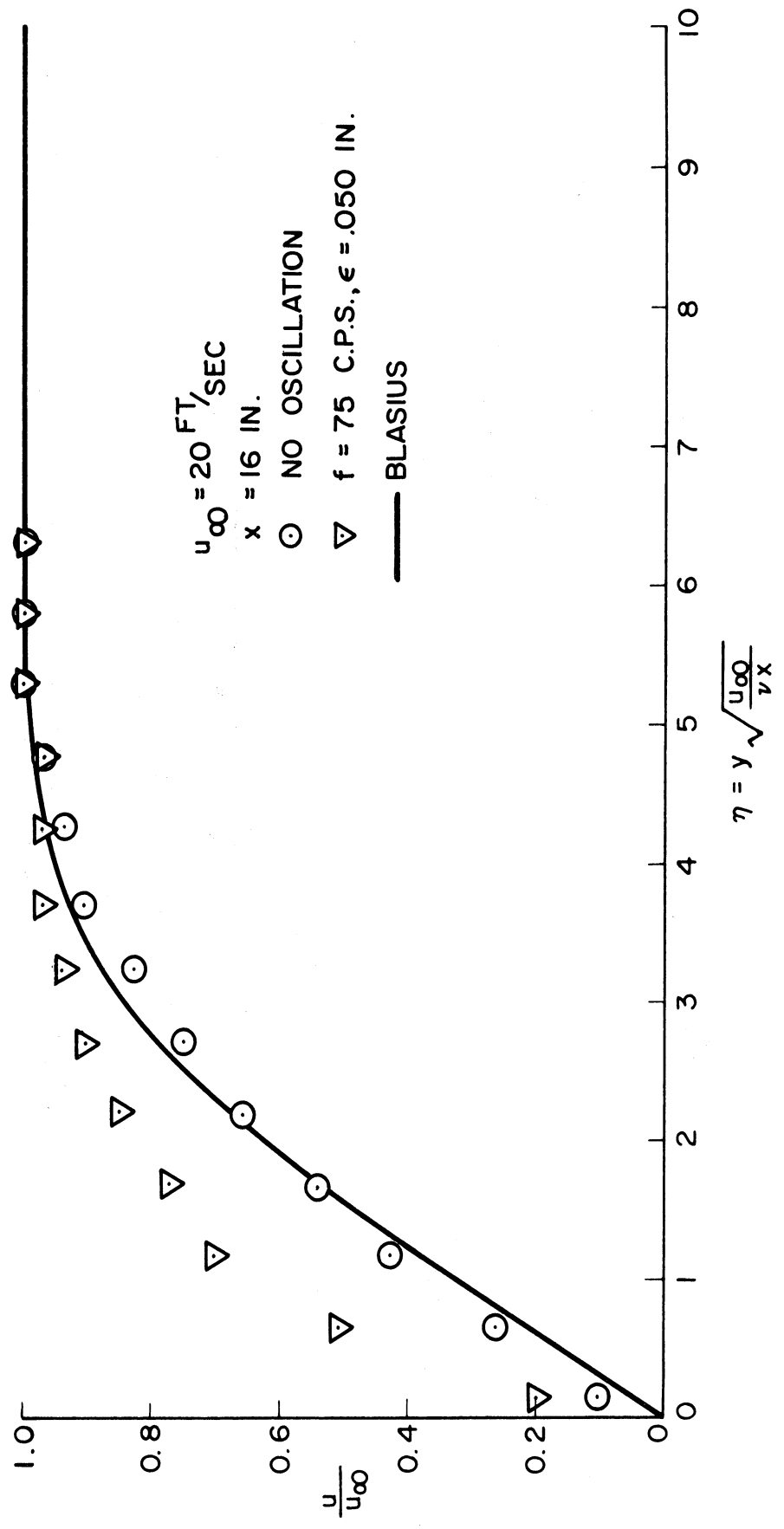
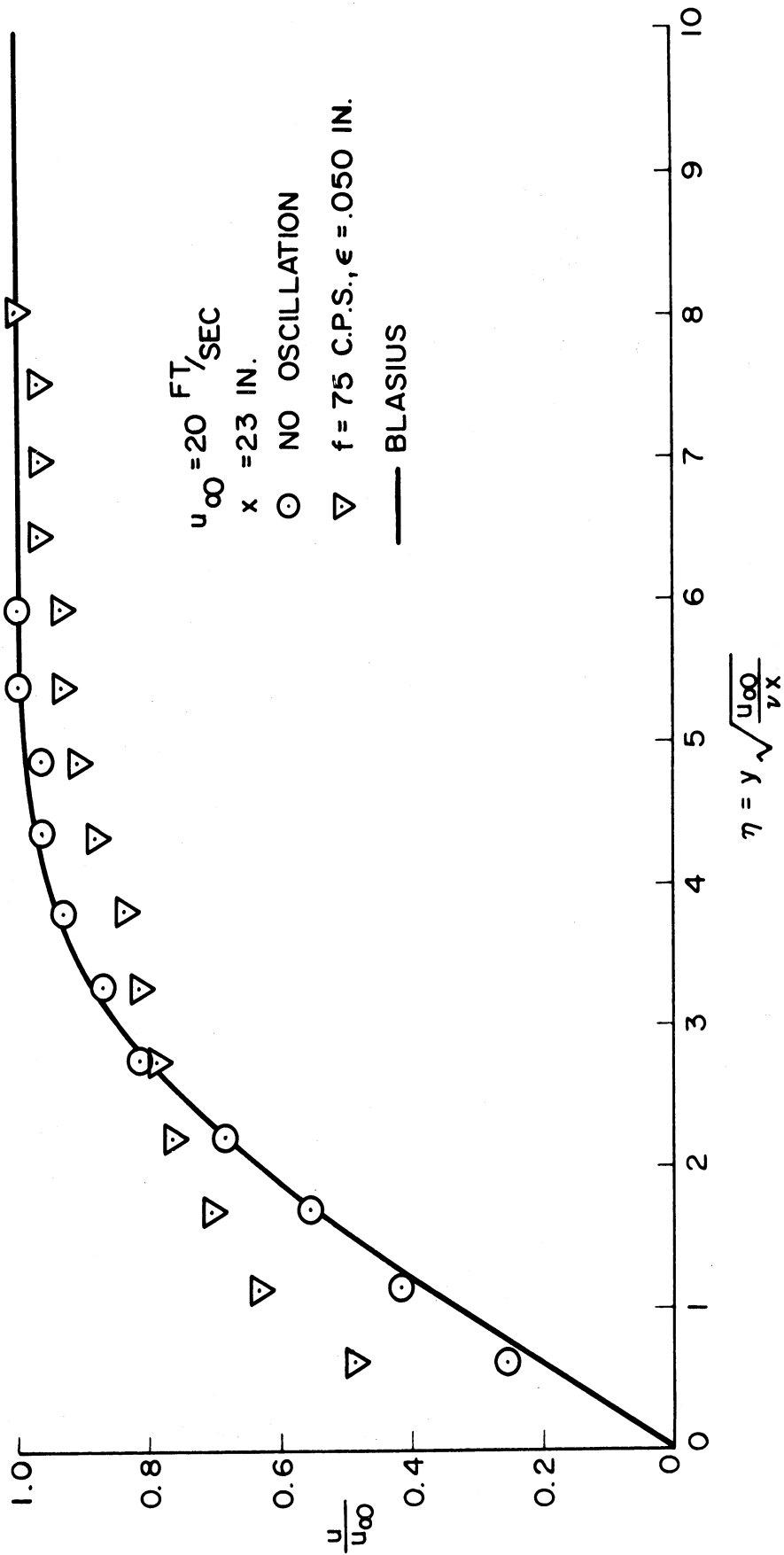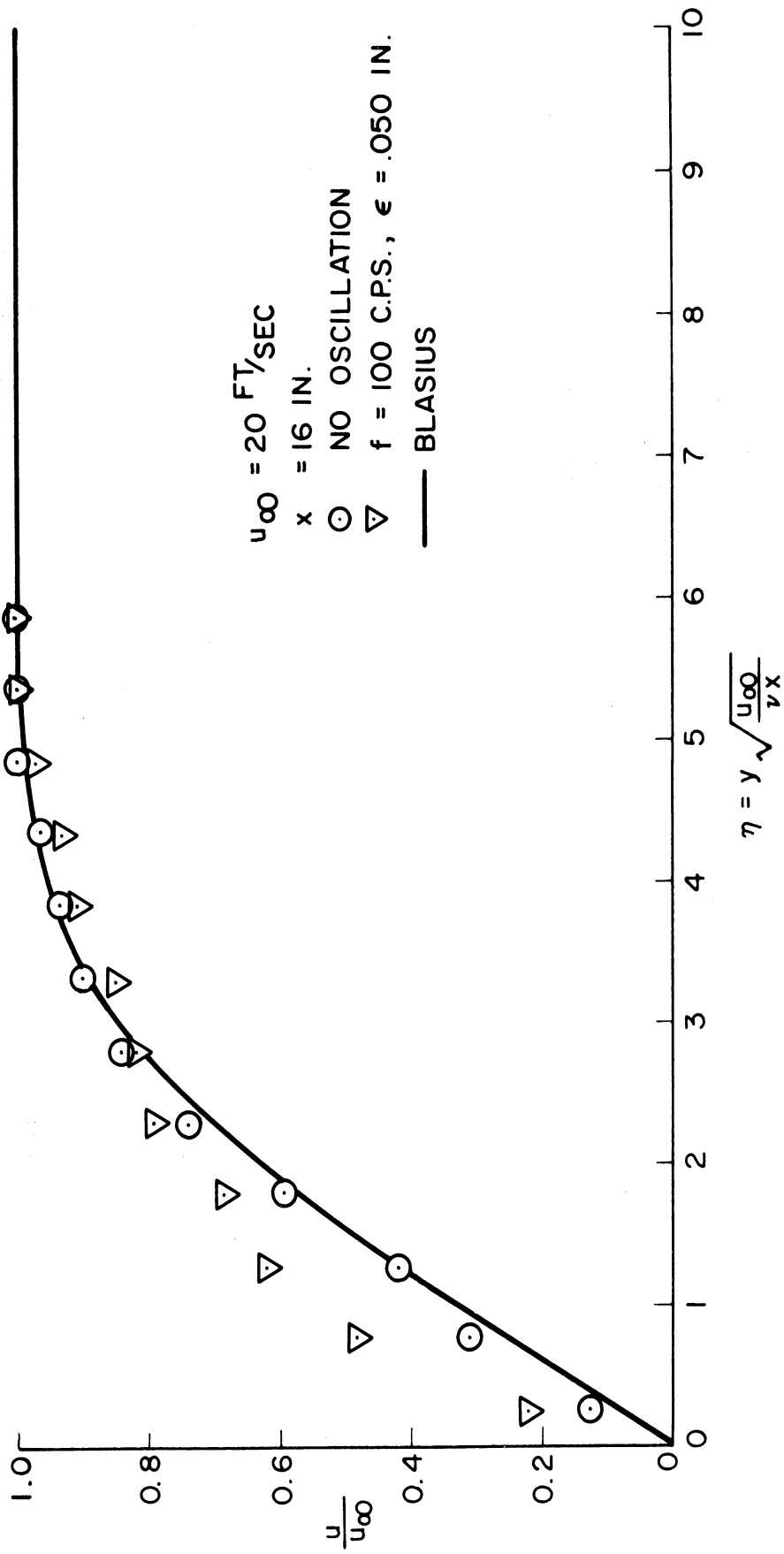Figure 6.48 Comparison of velocity profiles with and without oscillation ($u_\infty=20$, $x=16$, $f=100$)
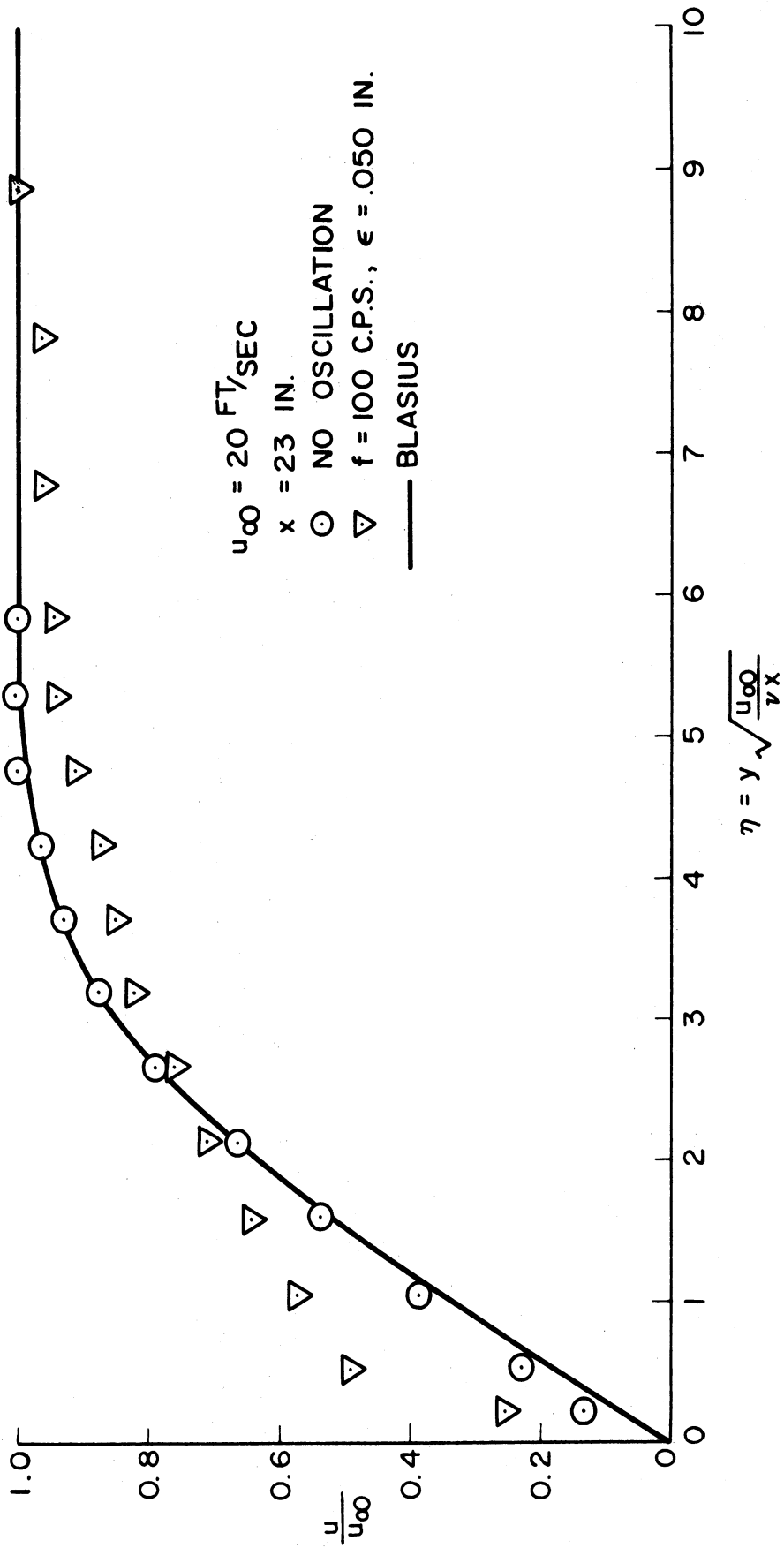
Figure 6.49 Comparison of velocity profiles with and without oscillation ($u_{\infty} =20$, $x=23$, $f=100$)
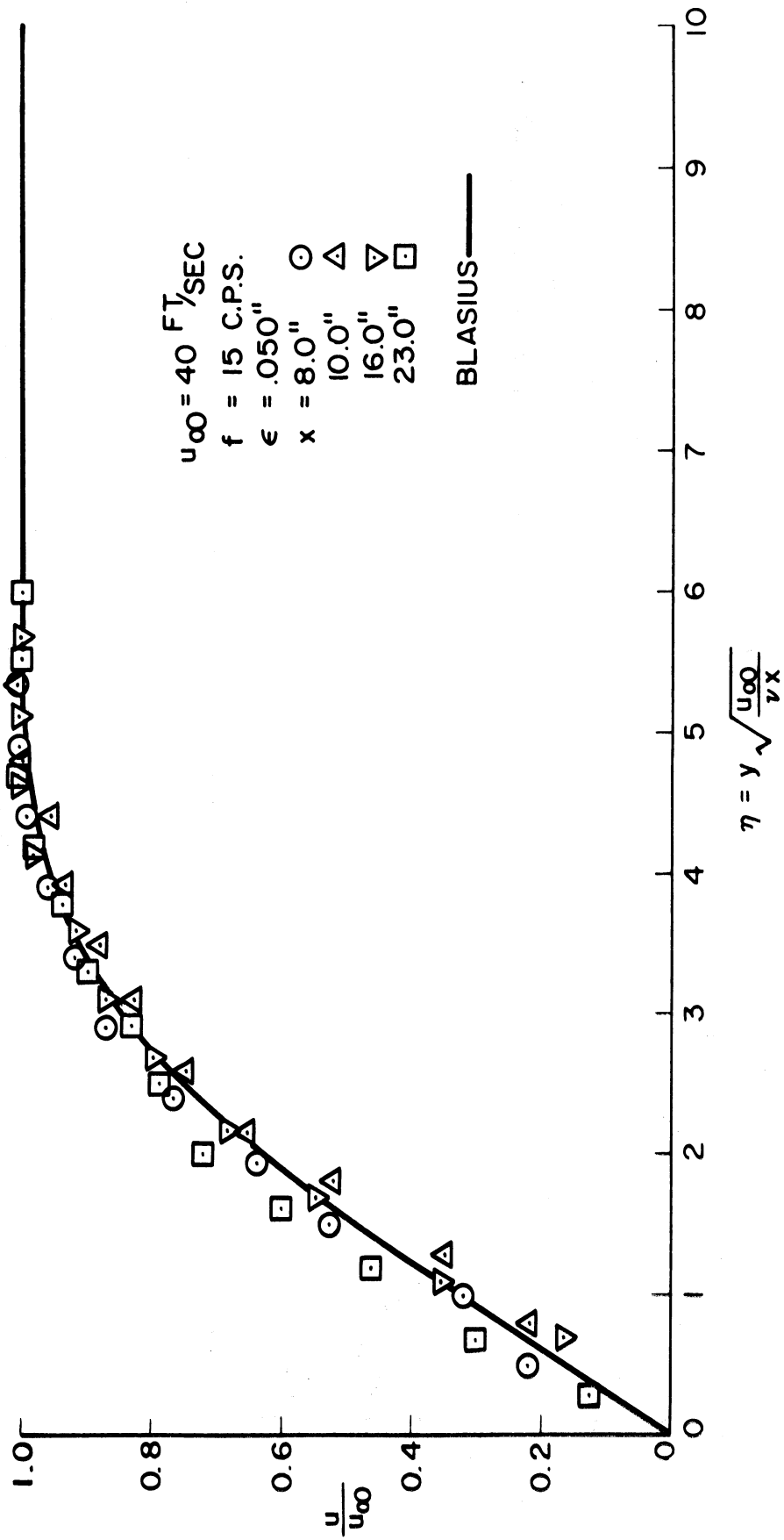
Figure 6.50 Profiles as a function of x
(u∞ =40, f = 15)
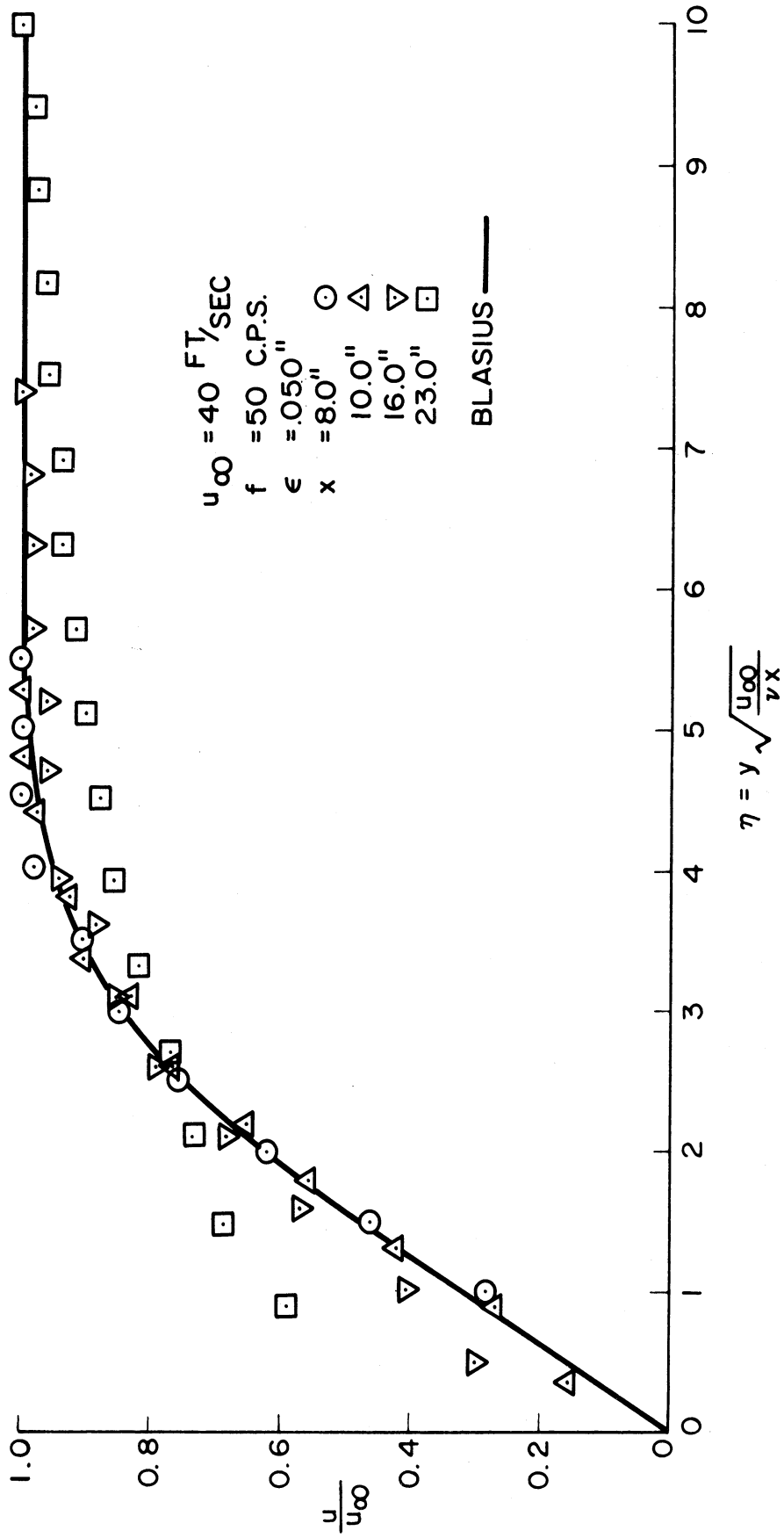
Figure 6.51 Profiles as a function of x
($u_\infty = 40$, f = 50)

Figure 6.52 Profiles as a function of x
$(u_\infty = 40,\ f = 75)$

Figure 6.53 Profiles as a function of x
(u∞ = 40, f = 100)

Figure 6.54 Profiles as a function of x
(u_∞ = 20, f = 15)
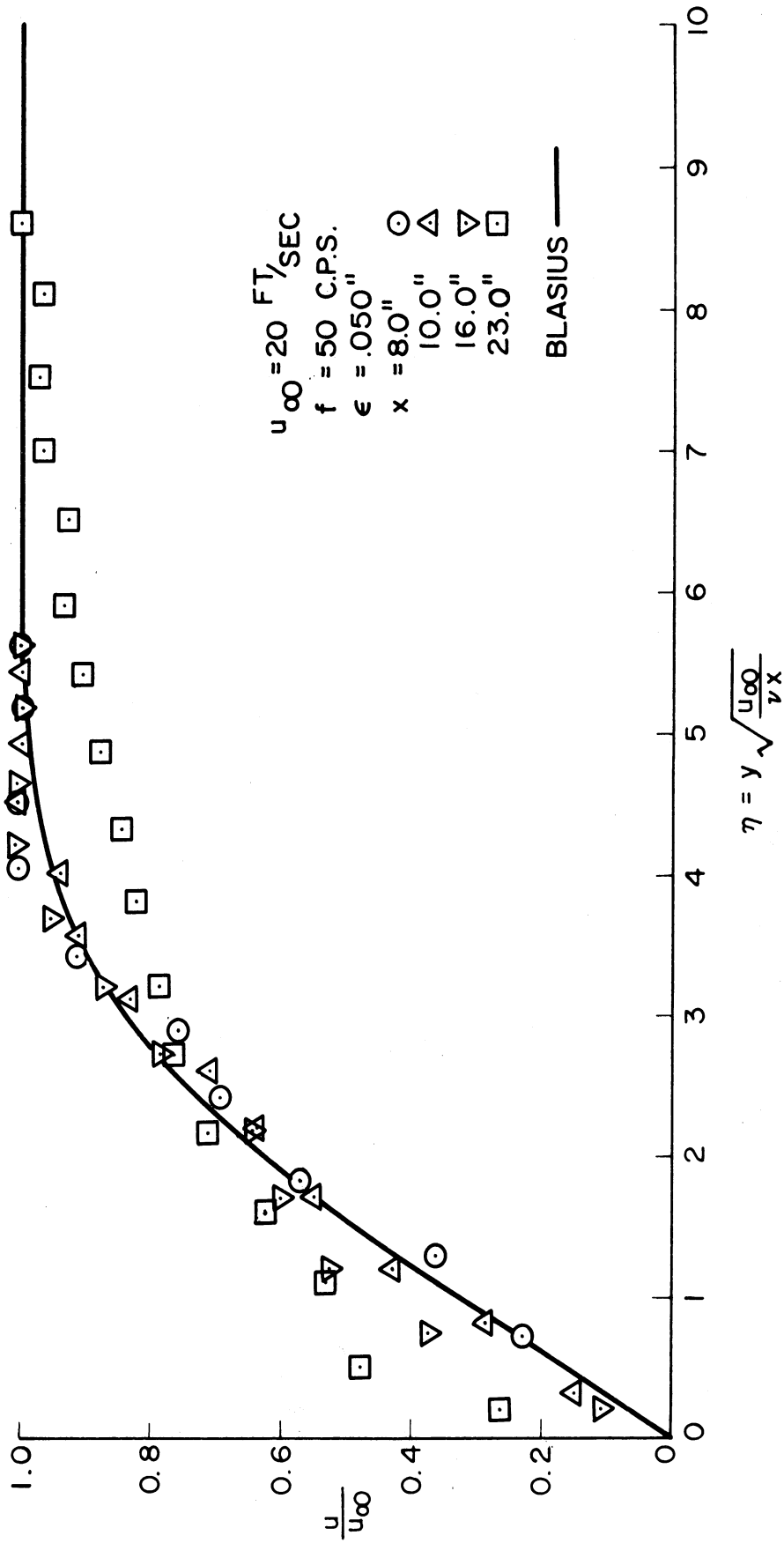
Figure 6.55 Profiles as a function of x
(u_∞ = 20, f = 50)

$\eta = y \sqrt{\dfrac{u_0O}{\nu x}}$

$\dfrac{u}{u_\infty}$

u_∞ = 20 $^{FT}/_{SEC}$
f = 50 C.P.S.
ϵ = .050"
x = 8.0"   ⊙
    10.0"   △
    16.0"   ▷
    23.0"   ⊡

BLASIUS ———
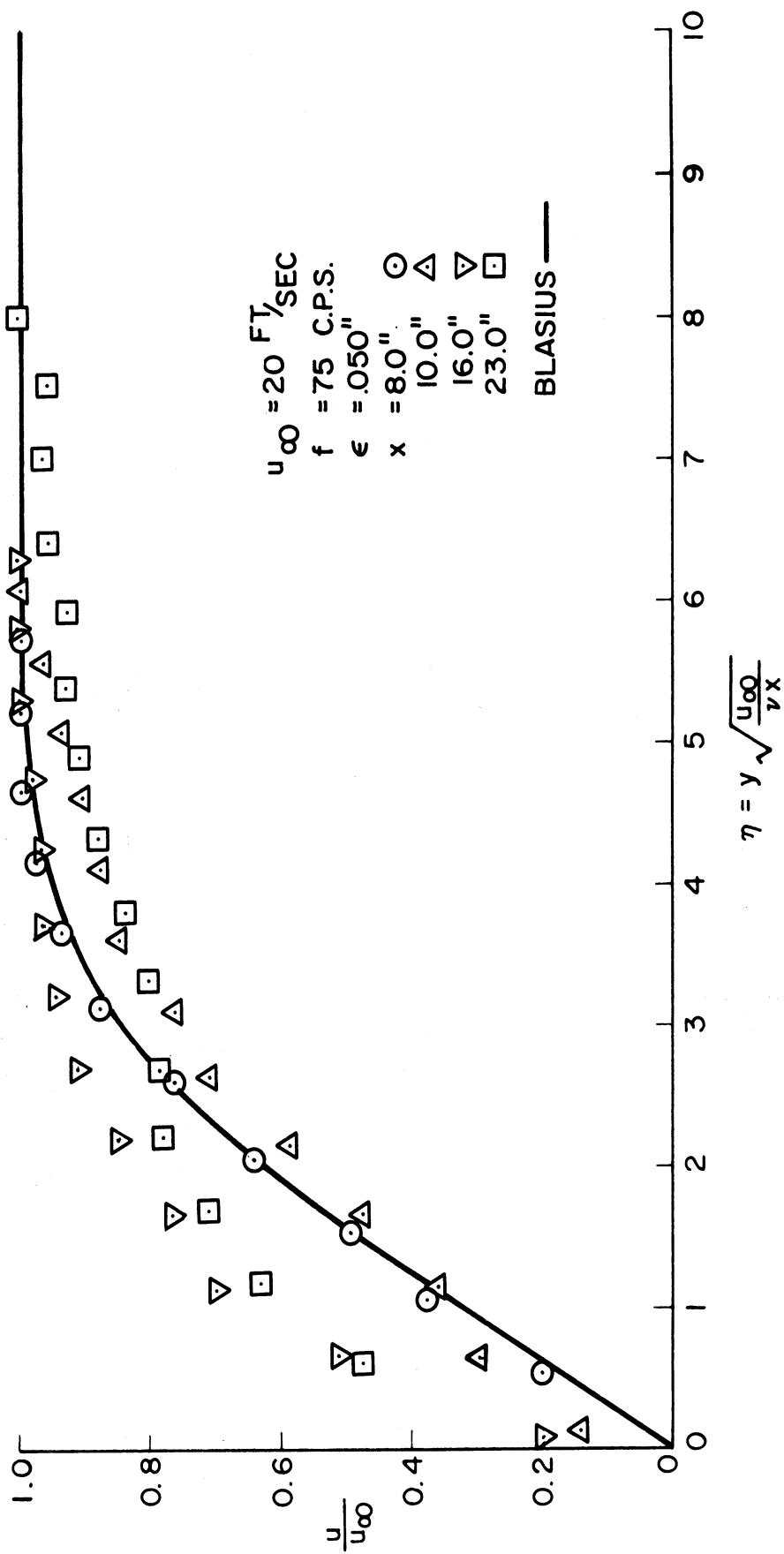
Figure 6.56 Profiles as a function of x
($u_\infty = 20$, f = 75)
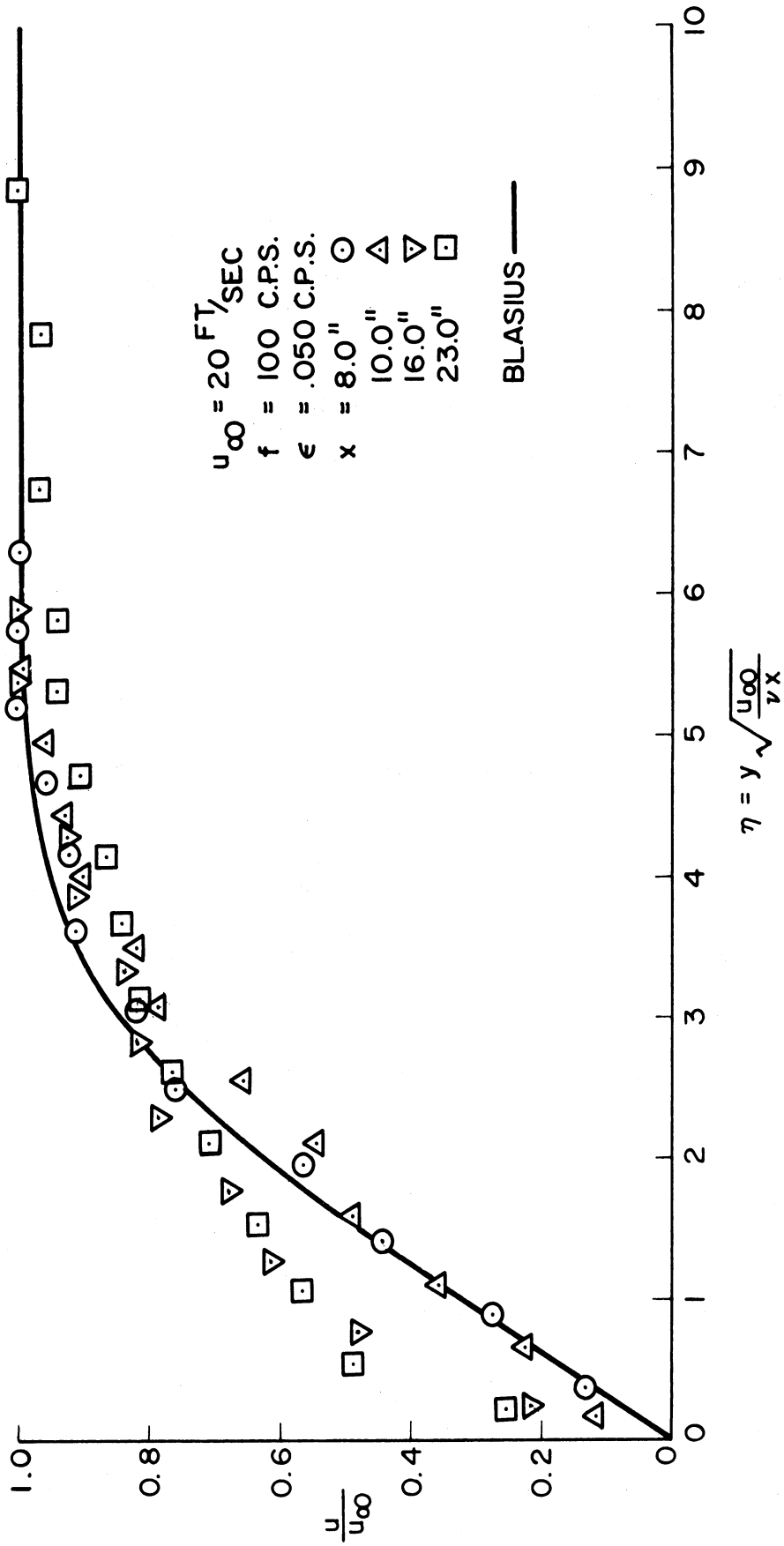
Figure 6.57 Profiles as a function of x
($u_\infty = 20$, f = 100)

6.6 Comparison of the time averaged oscillating profiles for various values of frequency.
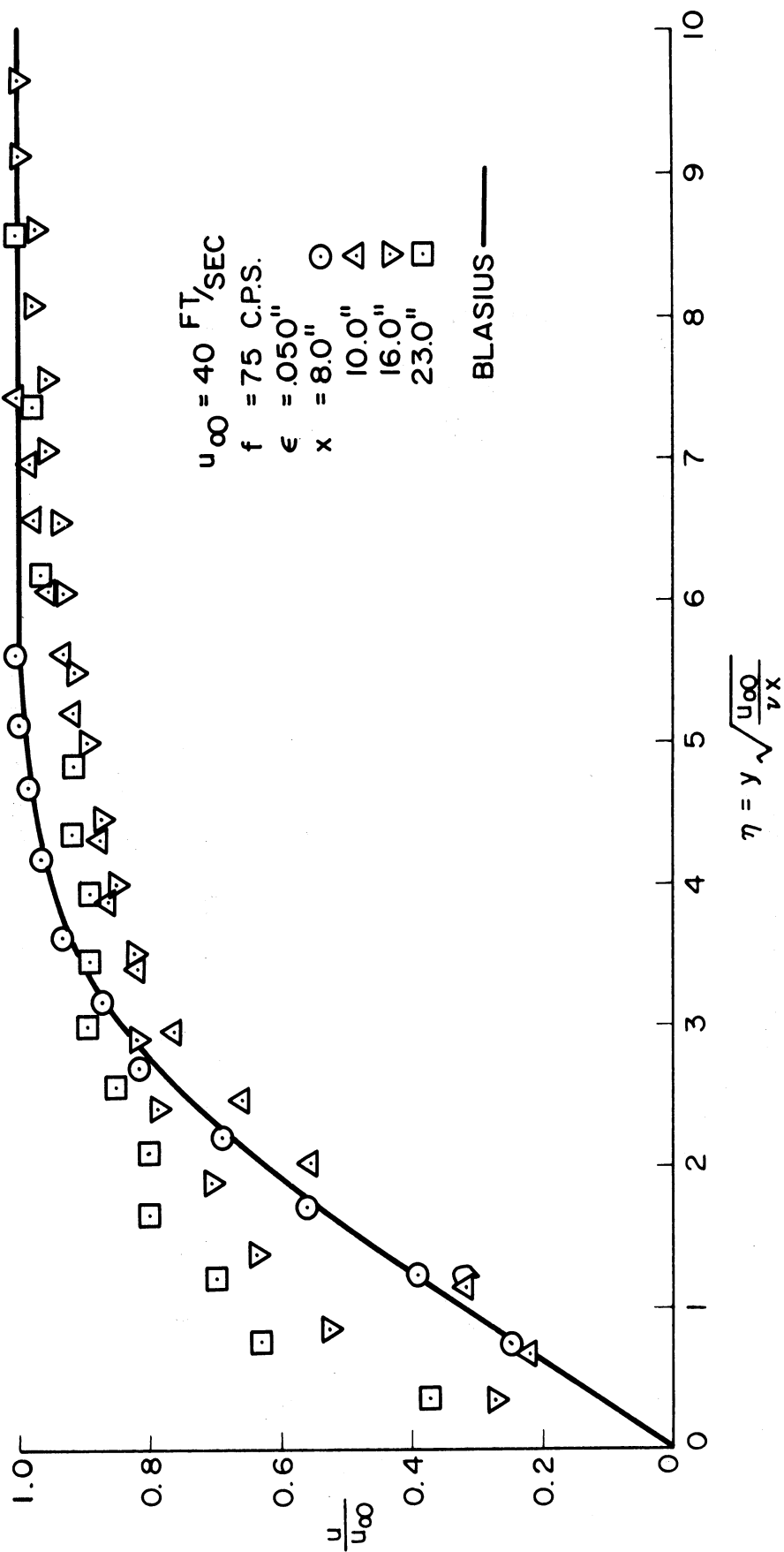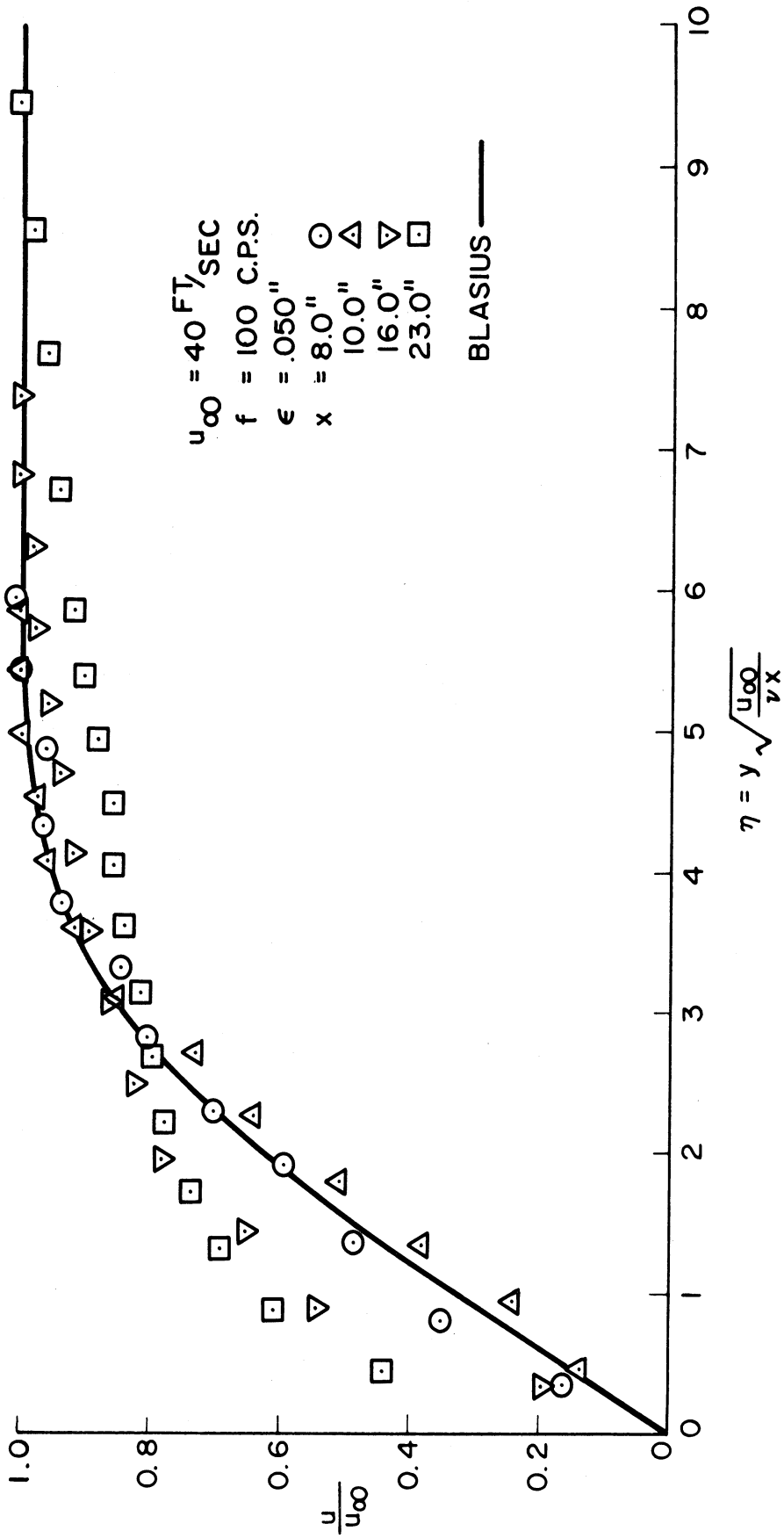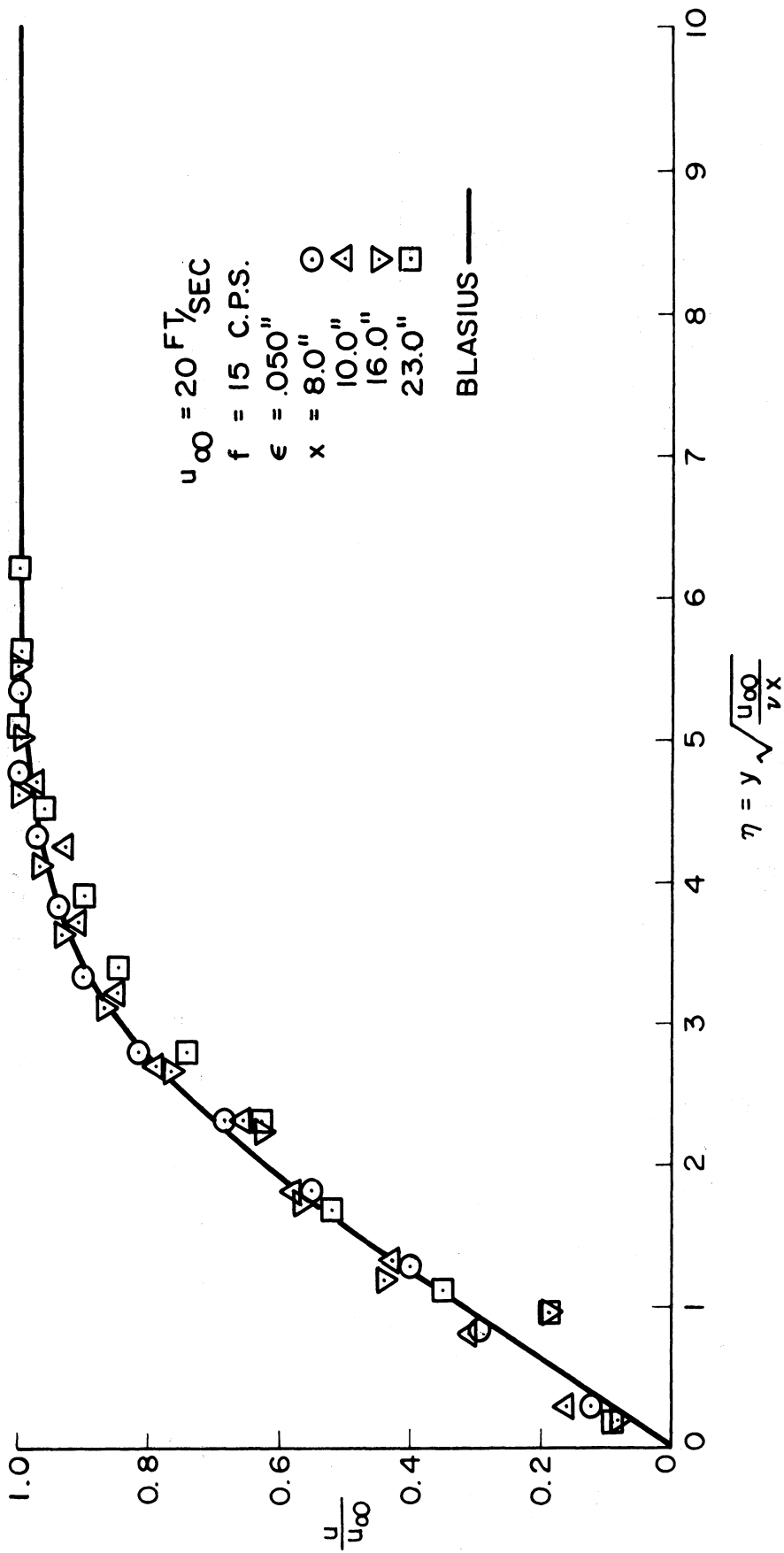
Figures 6.58 through 6.65 are a comparison of the oscillating profiles as a function of frequency with x and velocity held constant. Figures 6.58 through 6.61 are at a free stream velocity of 40 feet per second. Figure 6.58 indicates that at x = 8-inches the profiles all closely approximate the Blasius profile. At x = 10-inches in Figure 6.59 the profile for 75 cps decreases most markedly from the Blasius profile. At x = 16-inches in Figure 6.60 the profile for 15 cps closely approximates the Blasius profile. The profiles for 50 and 100 cps show the increase near the wall and the thickening of the boundary layer. The profile for 75 cps is a transition profile and shows the most deviation. The profiles at x = 23-inches in Figure 6.61 are transition profiles except for 15 cps which is a laminar profile closely approximating the Blasius profile. It is apparent that the maximum effect of the oscillation occurs at a frequency of 75 cps with a free stream velocity of 40 feet per second.

Figures 6.62 through 6.65 pertain to a free stream velocity of 20 feet per second. In Figure 6.62 the profiles at x = 8-inches again indicate a close approximation to the Blasius (2) profile. At x = 10-inches in Figure 6.63 the profiles progressively decrease from the Blasius profile as the frequency increases from 15 to 100 cps. At 75 cps a slight thickening of the boundary layer may be noted. Figure 6.64 at x = 16 inches indicates a progressive

Figure 6.58 Profiles as a function of frequency
($u_\infty = 40$, $x = 8$)

$$u_\infty = 40 \, ^{FT}/_{SEC}$$
$$x = 10.00''$$
$$\epsilon = .050''$$

f = 100 C.P.S.	⊙ △
75 C.P.S.	▽
50 C.P.S.	□
15 C.P.S.	

BLASIUS ———

$$\eta = y \sqrt{\frac{u_\infty}{\nu x}}$$
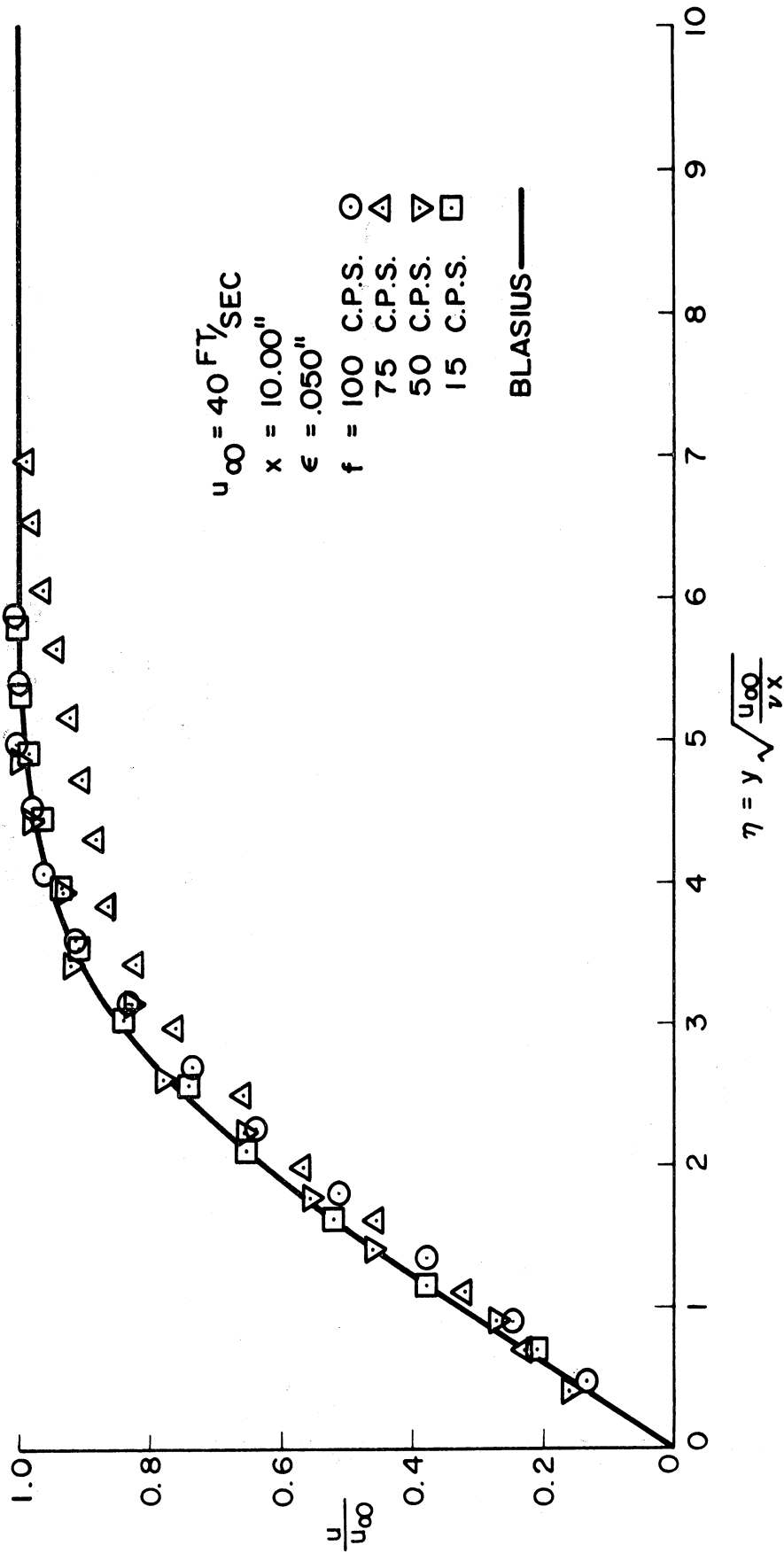
Figure 6.59 Profiles as a function of frequency
($u_\infty = 40$, x = 10)
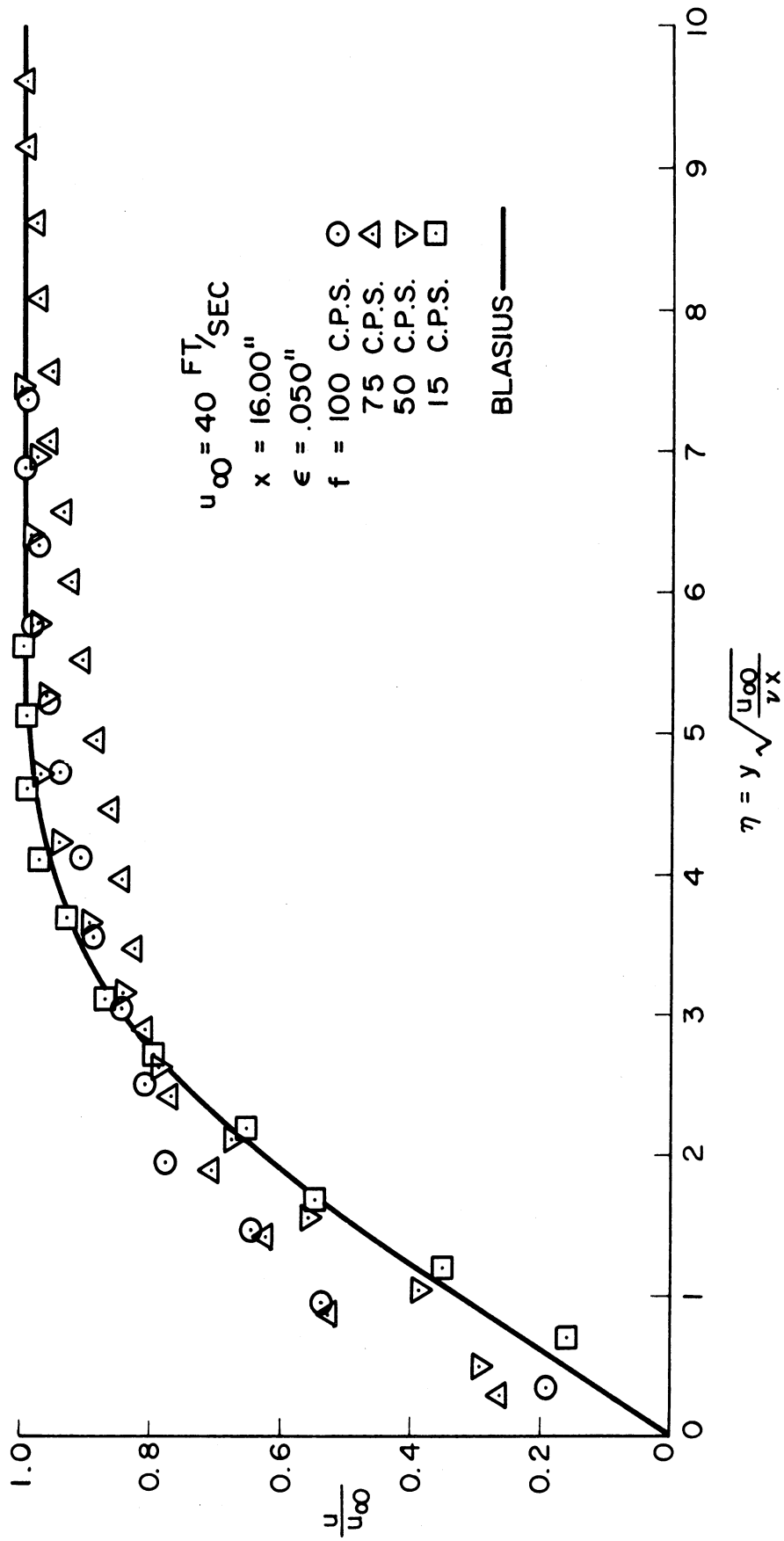
Figure 6.60 Profiles as a function of frequency
($u_\infty = 40$, $x = 16$)
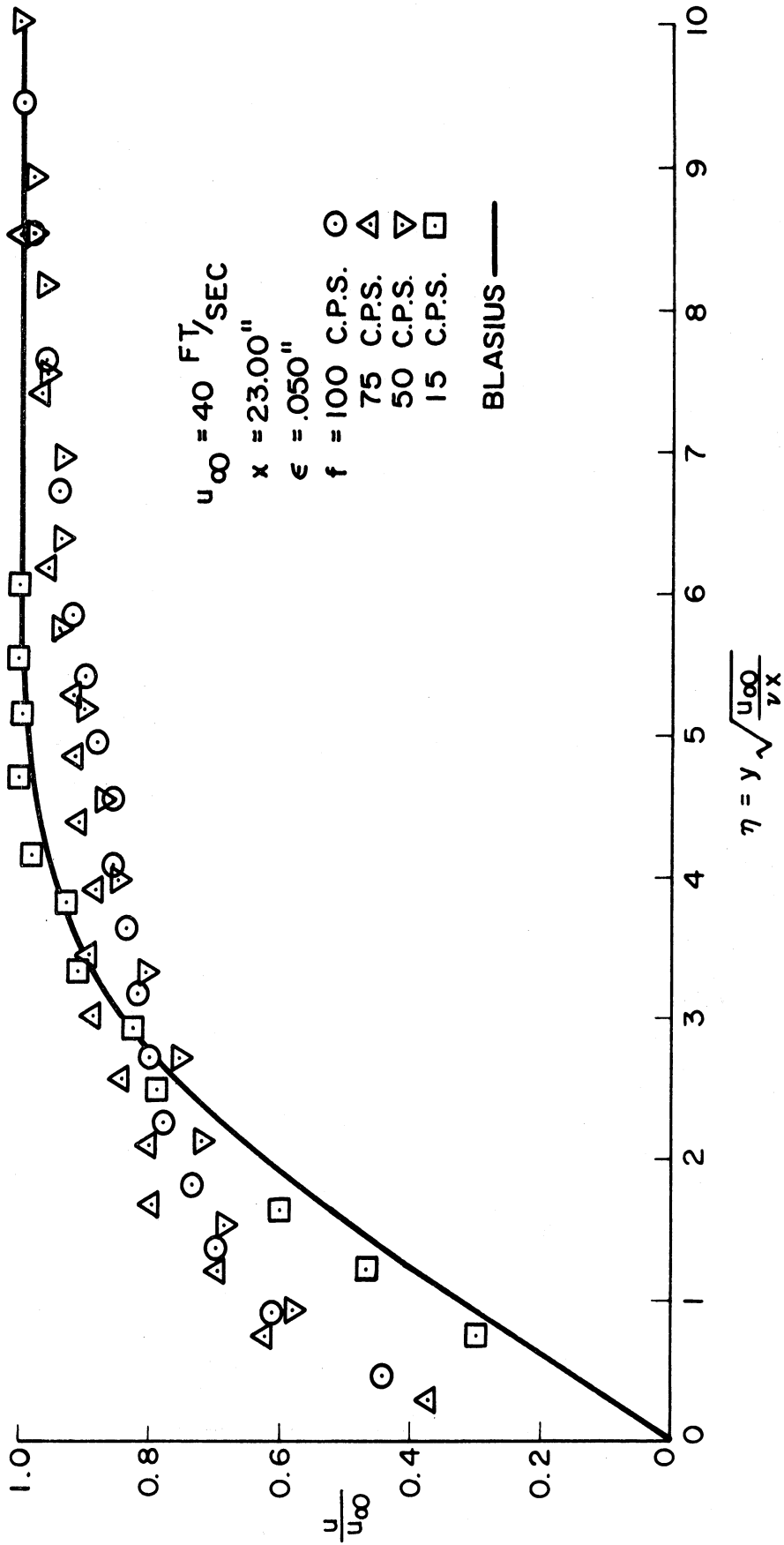
Figure 6.61 Profiles as a function of frequency
($u_\infty = 40$, $x = 23$)

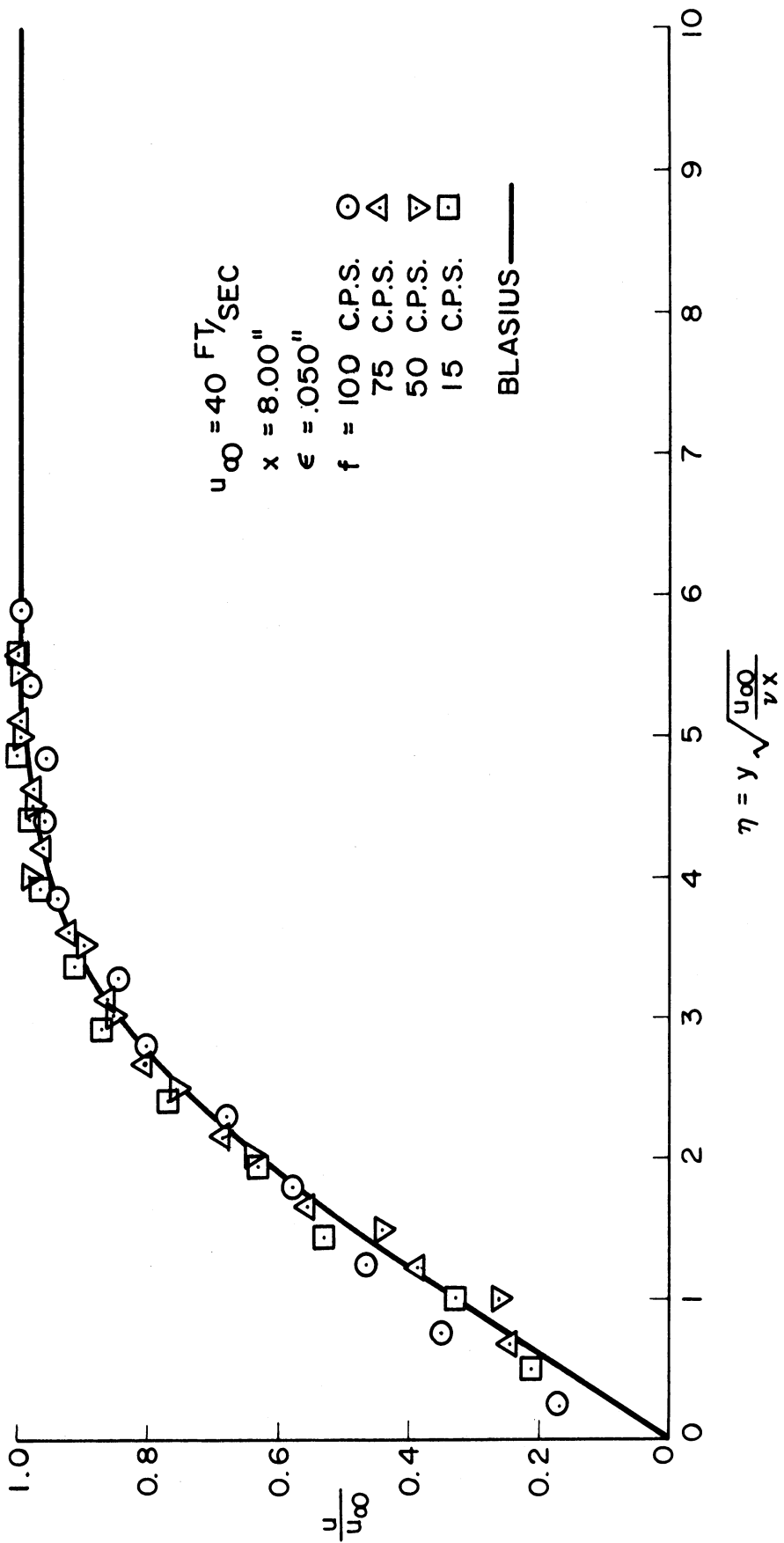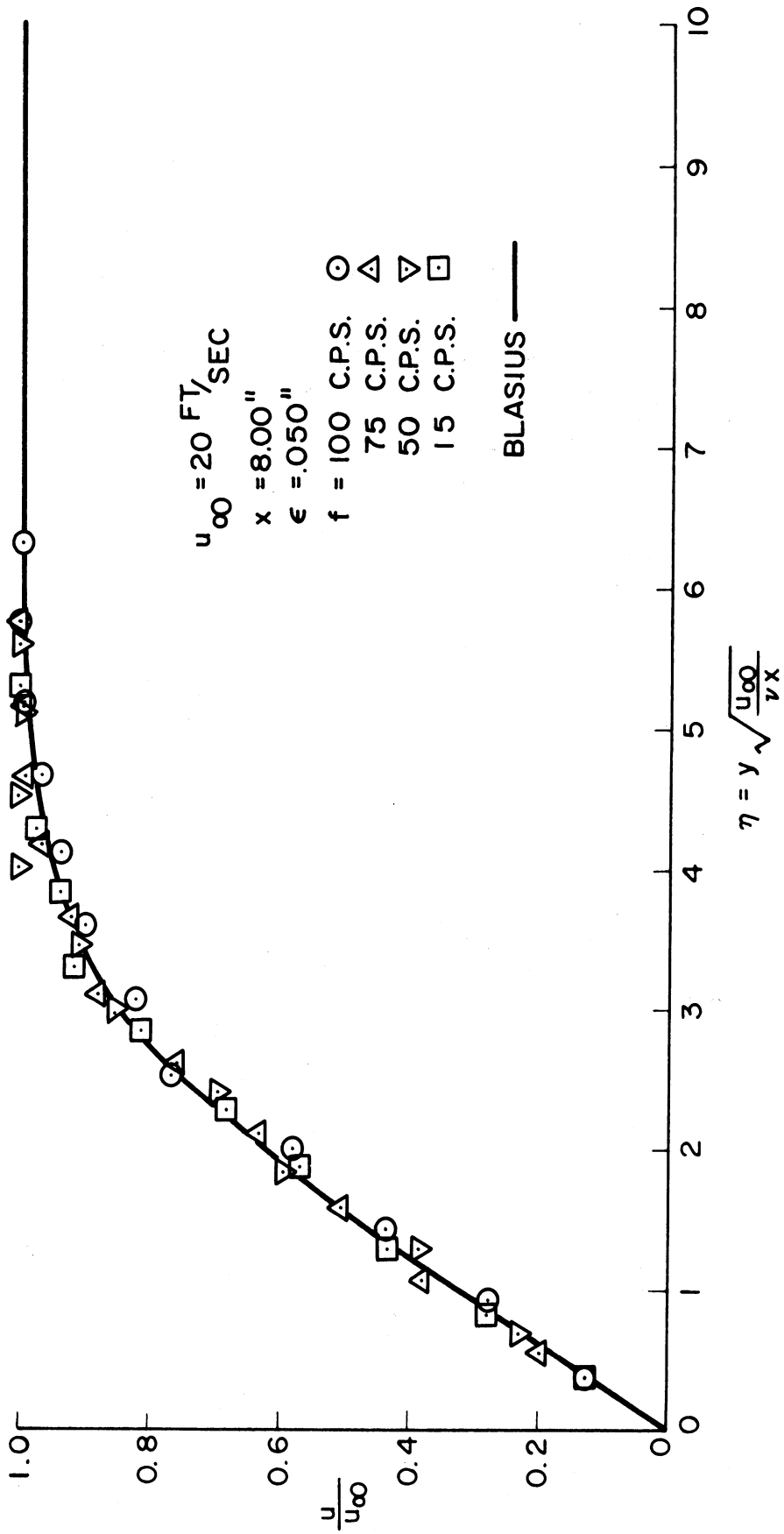Figure 6.62 Profiles as a function of frequency
(u ∞ = 20, x = 8)
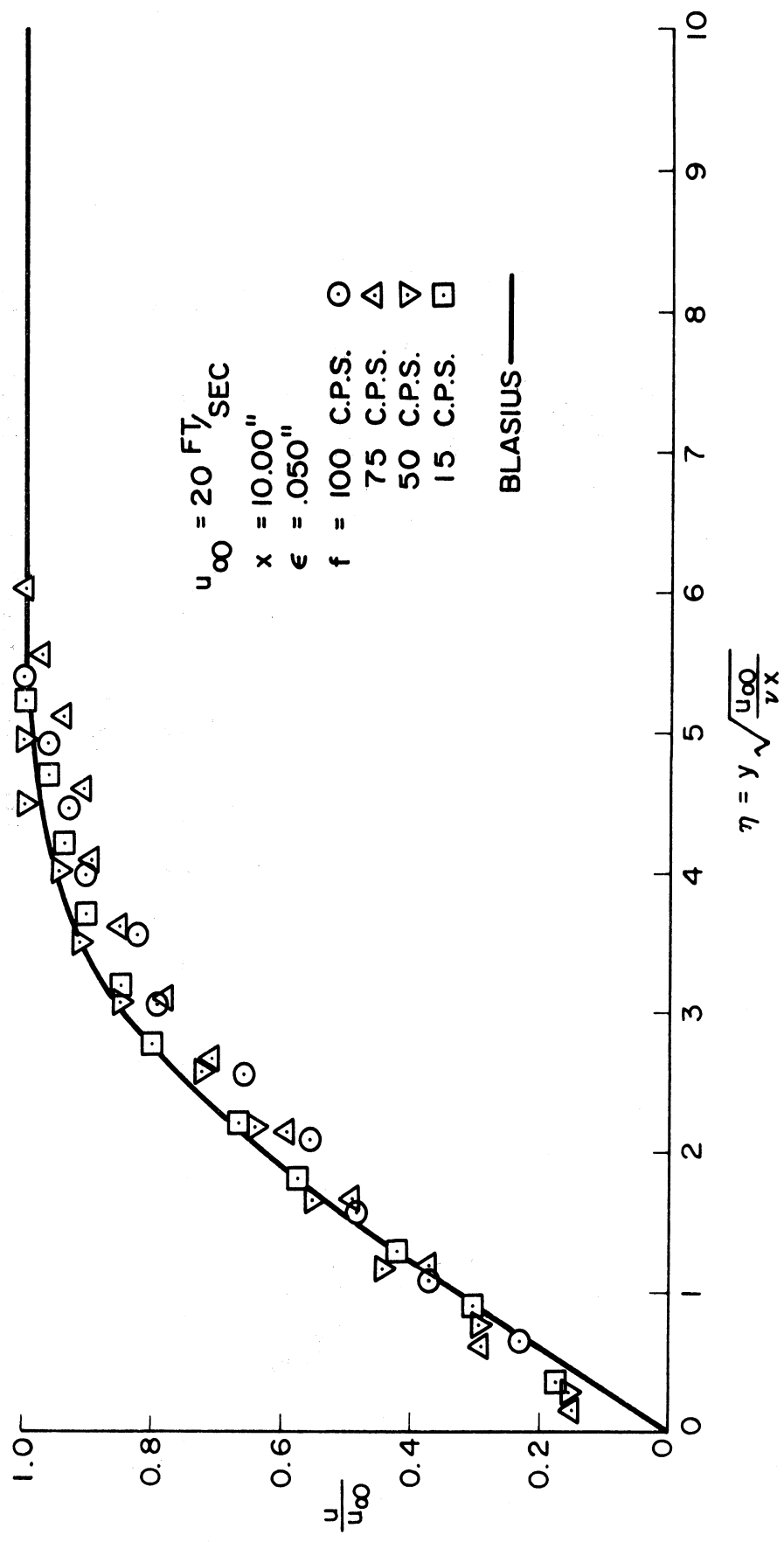
Figure 6.63 Profiles as a function of frequency
($u_\infty = 20$, $x = 10$)
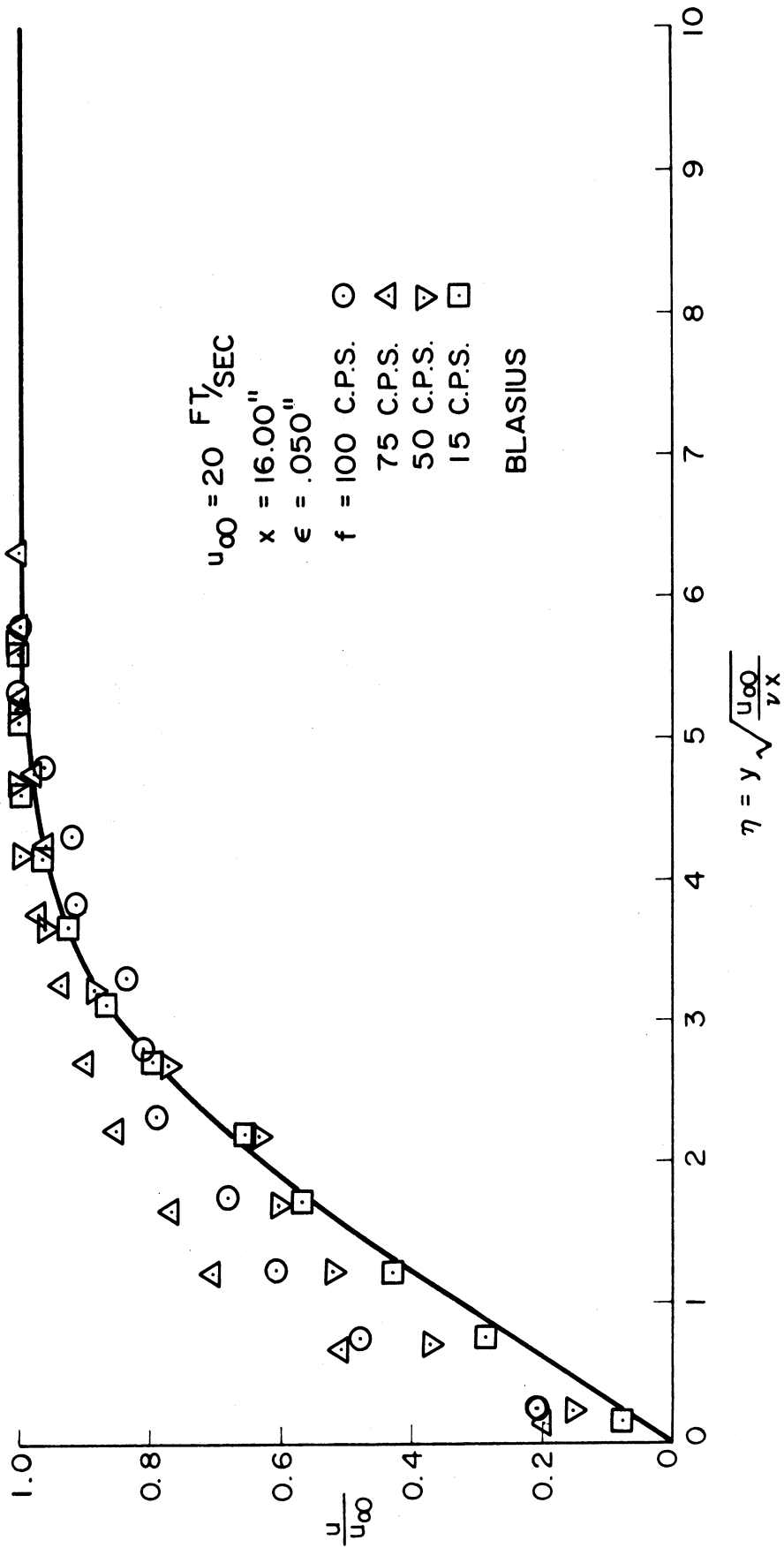
Figure 6.64 Profiles as a function of frequency
($u_\infty = 20$, $x = 16$)
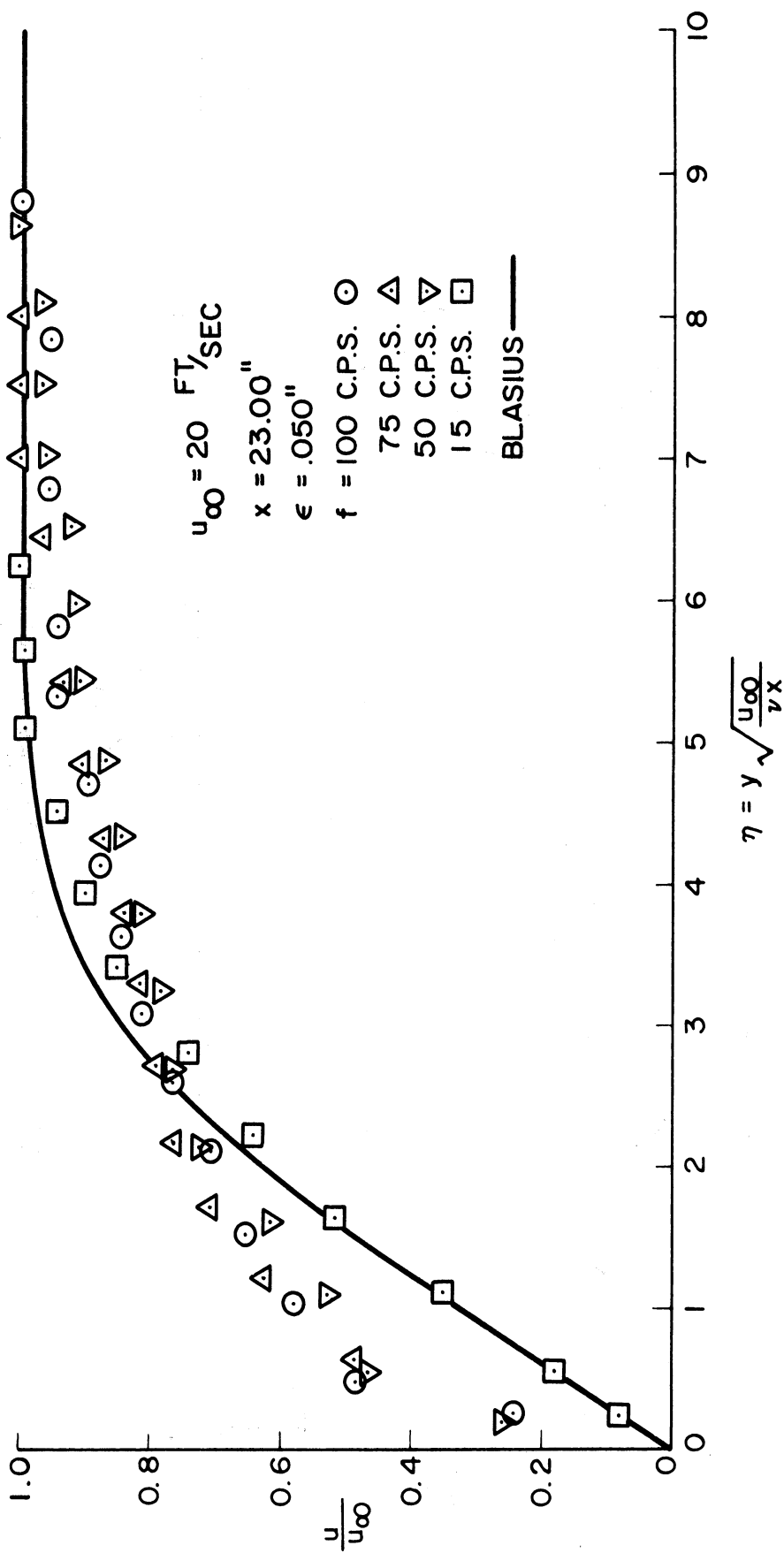
Figure 6.65 Profiles as a function of frequency
(u ∞ = 20, x = 23)

increase in the velocity profile from 15 to 75 cps.

At 100 cps the profile has begun the decrease in velocity

near the edge of the boundary layer. In Figure 6.65 for

x = 23-inches the profiles are transition profiles except

for the profile at 15 cps which is laminar but decreased

from the Blasius profile. There appears to be no

frequency within the range of frequencies studied that

produces a maximum effect for a free stream velocity of

20 feet per second.

Figure 6.66 is the difference between the Blasius

theoretical solution (2) and the experimental velocities for

the typical case of U_∞ = 40 feet per second and

f = 100 cycles per second. The plot is velocity difference

divided by the free stream velocity versus the Blasius η.

Only the profile at x = 10-inches appears to have a minimum

near η = 2.1 as predicted by the analytical solution

of Na (56). The transition profile at x = 23-inches has

a maximum at $\eta < 1$ and a minimum at about η = 4.5.

The profiles at x = 12 and 16 have maxima at about η = 1.5

and minima at about η = 3.5. The profile at x = 8-inches

also exhibits a small maximum and minimum but this may be

open to question because of the accuracy of the

measuring equipment.
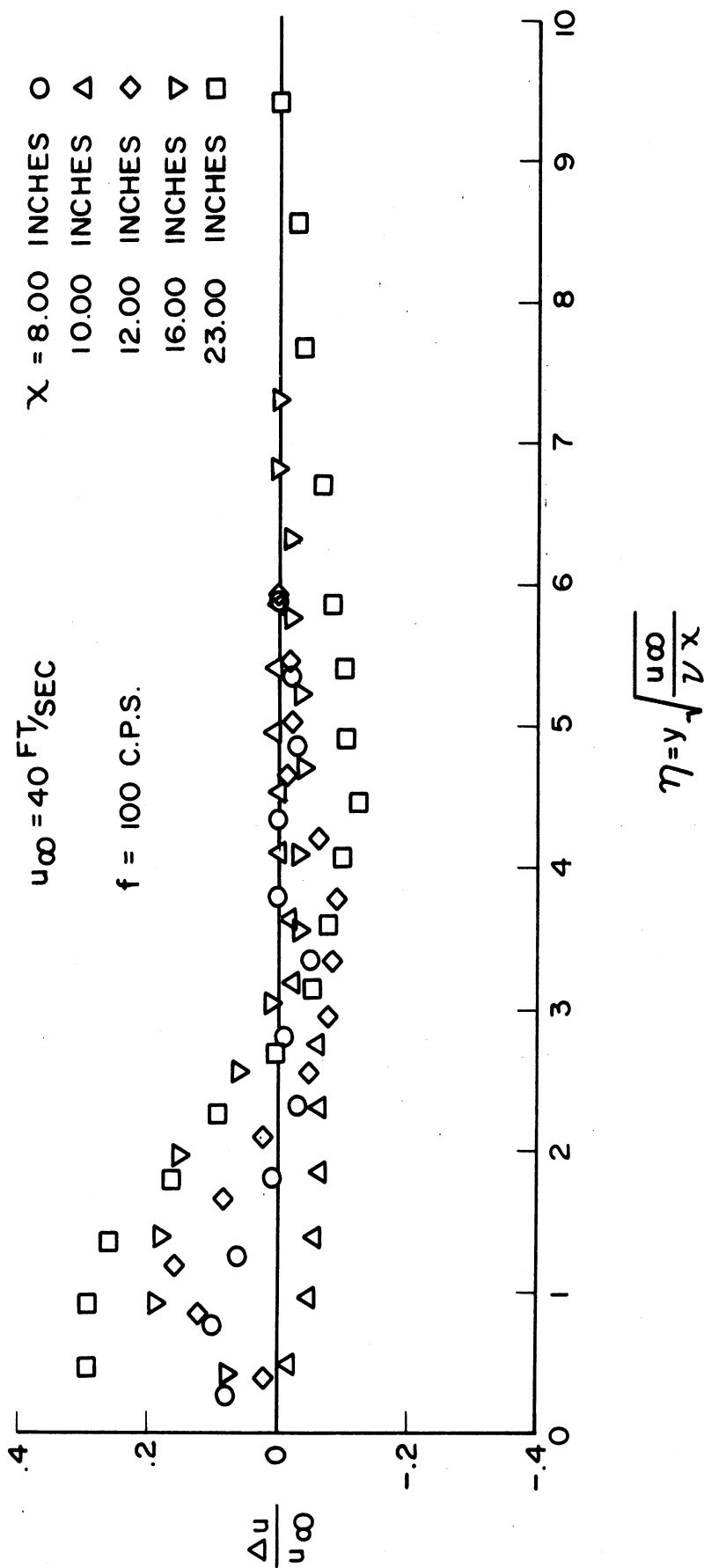
Figure 6.66 Oscillation Profile difference from
Blasius profile ($u_\infty = 40$, $f = 100$)

CHAPTER VII

Conclusions

Several definite conclusions may be made from the results of this investigation.

1. The analysis by Na(56) indicates that the maximum change in the mean value velocity profile for this type of oscillating flow occurs at $\eta \approx 2.1$. Fig. 6.66 shows that the maximum change in the experimental mean value velocity profiles occur at differing values of η . Nevertheless the experimental investigation shows that measurements made at various x and η = 2.1 will indicate the location of profiles in the oscillating flow that deviate from the Blasius (2) flow.

2. Separation will not occur behind a finite oscillating surface disturbance as large as 48% of the boundary layer thickness for velocities in the range tested, i.e., 20 to 40 ft/sec. This conclusion implies that the geometric shape of the disturbance is similar to the probability curve.

3. A definite change in the mean value velocity profile occurs for an oscillating disturbance of finite amplitude and is a function of free stream velocity, frequency, and position downstream from the disturbance. Immediately downstream of the disturbance the mean velocities at various η decrease. Subsequently, further downstream the mean velocities increase with respect to the mean

profile velocities without the disturbance. The

analysis by Na(56) for very small disturbances also in-

dicates the downstream decrease in mean velocities and

the subsequent increase. Unfortunately, quantitative

values obtained from the theory do not adequately pre-

dict the geometric location on the plate for the

decrease or increase. Therefore, the analysis by Na can

only be considered qualitatively valid for disturbances

of finite magnitude in the region downstream from the

membrane.

4. The data for 40 ft/sec indicate a maximum change in

the mean value velocity profiles at 75 cps. The entire

range from 50 to 100 cps lies below the neutral

stability curve in the damping region. Thus, the maxi-

mum in the experimental data is not explained by the

stability theory.

5. Thickening of the laminar boundary layer occurs

for an oscillating surface disturbance in a similar

manner to the thickening for a stationary bulge. The

present investigation indicates a thickness of up to

45% in excess of the boundary layer without the disturbance.

The boundary layer edge is defined as 99% of the free

stream mean velocity.

6. Early transition from laminar to turbulent flow is

definitely promoted in the frequency range of 50 cps

to 100 cps.

APPENDIX

Eccentric and connecting rod design and balance.

The eccentric configuration is shown in Figure A-1 and the counterweight configuration in Figure A-2.

Center of gravity for eccentric.

$$-\pi k^2 z = \pi D^2 (\epsilon - z)$$

(A-1)

$$z = \frac{D^2 \epsilon}{D^2 - k^2}$$

Eccentric unbalance .

$$\left[\pi/4 \, \rho_B \, (D^2 - k^2) \ell_c \right] \frac{D^2}{D^2 - k^2} \, \epsilon = \pi/4 \, \rho_B \, \ell_c \, D^2 \epsilon$$

(A-3)

where ρ_B = 0.3048 Lbm/in^3

The connecting rod rotating unbalance is $m_1 \epsilon$ where m_1 is the connecting rod crank end mass (0.050 Lbm). The connecting rod reciprocating unbalance is $\frac{1}{2}m_2 \epsilon$ where m_2 is the connecting rod wrist pin end mass (0.050 lbm). The total eccentric and connecting rod unbalance is,

$$\pi/4 \, \rho_B \ell_c \, D^2 \epsilon + \frac{1}{2} m_2 \epsilon + m_1 \epsilon$$

(A-4)

The counterweight ring unbalance is,

$$\rho_B \pi \left[r^2 - \left(\frac{D}{2}\right)^2 \right] \ell_{cw} \epsilon \qquad \text{(A-5)}$$

The total unbalance is,

$$\frac{\pi}{4} \rho_B \ell_c D^2 \epsilon + \frac{1}{2} m_2 \epsilon + m_1 \epsilon + \rho_B \pi \left[r^2 - \left(\frac{D}{2}\right)^2 \right] \ell_{cw} \epsilon \qquad \text{(A-6)}$$

The unbalance of the counterweight is,

$$\rho_B (0.00873)(150)(I^2 - r^2)(h - \epsilon) \ell_{cw} =$$
$$\rho_B (0.00873)(150)(I^2 - r^2)\left\{(38.197)\left(\frac{I^3 - r^3}{I^2 - r^2}\right) \frac{\sin 150}{150} - \epsilon\right\} \ell_{cw} \qquad \text{(A-7)}$$

The total unbalance is set equal to the unbalance of the counterweight and the resulting expression solved for outside radius I with ϵ a specified parameter. Therefore, for each eccentric a set of counterweights must be constructed.

The resulting expression is a cubic equation in I with the parameter ϵ as follows,

$$I^3 - 7.854 I^2 \epsilon - 5.354 \epsilon - 0.0406 = 0 \qquad \text{(A-8)}$$

For an eccentric with a stroke of ϵ = 0.050 inches the outside radius I is 0.803 inches.
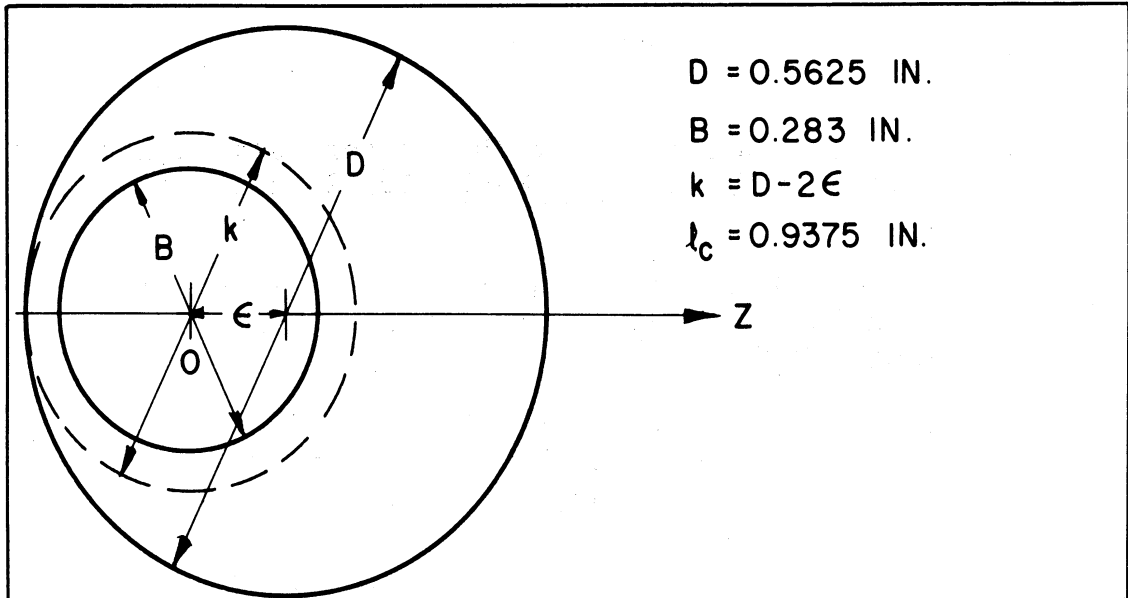
D = 0.5625 IN.

B = 0.283 IN.

k = D-2ϵ

ℓ_c = 0.9375 IN.

Figure A.1   Eccentric configuration

D = 0.5625 IN.

r = 0.3438 IN.

ℓ_{cw} = 0.500 IN.
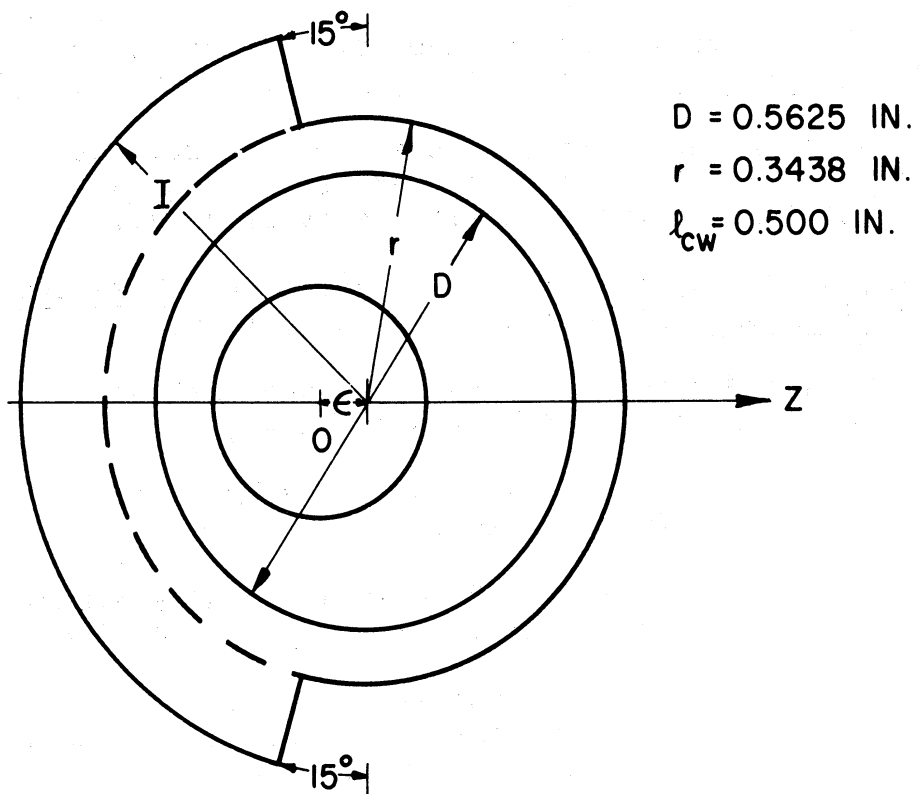
Figure A.2   Counterweight configuration

REFERENCES

1. Benney, D.J., "A Non-Linear Theory for Oscillations in a Parallel Flow", J. Fluid Mech. 10, 2 Mar. 1961, 209-236.

2. Blasius, H. "Grenzschichten in Flussigkeiten mit kleiner Reibung". Zeit, Mathe, Phys. 56, 1908, p.1, Also NACA, TM #.1256.

3. Bolt Beranek and Newman, Inc. "Effect of Localized Acoustic Excitation on the Stability of a Laminar Boundary Layer." Cambridge, Massachusetts, January 15, 1962.

4. Chang, P.K. "Drag Reduction of an Airfoil by Injection of Sound Energy ". J. Aerospace Sci. 28, 9, Sept. 1961, 742-743.

5. Charters, A.C., "Transition Between Laminar and Turbulent Flow by Transverse Contamination". NACA TN #891, March 1943.

6. Cheng, S.I., "Some Aspects of Laminar Boundary Layer Flows". Quart. Appl. Math. 14, 4, Jan. 1957, p. 337-352.

7. Cooper, Ralph D. and Tulin, Marshall P. "Turbulence Measurements with the Hot Wire Anemometer". AGARD # 12 August 1955, North Atlantic Treaty Organization.

8. Corcoran, Wm.H., Opfell, J.B. and Sage, B.H., Momentum Transfer in Fluids, Academic Press Inc., 1956.

9. Corsin, S. and Uberoi, M.S. "Spectra and Diffusion in a Round Turbulent Jet." NACA Rept. 1040, 1951.

10. Corsin, S. "Extended Applications of the Hot Wire Anemometer". NACA TN 1864, 1949.

11. Corsin, S. "Investigation of Flow in an Axially Symmetrical Heated Jet of Air", NACA Wartime Rept. W 94, 1946

12. Criminale, W.O., Jr. and Kovasznay, L.S.G., "The Growth of Localized Disturbances in a Laminar Boundary Layer", J. Fluid Mech, vol. 14, pt. 1, Sept, 1962, p. 59-80

13. Davies, E.B. and Young, A.D. "Streamwise Edge Effects in the Turbulent Boundary Layer on a Flat Plate Finite Aspect Ratio", A.R.C. R&M #3367

14. Dean, Robert C. Jr., et al. "Aerodynamic Measurements" Massachusetts Institute of Technology, Summer Session 1952.

15. Dhawan, S. and Narasimha, R. "Some Properties of Boundary Layer Flow during the Transition from Laminar to Turbulent Motion." J. Fluid Mech. 3,4, Jan. 1958, 418-436.

16. Dhawan, S. "Direct Measurements of Skin Friction". NACA Rept. 1121, 1953.

17. Dryden, H.L., Schubauer, G.B., Moc, W.C. and Skramstad, H.K., "Measurements of Intensity and Scale of Wind Tunnel Turbulence and Their Relation to the Critical Reynolds Number of Spheres". NACA Rept. 581, 1953.

18. Dryden, H.L., "Air Flow in the Boundary Layer near a Plate". NACA Rept. 562, 1936.

19. Dryden, H.L., and Kuethe, A.M., "The Measurement of the Fluctuations of Air Speed by the Hot Wire Anemometer", NACA Rept. 320, 1929.

20. Emmons, H.W. "The Laminar Turbulent Transition in a Boundary Layer, Part I". Jour. Aero. Sci. Vol. 18, 7, July 1951 p. 990-998.

21. Ferri, A., Kuchemann, D. and Sterne, L.H.G., Progress in Aeronautical Sciences Volume II. Boundary Layer Problems New York, Pergamon Press, Inc. 1962.

22. Gault, Donald E., "An Investigation at Low Speed of the Flow over a Simulated Flat Plate at Small Angles of Attack Using Pitot Static and Hot Wire Probes." NACA TN 3876, March 1957.

23. Greenspan, H.P. and Benney, D.J., "On Shear Layer Instability, Breakdown and Transition". J. Fluid Mech vol. 15, pt. 1, 133-153.

24. Grohne, D. "On the Spectrum of Natural Oscillations of Two Dimensional Laminar Flows." NACA TM 1417.

25. Hall, A.A., "Measurements of the Intensity and Scale of Turbulence". ARC R&M 1842, 1938.

26. Hall, A.A. and Hislop, G.S., "Experiments on the Transition of the Laminar Boundary Layer on a Flat Plate". ARC R&M 1843, 1938.

27. Hansen, M. "Velocity Distribution in the Boundary Layer of a Submerged Plate" NACA TM #585.

28. Hassan, H.A., "On Unsteady Laminar Boundary Layers".
J. Fluid Mech. vol. 9, pt 2, October 1960, p. 300-304.

29. Hassan, H.A. "On a Solution to the Unsteady Laminar
Boundary Layer", J. Aero/Space Sci, 27, 6, pp 474-476
(Readers Forum) June 1960.

30. Hayasi, N., "On the Approximate Solution of the Unsteady
Quasi-two-dimensional Incompressible Laminar Boundary
Layer Equations". Physics Society of Japan, J. Vol. 17,
Jan. 1962, p. 203-212.

31. Hayasi, N., "On Semi-similar solutions of the Unsteady
Quasi-two-dimensional Incompressible Laminar Boundary
Layer Equations". Physics Society of Japan, J. Vol. 17,
Jan, 1962 p. 194-203

32. Hayasi, N., "On Similar solutions of the Unsteady Quasi-
two-dimensional Incompressible Laminar Boundary Layer
Equations". Physics Society of Japan, J. vol. 16,
Nov. 1961.p. 2316-2329.

33. Hildebrand, F.B., Advanced Calculus for Engineers,
Prentiss-Hall, Inc. 1949, p. 138.

34. Hill, P.G.and Stenning, A.H., "Laminar Boundary Layer
in Oscillatory Flow" ASME Trans. 82B (J. Basic Engn.)
3, Sept. 1960, p. 593-608.

35. Hinze, J.O., Turbulence, An Introduction to its
Mechanism and Theory, McGraw-Hill, 1959.

36. Holstein, H. and Bohlen, T. "Ein Einfaches Verfahren
zur Berechnung Laminarer Reibungschlichten die dem
Nahungsansatz von K. Pohlhausen genugen,"
Lilienthal-Bericht S 10, 1940, P. 5.

37. Kestin, J., Maeder, P.F. and Wang, H.E., "On Boundary
Layers Associated with Oscillating Streams". Appl. Sci
Res., Sect. A. vol. 10, no. 1, 1961, p. 1-22.

38. Klebanoff, P.S., Tidstrom, K.D. and Sargent, L.M.
"The Three Dimensional Nature of Boundary Layer
Instability". J. Fluid Mech. vol. 12, pt. 1, Jan. 1962
p. 1-34.

39. Klebanoff, P.S. and Tidstrom, K.D., "Evolution of
Amplified Waves Leading to Transition in a Boundary
Layer with Zero Pressure Gradient." NASA TN D-195
Sept. 1959.

40. Knudsen, James G. and Katz, Donald L., Fluid Dynamics
and Heat Transfer, McGraw-Hill, 1958.

41. Kovasznay, L. "Calibration and Measurement in Turbulence Research by the Hot Wire Method," NACA TM 1180, 1947.

42. Laufer, J. "The Structure of Turbulence in Fully Developed Pipe Flow," NACA Rept. 1174, 1954.

43. Liepmann, H.W. and Dhawan, S. "Direct Measurement of Local Skin Friction in Low Speed and High Speed Flow." Procedure of the First U.S. Nat. Congr. of Appl. Mechanics, 1951, p. 869.

44. Liepmann, H.W. and Fila, G.H., "Investigation of Effects of Surface Temperature and Single Roughness Elements on Boundary Layer Transition". NACA Rept. 890, 1947.

45. Lighthill, M.J., "The Response of Laminar Skin Friction and Heat Transfer to Fluctuations in the Stream Velocity". Proc. Roy. Soc. A-224, 1954, p. 1.

46. MacPhail, D.C., "Turbulence Changes in Contracting and Distorted Passages". ARC R&M 2437, 1951.

47. Mark, Richard M. "On Shear Flow Past Plates". J. Fluid Mech. vol. 14, pt. 3, Nov. 1962, p. 452-462.

48. Martin, E.D. "Note on the Three Point Boundary Value Problem for the Blasius Equation." J. Aero/Space Sci. vol. 29, no 9, Sept 1962, p. 1133-1134.

49. Martinelli, R.C. and Randall, R.D., "The Behavior of a Hot Wire Anemometer Subjected to a Periodic Velocity" ASME Trans. Jan. 1946.

50. McClure, J.D. "On Perturbed Boundary Layer Flows" Appendix A. "Stability of a Flexible Surface Exposed to Potential and Laminar Viscous Flows" MIT Fluid Dynamics Research Lab. Rept. 62-2 (AFOSR 62-187) June 1962.

51. Mechel, F, Mertens, P. and Sehilz, F. "Research on Sound Propagation in Sound Absorbent Ducts with Super Imposed Air Stream" Physihalisches Institut der Universitat Gottingen, Technical Report No. 2, Contract No. AF-61(052)-112 Wright Air Development Center.

52. Mitchner, Morton "Propagation of Turbulence, from an Instantaneous Point Disturbance" J. Aero Sci. vol. 21 no. 5, May 1954 (Reader's Forum) p. 350-351.

53. Moore, P.K. and Ostrach, S. "Displacement Thickness of the Unsteady Boundary Layer". J. Aero. Sci. vol. 24 no. 1, Jan 1957 (Reader's Forum) p. 77-78.

54. Moore, F.K. and Ostrach, S. "Average Properties of
Compressible Laminar Boundary Layer on Flat Plate
with Unsteady Flight Velocity." NACA TN 3336
Dec. 1956.

55. Moore, F.K. "Unsteady Laminar Boundary Large Flow"
NACA TN 2471, 1951.

56. Na, Tsung Yen "The Influence of Localized Normal Surface
Oscillations on the Steady, Laminar Flow over a Flat
Plate" Ph.D. Thesis, University of Michigan.

57. Ostrach, Simon "Compressible Laminar Boundary Layer
and Heat Transfer for Unsteady Motions of a Flat
Plate" NACA TN 3569, 1955.

58. Pai, Shih-I Viscous Flow Theory, I - Laminar Flow, D.
Van-Nostrand Co., Inc. 1956

59. Pohlhansen, K. "Zur Haberumgsweisen Integration der
Differentialgleichung der Laminaren Reibungsschzicht"
ZAMM 1, 1921, p. 252.

60. Richardson, E/G., "The Correction of Hot Wire Readings
in a Boundary Layer for Proximity to the Solid Boundary"
J. Aero. Sci. vol. 23, no. 10, Oct. 1956 (Reader's
Forum) p. 970-971

61. Sandborn, V.A., "An Equation for the Mean Velocity
Distribution of Boundary Layers", NASA Memorandum
2-5-59E.

62. Sandborn, V.A., "Application of the Hot Wire Resistance
Temperature Transducer to the Measurement of Transient
FlowQuantities" ASME Symposium on Measurements in
Unsteady Flow, May 1962.

63. Sato, H. and Kuriki, K. "The Mechanism of Transition
in the Wake of a Thin Flat Plate Placed Parallel
to a Uniform Flow." J. Fluid Mech. II, 3, Nov. 1961.
p. 321-352.

64. Schlichting, H. Boundary Layer Theory, 4th ed. McGraw-
Hill, 1960.

65. Schubauer, G.B. and Klebanoff, P.S., "Contributions
on the Mechanics of Boundary Layer Transition".
NACA TN 3489, 1955.

66. Schubauer, G.B. and Kelbanoff, P.S. "Investigation of
Separation of the Turbulent Boundary Layer". NACA
Rept. 1030, 1951 (Formerly NACA TN 2133).

67. Schubauer, G.B. and Skramstad, H.K. "Laminar Boundary
     Layer Oscillations and Stability of Laminar Flow."
     NBS Research Paper #1772 or, J. Aero Sci. 14, 69,
     1947 or, NACA Rept. 909.

68. Schubauer, G.B. and Klebanoff, P.S. "Theory and Applica-
     tion of Hot Wire Instruments in the Investigation of
     Turbulent Boundary Layers". NACA ACR 5K27, W-86, 1946.

69. Squire, H.B. "Heat Transfer Calculation for Aerofoils"
     ARC R&M, 1942, p. 1986.

70. Vrebalovich, Thomas "Application of Hot Wire Techniques
     In Unsteady Compressible Flows" ASME Symposium on
     Measurement in Unsteady Flow, May 1962.